NUMERICAL AND EXPERIMENTAL INVESTIGATION OF PERFORATION OF ST-37 STEEL PLATES BY OBLIQUE IMPACT

A THESIS SUBMITTED TO
THE GRADUATE SCHOOL OF NATURAL AND APPLIED SCIENCES
OF
MIDDLE EAST TECHNICAL UNIVERSITY

BY

GÖKHAN ÖZTÜRK

IN PARTIAL FULFILLMENT OF THE REQUIREMENTS
FOR
THE DEGREE OF MASTER OF SCIENCE
IN
MECHANICAL ENGINEERING

JUNE 2010

Approval of the thesis:

NUMERICAL AND EXPERIMENTAL INVESTIGATION OF PERFORATION OF ST-37 STEEL PLATES BY OBLIQUE IMPACT

submitted by **GÖKHAN ÖZTÜRK** in partial fulfillment of the requirements for the degree of **Master of Science in Mechanical Engineering Department, Middle East Technical University** by,

Prof. Dr. Canan ÖZGEN _____
Dean, Graduate School of **Natural and Applied Sciences**

Prof. Dr. Suha ORAL _____
Head of Department, **Mechanical Engineering**

Prof. Dr. R. Orhan YILDIRIM _____
Supervisor, **Mechanical Engineering Department**

Examining Committee Members:

Prof. Dr. Metin AKKÖK
Mechanical Engineering, METU _____

Prof. Dr. R. Orhan YILDIRIM
Mechanical Engineering, METU _____

Prof. Dr. Mustafa İlhan GÖKLER
Mechanical Engineering, METU _____

Prof. Dr. Haluk DARENDELİLER
Mechanical Engineering, METU _____

Dr. Rıdvan TOROSLU
ASELSAN Elektronik Sanayi ve Ticaret A.Ş. _____

Date: _____

I hereby declare that all information in this document has been obtained and presented in accordance with academic rules and ethical conduct. I also declare that, as required by these rules and conduct, I have fully cited and referenced all material and results that are not original to this work.

Name, Last Name: GÖKHAN ÖZTÜRK

Signature :

ABSTRACT

NUMERICAL AND EXPERIMENTAL INVESTIGATION OF PERFORATION OF ST-37 STEEL PLATES BY OBLIQUE IMPACT

Öztürk, Gökhan
M.S., Department of Mechanical Engineering
Supervisor : Prof. Dr. R. Orhan YILDIRIM

June 2010, 103 pages

In this thesis, it is aimed to determine the ballistic limit thicknesses of ST-37 steel plates under oblique impact of bullets having hard steel core (DIN 100Cr6 at 61-62 HRc) by using both experimental and numerical methods. In experimental part, angles of attack of the bullets are changed from 0° to 70° by 10° increments. Bullet velocities are measured for each shot just before the impact and they are found to be between 790-830 m/s. The minimum plate thickness that is not perforated and the maximum plate thickness that is perforated are determined by conducting three shots for each angle of attack - plate thickness combination. After the monolithic case, for some angles, layered plate combinations are also investigated. In the numerical analysis part, Johnson Cook constitutive and failure models are used together with the data obtained from literature. Experiments are simulated numerically by using a commercial non-linear explicit hydrocode software package, ANSYS AUTODYN. Results of the numerical simulations and the experimental findings are presented in tabular and graphical forms and then compared to each other.

Keywords: Ballistic, Oblique Impact, Perforation, ST-37 Steel

ÖZ

ST-37 ÇELİĞİNİN EĞİK ÇARPMA KOŞULLARINDA DELİNMESİNİN SAYISAL VE DENEYSEL YÖNTEMLERLE İNCELENMESİ

Öztürk, Gökhan
Yüksek Lisans, Makina Mühendisliği Bölümü
Tez Yöneticisi : Prof. Dr. R. Orhan YILDIRIM

Haziran 2010, 103 sayfa

Bu tez çalışmasında ST-37 çeliğinin, değişik açılarla çarpan sert çelik çekirdekli (DIN 100Cr6, 61-62 HRc) mermilere karşı balistik limit kalınlığının deneysel ve sayısal yöntemlerle belirlenmesi amaçlanmaktadır. Çalışmanın deneysel kısmında, mermilerin çarpma açıları 0°'den 70°'ye kadar 10°'lik adımlarla arttırılmıştır. Mermi hızı atışlar öncesinde ölçülmüş ve 790-830 m/s değerleri arasında olduğu görülmüştür. Her plaka kalınlığı - çarpma açısı kombinasyonu için üçer adet atış yapılmış ve sonuç olarak her çarpma açısı için delinen en kalın ve delinmeyen en ince plakalar belirlenmiştir. Yekpare plakalar için gerçekleştirilen atışlardan sonra belirli açılar için katmanlı plaka kombinasyonları da denenmiştir. Çalışmanın sayısal benzetim çalışmaları kısmında Johnson-Cook dayanım ve kırılma modelleri literatürden elde edilen parametrelerle kullanılmış ve deneysel çalışmaların sayısal benzetimleri gerçekleştirilmiştir. Bunu yaparken ticari bir doğrusal olmayan açık hidrokod yazılımı olan ANSYS AUTODYN kullanılmıştır. Deneysel çalışmaların sonuçları ile sayısal benzetim çalışmalarının sonuçları çizelgeler ve şekiller yardımıyla sunulmuş ve birbirleriyle karşılaştırılmıştır.

Anahtar Kelimeler: Balistik, Eğik Çarpma, Delme, ST-37 Çeliği

özlenen barış ve kardeşliğe...

ACKNOWLEDGMENTS

First of all, I would like to thank to my supervisor, Prof. Dr. R. Orhan YILDIRIM, for his guidance during my graduate education.

I also would like to thank to Prof. Dr. Mustafa İ. GÖKLER, director of METU BİLTİR Center, for providing the necessary computer and software support to make the numerical simulation studies and to patient personnel of MKEK Small Arms Weapon Factory for allowing and helping us to use the ballistic shooting range.

I would like to thank to my family for their priceless love, care and support. Without them, I would be nothing.

Finally, I would like to thank to my dear friend, Şebnem GÜZELBAYRAM, for her invaluable support throughout the last four years and hopefully the rest of my life.

TABLE OF CONTENTS

LIST OF TABLES

TABLES

LIST OF FIGURES

FIGURES

CHAPTER 1

INTRODUCTION

Perforation of steel plates by bullets is an important research topic for defence applications. Although armor materials are already evolved to more complicated systems and/or material combinations, investigating the perforation of steel plates is quite important to understand the basic mechanisms of protection against bullet impact and armor design.

Normal impact of bullets is the most critical case and has been examined widely in literature. But in reality, most of the bullet-armor encounters involve more or less obliquity. To have a command of oblique impact and its results (i.e. perforation, ricochet etc.) it is important to analyze and understand the behavior of steel plates under oblique impact conditions.

In examining a physical phenomenon, many methods can be implemented solely or in combinations. In solving ballistic impact problems, there are generally three ways to follow. First one is the experimental approach. This approach is the most reliable yet the most time consuming and costly method. Apart from those, another drawback of experimental analysis is difficulty of measuring some variables during high speed impact. For an oblique impact condition, for example, it is almost impossible to measure the exit direction (angle) and velocity of the bullet unless there exist two or three high speed cameras positioned accurately.

The second method of solving high speed penetration/perforation problems is the analytical method. There are several analytical methods developed for normal and oblique impact conditions. Considering the severity of defence systems, it is obvious that a purely analytical approach can only be used to have a general intuition of the nature of penetration/perforation process. Before conducting experiments, for example, preliminary analytical approach can be used to find a starting point and to decrease the number of total experiments.

The third and the final approach is the use of numerical methods. Main advantage of this approach is the ability of dealing with very complex geometries without any difficulty. Depending on the complexity of the materials models used, results starting from the level of analytical models to the level of experimental methods can be obtained. Once the model for a material is obtained, any kind of penetration/perforation simulation can be conducted by fine tuning the parameters such as impact velocity, plate thickness, angle of attack etc. Considering the rapid development in hardware and software systems, number crunching operations can now be done in a short time spending very little effort.

In this thesis, both numerical and experimental methods are used providing the opportunity of comparing these methods and tuning material constitutive model parameters. By comparing the results of both methods, ability of the numerical solver in explaining the true physical behavior of perforation/penetration can also be determined.

1.1 Scope of the Thesis

Main aim of this thesis is to determine the ballistic limit thicknesses of ST-37 steel plates under oblique impact of bullets having hard steel core (DIN 100Cr6 at 61-62 HRc) by using both experimental and numerical methods.

In Chapter 2, theoretical background of the thesis is presented using the results of literature survey. First of all, general information about ballistics (Section 2.1), threat types (Section 2.2) and means of protection from these threats (Section 2.3) is presented. In Section 2.4, some basic information about penetration, perforation and ricochet is given. Afterwards, in Section 2.5, results of the literature survey on oblique impact are presented. Then the effects of strain rate and temperature on the mechanical behavior of materials are explained generally in Section 2.6. As a final topic of Chapter 2, in Section 2.7, the term *Areal Density* and its use in the armor systems is explained.

In the experimental analysis part (Chapter 3), information about the experimental work conducted for this thesis is presented. In Sections 3.1-3.4, preparations done for the experimental studies and testing procedure are explained. Finally results of the experimental shots are presented in Section 3.5

In Section 4.1 of the numerical analysis part (Chapter 3), some preliminary information about modeling the impact phenomenon is given. In Section 4.2, numerical modeling process conducted for the numerical simulation part of the thesis is explained and finally in Section 4.3, results of the numerical simulation studies are presented.

In Chapter 5, results obtained from the numerical simulations are compared with the experimental findings. In Section 5.1 of this chapter is dedicated to the comparison of monolithic plate experiments and simulations while in Section 5.2, comparison is done for the layered plate combinations.

Finally in Chapter 6, conclusions of the thesis are presented (Section 6.1) together with recommendations for the future researchers of this topic (Section 6.2).

CHAPTER 2

THEORETICAL BACKGROUND

Before mentioning the methods used to solve the ballistic perforation/penetration of armors, some preliminary information about the terms *ballistics*, *threat* and *armor* is crucial. In addition to these, investigating the situation of a high speed bullet hitting a target also requires a deep knowledge of the disciplines such as mechanics of penetration, perforation and ricochet, impact mechanics in oblique impact conditions and material behavior at high strain rates and temperatures. Furthermore, the term *Areal Density* plays an important role in determining the effectiveness of armor systems. Detailed information on these subjects can be seen in the following sections of this chapter.

2.1 General Information about Ballistics

Ballistics is defined as the science of the propulsion, flight, and impact of projectiles [1]. It has been studied for centuries at different branches of academic world from ethics to flight characteristics. In literature, ballistics is divided into three main types as follows [2, 3]:

1. Interior (Internal) Ballistics
2. Exterior (External) Ballistics
3. Terminal Ballistics

2.1.1 Interior (Internal) Ballistics

In practice, all cartridges made up of the following components [4];

1. Case
2. Primer
3. Powder (Propellant)
4. Projectile (Core) (Figure 2.1)

Interior ballistics investigates the period of time starting with the hit of the firing pin to the primer and ending with the exit of the bullet from the muzzle of the gun. In short, it is interior ballistics' job to examine what happens inside the barrel of a gun.

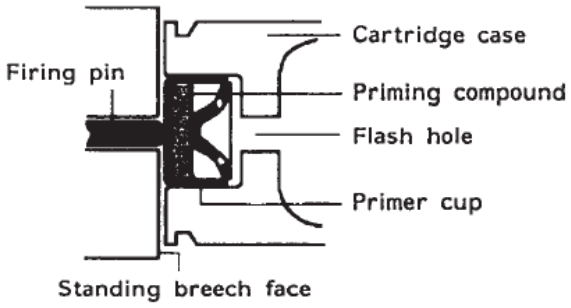

Figure 2.1: Center Fire System [2]

The area of interior ballistics is quite complex. But simply, the process starts when the firing pin hits the primer . This results with the explosion of the priming compound and emergence of a extremely high temperature (around 2000 °C) jet of flame. This jet of flame passes through the flash hole, into the propellant charge and ignites the propellant (Figure 2.2). Burning at high speed, propellant creates a large volume of gas at high pressure which accelerates the bullet through the barrel until it leaves the muzzle of the gun [2].

2.1.2 Exterior (External) Ballistics

When the bullet leaves the muzzle of the gun and starts its flight without any lateral constraints, it is in the area of exterior ballistics until it hits a target. During the flight, it is under the effects of atmospheric pressure, the force induced by its spin and the force created by the gravitational acceleration. Person investigating the trajectory of the bullet during its flight

(Figure 2.3) is called the exterior ballistician or the aero-ballistician [3]. Aerodynamic forces acting on a projectile during its flight can be seen in Figure 2.4.

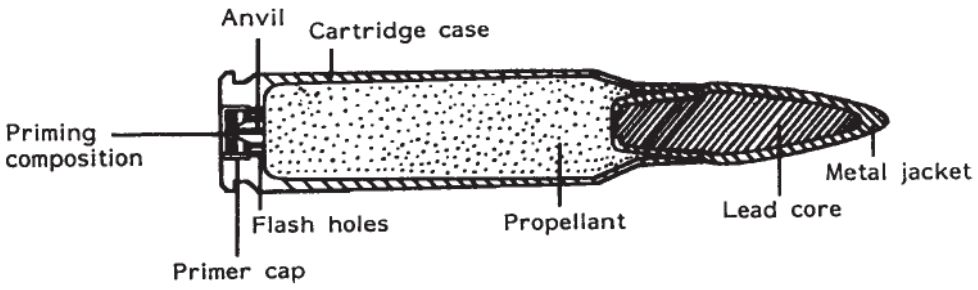

Figure 2.2: Center Fire Bullet [2]

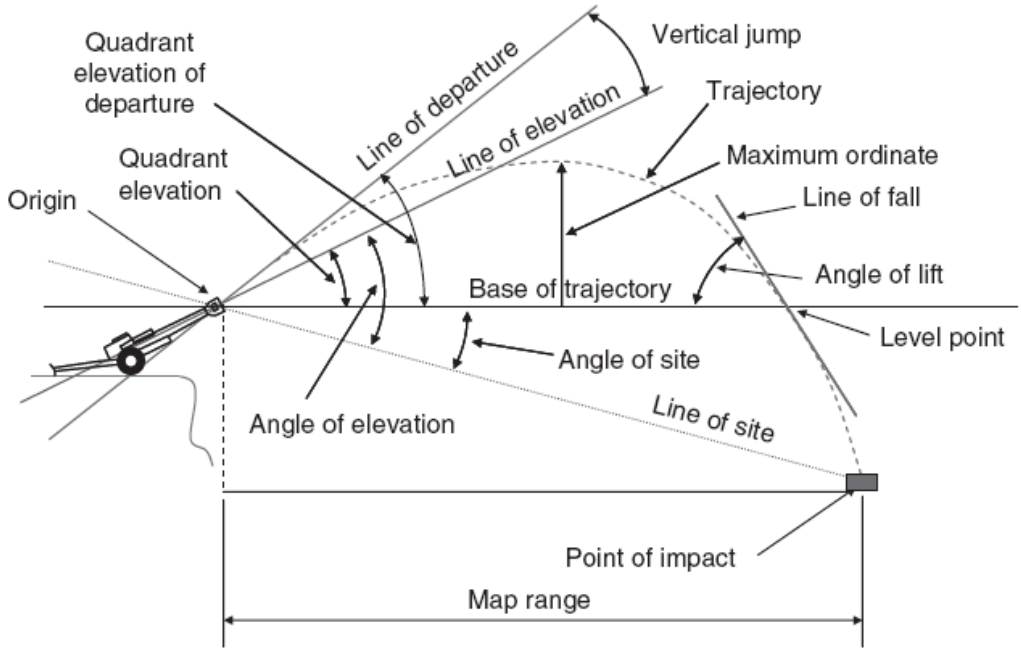

Figure 2.3: Elements of Trajectory [3]

2.1.3 Terminal Ballistics

Most of the projectiles are aimed to hit and defeat a target and it is terminal ballistician's duty to investigate what happens after that instance, how the projectile affects the target and how

the target affects the projectile. Terminal effects on a projectile while defeating its target are highly dependant on the mission and design of the projectile. The most common of these missions are as follows [3]:

1. Fragmentation of the projectile body by its cargo of high explosives

2. Penetration or perforation of the target by the application of kinetic or chemical energy

3. Blast at the target area delivered by the chemical energy of the explosive cargo

4. The dispersal of the cargo for lethal or other missions, e.g., smoke, illumination, propaganda dispersal, etc.

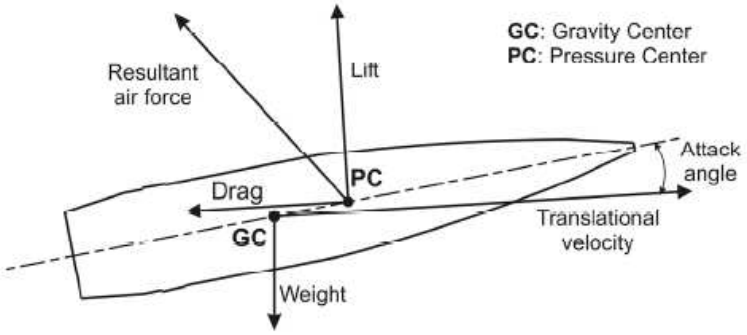

Figure 2.4: Aerodynamic Forces Acting on a Projectile [5]

Main area of interest of this thesis is also terminal ballistics investigation of a specific case, i.e. perforation of a ST 37 steel target by a 7.62 mm AP (Armor Piercing) bullet under oblique impact conditions.

In some resources a fourth type of ballistics, *intermediate ballistic*, is also mentioned. Intermediate ballistics investigates the motion of the bullet as it exits from the muzzle, including the initial tip-off, tube and bullet jump, muzzle device effects and sabot discard. It can be seen that the area of investigation of the intermediate ballistics is quite overlapping with external ballistics [3].

2.2 Threat Types

Men started to create and develop arms, instinctively, to hunt and feed himself starting from the ancient times. Today, however, hunting is not solely enough to survive. Countries have to defend themselves against not only the terrorist attacks but also the other countries looking for more natural resources. It is obvious that a simple bow and arrow is not an efficient way of protection since they are not capable of perforating modern armors.

Generally speaking, any item that can be launched is a potential projectile. Although military type of projectiles are the most famous ones, in fact, they constitute a small group [7]. Even a chair, standing in front of your house can be a high speed projectile when accelerated by a sudden tornado. General characteristics of projectiles can be seen in Table 2.1.

Table 2.1: General Characteristics of Projectiles [7]

	Basic Shape	**Nose Configuration**
Geometry	Solid Rod	Cone
	Sphere	Ogive
	Hollow Shell	Hemisphere
	Irregular Solid	Right Circular Cylinder

	Light Weight	**Intermediate**	**Heavy**
Material Density	Wood	Steel	Lead
	Plastics	Copper	Tungsten
	Ceramics		
	Aluminum		

	Trajectory	**Impact Condition**
Flight Characteristics	Straight (Stable)	Normal
	Curved (Stable)	Oblique
	Tumbling (Unstable)	

	Shape	**Location**
Final Condition	Undeformed	Rebound
	Plastically Deformed	Partial Penetration
	Fractured	Perforation
	Shattered	

Since the main area of interest of this thesis is the military projectiles (Armor Piercing bullets, to be specific) we will limit our explanation to the military projectiles. In general, we can divide modern types of military threats into two main categories [6]:

1. Kinetic Energy Projectiles

2. Chemical Energy Projectiles

Detailed information about these categories of projectiles are presented in Sections 2.2.1 and 2.2.2.

2.2.1 Kinetic Energy Projectiles

Large amount of energy is required to accelerate any type of projectile that will defeat a target. In kinetic energy projectiles, this energy is provided by the compressed gases which are generated by the high speed burn of the propellants in a barrel. As a result, they need to be launched from a gun. Armor Piercing (AP) bullets and kinetic energy penetrators are in this category [6].

Common types of kinetic energy projectiles can be seen in Figure 2.5. First one (a) is the 0.50 caliber armor piercing bullet. It has a steel jacket and lead core. Another example of this type of bullet is the 7.62 mm AP bullet used in the experimental and numerical analysis parts of this thesis having a brass jacket and hard steel core. The second projectile (b) shown in Figure 2.5 is the Armor Piercing Fin Stabilized Discarding Sabot (APFSDS) projectile. It is a long rod projectile generally launched from a tank. Material of the rod is a high density alloy (tungsten alloy or depleted uranium). Fins facilitate a more stable flight. While projectile is being launched from the barrel (interior ballistics duration) the sabot projects the projectile and discards during flight (Figure 2.6). The third one (c) is an armor piercing charge-bursting projectile. It carries an explosive cargo which detonates when the projectile penetrates into the target [6].

2.2.2 Chemical Energy Projectiles

Contrary to kinetic energy projectiles (Section 2.2.1), chemical energy projectiles do not need to be launched from a from a gun. They use the energy created by the detonation of an explosive. The most common types of chemical energy projectiles are [8]:

1. Shaped Charges

2. Hemispherical Charges

3. Explosively Formed Projectiles (EFP)

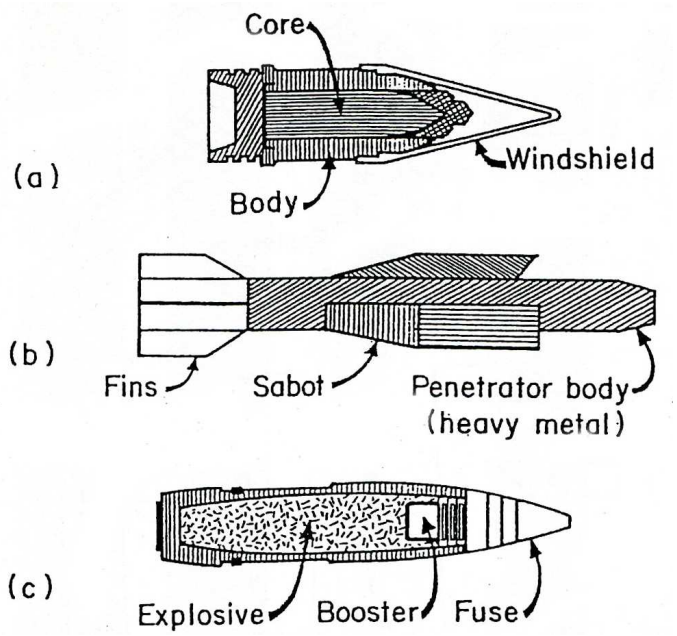

Figure 2.5: Description of Kinetic Energy Projectiles [6]

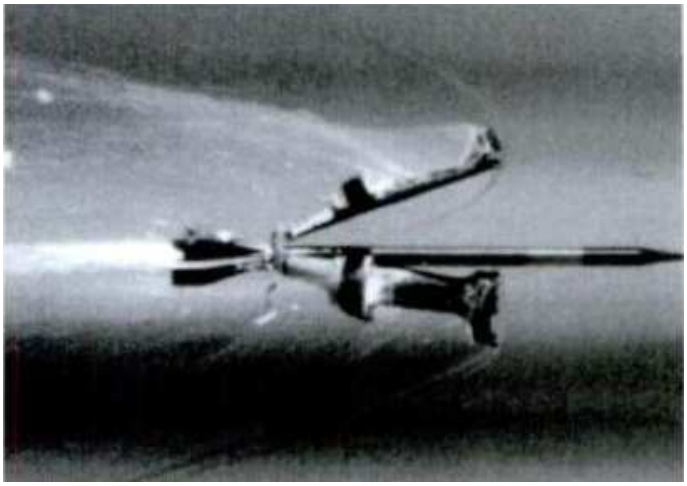

Figure 2.6: A View of 120mm APFSDS Projectile, Discarding Its Sabot [10]

Chemical energy projectiles consist of a cylinder filled with high explosive. Frontal face of the explosive is covered by a thin layer of metal called the *liner* (Figure 2.7). When the high

explosive is detonated, the liner turns into a high speed jet and penetrates the target [10]. Generally, almost 15-20% of the total kinetic energy of the explosive is employed to form and accelerate a jet made of the liner material [8].

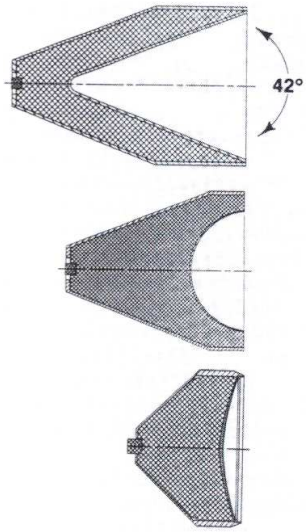

Figure 2.7: Chemical Energy Projectiles; Top to Bottom: Shaped Charge, Hemispherical Charge, EFP [8]

Two extremes of the chemical energy projectiles are shaped charges and explosively formed projectiles. Shaped charges produce a low mass (15% of the total liner mass) jet having high speed (7-10 km/s) while explosively formed projectiles form a heavy rod of fragment having moderate velocity (2-3 km/s) [8].

2.3 General Information about Armors and Armor Types

Parallel to the development of threat mechanisms (Section 2.2), the need of defeating these new threats emerges, triggering the development of new armor types (Figure 2.8). The endless cycle completes itself by the development of a new threat that perforates the new armor. For example, steel has been the prime armor material traditionally but the use of other materials such as ceramics, composites, glass and even explosives is the new trend.

Armors are divided into three main groups [6]:

1. Body Armors (Personnel Armors)

2. Light Armors (Aircraft and Vehicle Armors)

3. Heavy Armors (Tank Armors)

Body Armors are intended to protect the torso and the head of the personnel primarily against gunfire, fragments from mines and high explosive artillery shells and grenades. Traditional steel helmets are replaced by Kevlar and Spectra fiber-reinforced composite helmets nowadays and application of fiberglass reinforced plastics and ceramic plates backed with aluminum can be seen in body armors [4, 6, 11, 12].

Light Armors are used to protect the seats of the helicopters, light vehicles and airplanes. These armors use the principle of breaking and fragmenting the projectile by a hard surface and absorbing the residual energies of the fragments by a softer material backing the hard surface. For example, for light vehicles and airplanes, while ceramic armor plates break the projectiles, a ductile organic composite (e.g. graphite reinforced plastic) backing absorbs the residual energy and provides a successful protection [6, 13].

Protection of tanks is the provided by Heavy Armors. Steel has been the traditional armor material for tanks. But as threats develop, it started to be inefficient. Since threats like shaped charges can penetrate into steel about 250 mm or more, it is almost impossible to use solely steel as tank armor. Main reason for this is the weight consideration. To overcome this difficulty, other materials such as ceramics backed by a ductile material (e.g. aluminum) are employed nowadays [6]. Another type of heavy armor is Reactive Armor (RA or Explosive Reactive Armor, i.e. ERA). In RA applications, an explosive is sandwiched between two layers of metal. These tiles of RA are placed around the tank. As a shaped charge jet or a kinetic energy projectile penetrates the front plate, the explosive under the plate ignites and erodes the projectile. RA tiles are even used in light armored vehicles [14, 15].

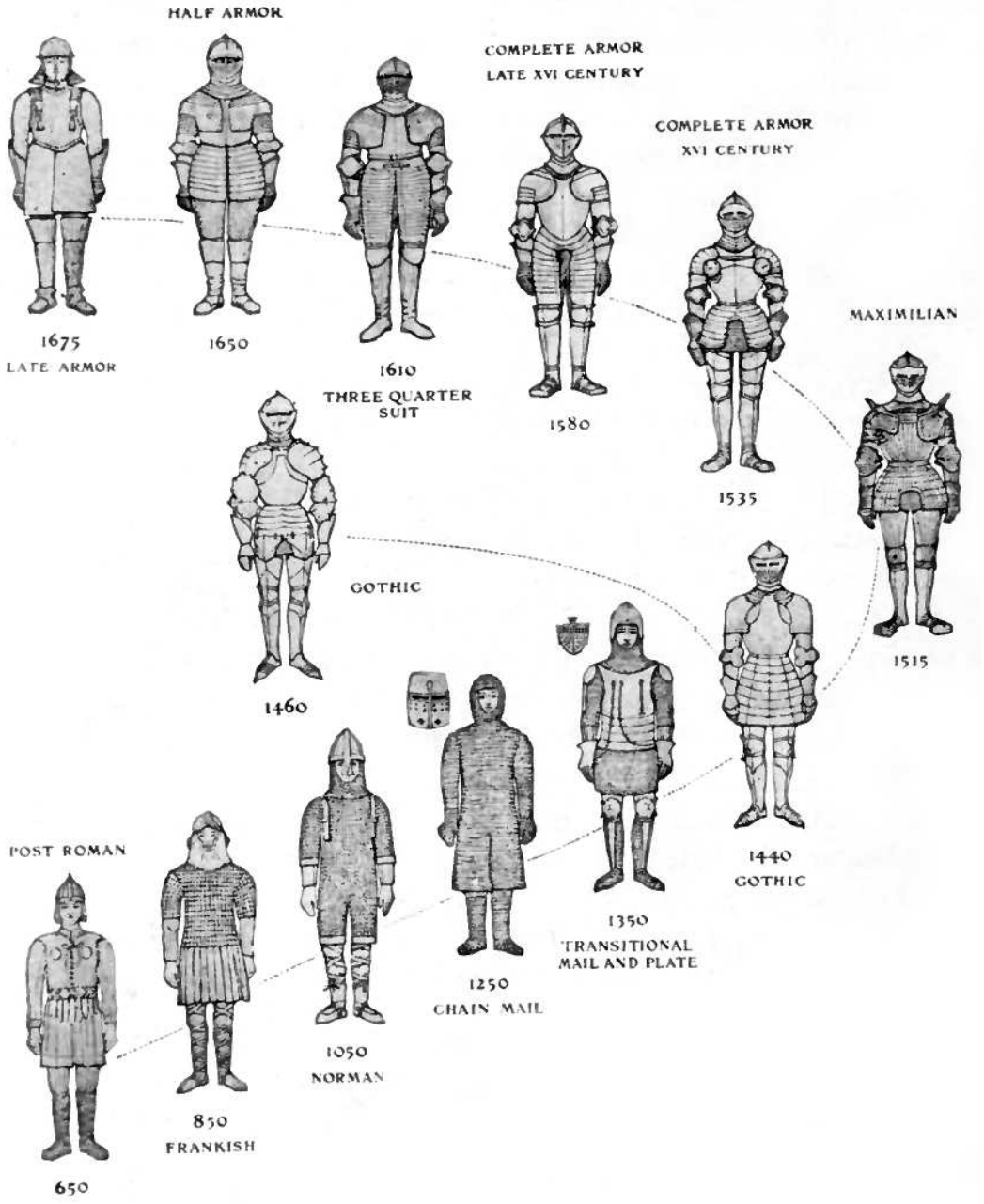

Figure 2.8: European Armor and Its Development during a Thousand Years (A.D. 650 to 1650)[9]

2.4 Definitions of Penetration, Perforation and Ricochet

In general, penetration is defined as the entrance of a missile into a target without completing its passage through the body, generally resulting in the embedment of the striker into the target and formation of a crater [16]. The term *ricochet*, on the other hand, defines the rebound of the projectile from the target or the emerging of the projectile from the impacted surface after penetrating and following a curved penetration path in the impacted body. Finally, perforation may be defined as the complete passage of a missile through a target material by completely piercing it [7]. In other words, perforation may be referred as *complete penetration*. Definitions of the partial and complete penetration processes can be seen in Figure 2.9.

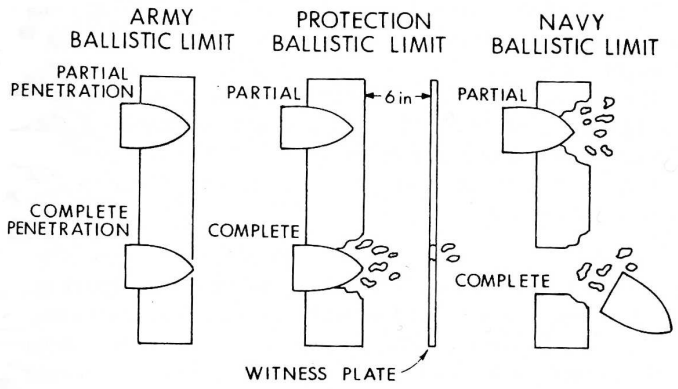

Figure 2.9: Definitions of Complete and Partial Penetration for Normal Impact of Projectiles [7]

When a target plate is impacted by a projectile, failure may occur in several ways, namely *brittle fracture*, *ductile hole growth*, *radial fracture*, *plugging*, *fragmentation* and *petaling*. These failure types can be seen in Figure 2.10.

2.5 An Overview of the Studies in Literature about Oblique Impact

Since the normal impact condition is the worst impact case for an armor, it has been investigated widely in the literature. Although being not as common as normal impact, oblique impact is also investigated analytically, experimentally and numerically in the literature by some researchers.

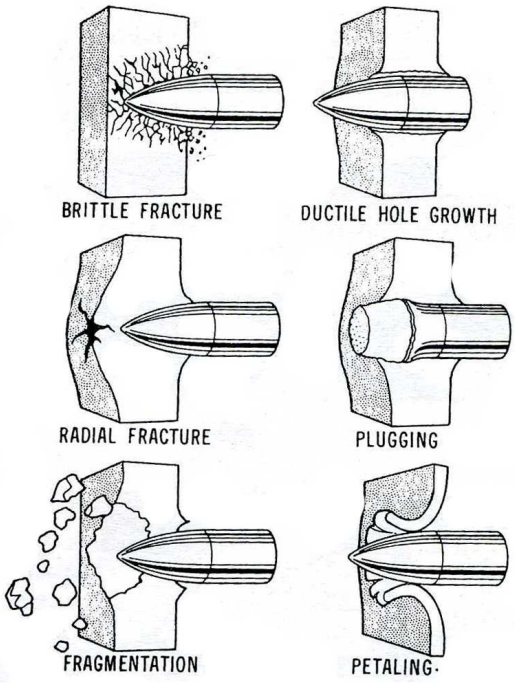

Figure 2.10: Types of Failure for Normal Impact of Projectiles [7]

To give a general overview of the publications in the field of oblique impact, we can firstly mention Awerbuch and Bodner [17]. In 1975, they investigated the oblique impact of 5.6 mm lead core bullets to pure aluminum (1100-H14) and aluminum alloy (6061-T6) target plates up to 75 ° angle of attack both analytically and experimentally. In 1997, Gupta and Madhu [18] investigated the perforation of mild steel, aluminum and RHA (Rolled Homogeneous Armor) plates by 7.8 mm hard steel core bullets impacting at 800-880 m/s speeds up to 60 °. This work resulted in an analytical model for oblique perforation studies. They also examined the perforation of layered plates. Five years later; Woong Lee, Heon-Joo Lee and Hyunho Shin [19] published a paper including analytical, experimental and numerical investigation of oblique impact phenomenon. In their work, they investigated the oblique impact of a 7 mm diameter Tugsten alloy long rod impacting at 1000 - 2000 m/s to RHA and S-7 plates having 6.25 mm thickness from 3 ° to 25 ° angles of attack. They derived the critical ricochet angles both numerically and experimentally and proved that ricochet can occur at lower angles by employing harder target materials for a given impact velocity, which was appreciable at lower velocities in particular. In 2008, Daneshjou and Sahravi [20] added the mesh free Lagrangian method, SPH (Smooth Particle Hydrodynamics), to the previous work ([19]). As a result,

they showed that long rods shatter into spray of particles under oblique impact conditions and this behavior can be more successfully represented by SPH method. Finally, again in 2008, Zhou and Stronge [21] conducted numerical and experimental analysis of impact of flat and hemispherical nosed hard steel projectiles having 12.68 mm diameter and impacting at 50-150 m/s speeds to 316L steel plates at 0 °, 30 ° and 45 °. This paper includes the investigation of sandwich plates. They concluded that when impacted obliquely by flat nosed projectiles, layered plates have a larger ballistic limit compared to single plates of the same material and same total thickness.

2.6 Material Behavior at High Strain Rates and Temperatures

The last topic that will be investigated in the theory chapter of this thesis is the material response at high strain rates and temperatures. Speed of loading is an extremely important parameter when determining the characteristics of a material. A material acting in a ductile manner under static loading can respond in a completely different manner to an impact loading. We can even classify the term "impact" according to the strain rate ($\dot{\varepsilon}$) and velocity of impact (V_s) as it can be seen in Figure 2.11 [7].

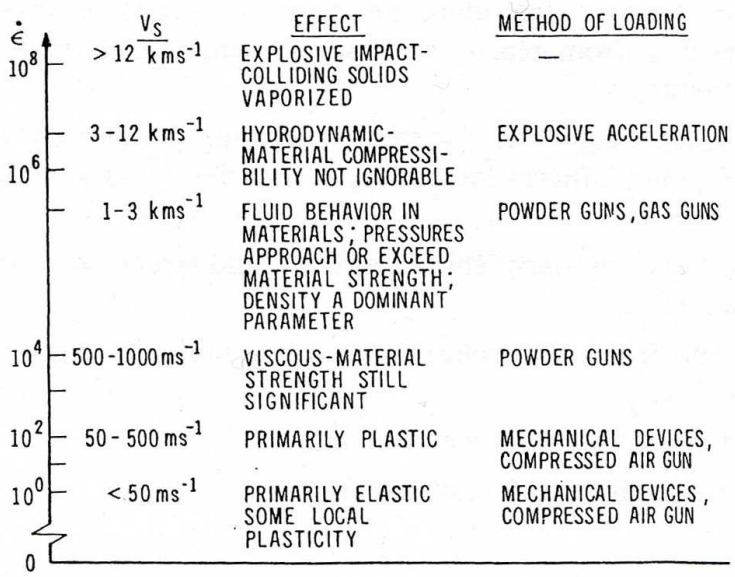

Figure 2.11: Impact Response of Materials [7]

It is also known that high strain rate deformation is an adiabatic process. In this process, a great proportion of the plastic work is converted into heat energy causing a temperature rise around impact region [22].

In general, we can say that the general flow curve of a material will decrease (material will soften) with decreasing strain rate (Figure 2.12) and increasing temperature (Figure 2.13) [22, 23, 24].

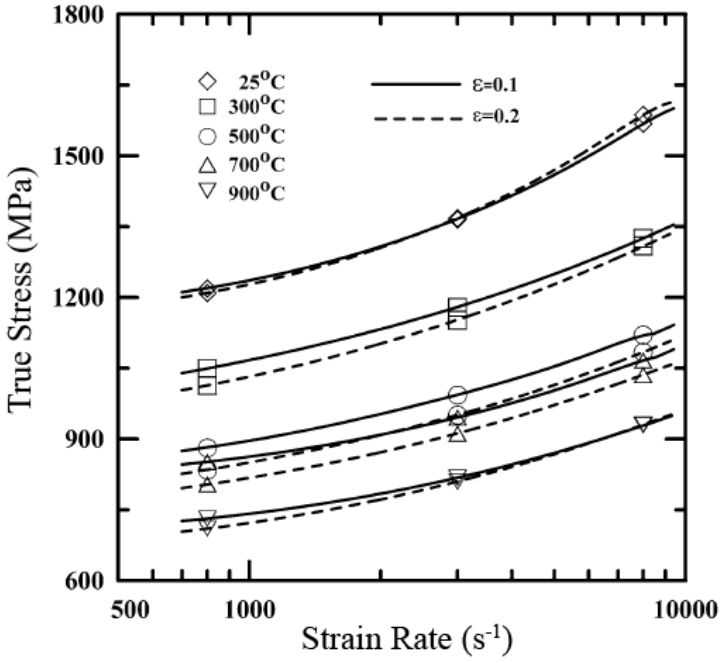

Figure 2.12: Variation of Flow Stress of a Ti Alloy with Strain Rate [24]

As a last note, it can be said that the strain rate sensitivity of steels decrease with the increasing temperature and decreasing carbon content (Figure 2.14) while the temperature sensitivity increases with increasing temperature and and increasing carbon content but decreases with the strain rate (Figure 2.15) [22].

While creating numerical simulation models of a high strain rate problem (e.g. ballistic impact), it has great importance to take into account such effects by implementing a constitutive equation like Johnson-Cook (Equation 4.2) wherever possible.

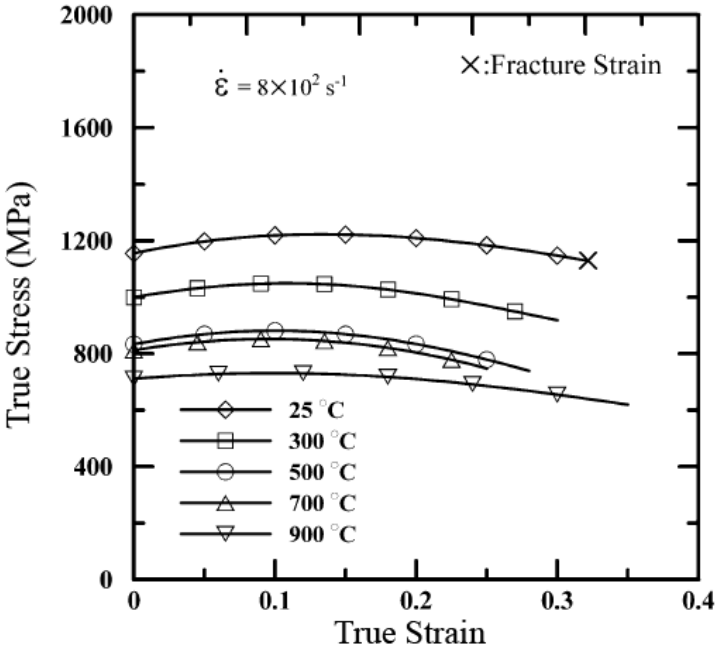

Figure 2.13: Variation of Flow Stress of a Ti Alloy with Temperature [24]

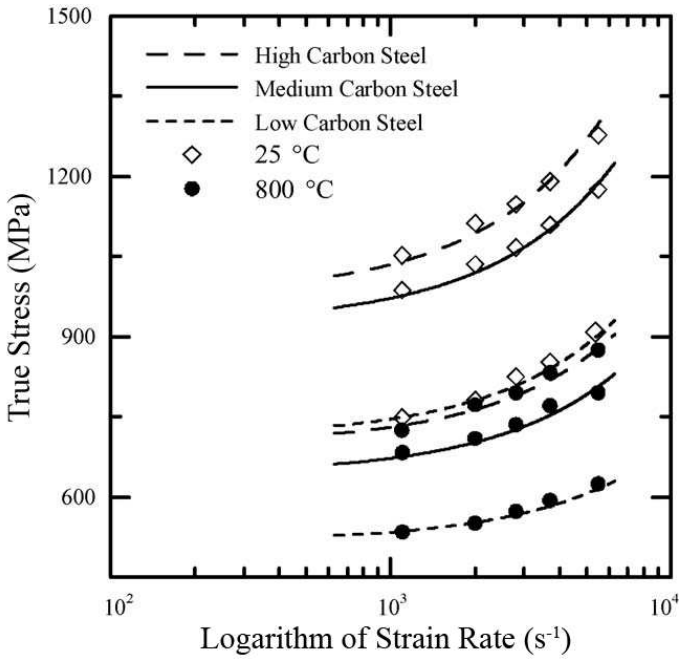

Figure 2.14: Flow Stress of S15C Low Carbon Steel, S50C Medium Carbon Steel and SKS93 High Carbon Steel as Function of Logarithmic Strain Rate at True Strain of 0.3 and Temperatures of 25 and 800 °C [22]

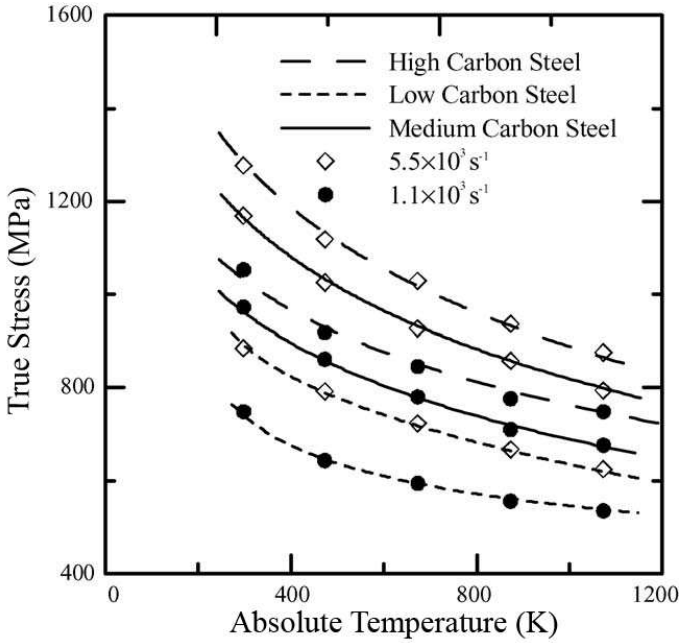

Figure 2.15: Flow Stress of S15C Low Carbon Steel, S50C Medium Carbon Steel and SKS93 High Carbon Steel as Function of Temperature at True Strain of 0.3 and Strain Rate of 5.5 and 1.1×10^3 s^{-1} [22]

2.7 Definition of Areal Density

To compare the effectiveness of obliquity in armor systems, the term *Areal Density* should be investigated. Areal density is the weight of an armor system for a unit area. When we change the orientation of a plate, to have the same areal density, we should also change its thickness. For example, assume that the areal densities of plates 1 and 2 in Figure 2.16 are A_1 and A_2, respectively. We can define A_1 and A_2 as in Equations 2.1 and 2.2.

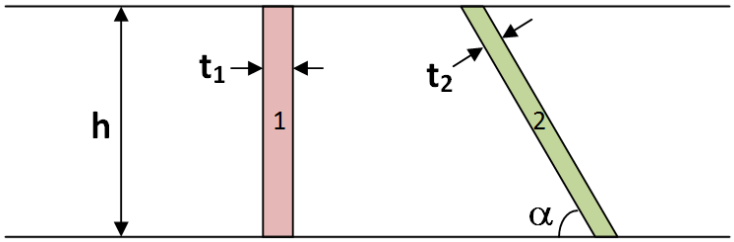

Figure 2.16: Cross-sectional View of Two Plates

$$A_1 = h \cdot t_1 \cdot \rho_1 \tag{2.1}$$

$$A_2 = \frac{h}{\sin(\alpha)} \cdot t_2 \cdot \rho_2 \tag{2.2}$$

In Equations 2.1 and 2.2;

t_1 and t_2 : Plate thicknesses

ρ_1 and ρ_2 : Plate densities

h : Cross sectional height

Assuming the same material for two plates, ρ_1 and ρ_2 cancel each other. For these plates to have the same areal density, A_1 should be equated to A_2;

$$h \cdot t_1 = \frac{h}{\sin(\alpha)} \cdot t_2 \tag{2.3}$$

As a result of Equation 2.3, we get;

$$t_2 = t_1 \cdot \sin(\alpha) \tag{2.4}$$

As defined in Figure 3.10 in Chapter 3, angle of attack (θ) used in this thesis is simply $90 - \alpha$. Inserting θ in Equation 2.4, it can be concluded that;

$$t_2 = t_1 \cdot \cos(\theta) \tag{2.5}$$

Equation 2.5 means that when the obliquity of a plate is changed, to keep the areal density constant, the plate thickness should be decreased to t_2. If the minimum plate thickness that is not perforated for a specific angle of attack is less than the calculated t_2 value, we can say that the areal density (as a result, the weight) of the total armor system is decreased and vice versa. Necessary comparisons according to constant areal density are presented in the related sections of experimental (Chapter 3) and numerical simulation (Chapter 4) studies.

CHAPTER 3

EXPERIMENTAL STUDIES

In this chapter, experimental part of the thesis is presented.

3.1 Test Setup

Ballistic impact experiments require special places designed for the test. For this thesis, ballistic testing (shooting) range of MKEK Small Arms Weapon Factory in Kırıkkale is used. In addition to existing systems in the shooting range, a clamping device that is designed in a previous work [25] is improved to be able to incline the target plates to a specified angle of attack and manufactured in the workshop of the Department of Mechanical Engineering, METU.

3.1.1 Existing Systems in MKEK

In the shooting range of the MKEK Small Arms Weapon Factory, there is a rifle that is fixed to a table (Figure 3.1) with horizontal and vertical movement (adjusting for aiming) capability. After 7.5 m distance from the bullet exit point (muzzle of the rifle) there is a speed measurement system consisting of two optical sensor units (Figure 3.2) having 5 m distance in between and a measurement device with display (Figure 3.3). By the help of two optical sensors, the measurement device measures and displays the speed of the 7.62 mm AP bullet before impacting the target plate. After 3.6 m from the second sensor, the clamping mechanism (Section 3.1.2) is installed. Under the clamping mechanism, a ricochet box is placed. The ricochet box is a rectangular prism made of sheet steel. It is filled with blocks of wood to

stop the ricocheted bullets and to prevent any injury that can occur to the personnel who aims and triggers the rifle. Whole set-up can be seen in Figure 3.4.

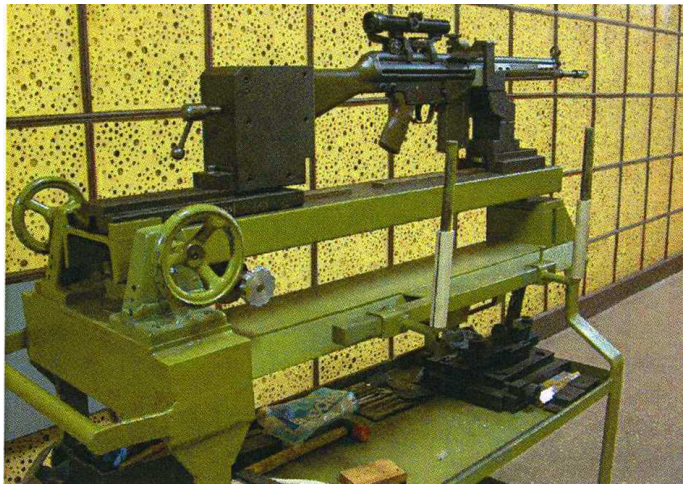

Figure 3.1: Rifle Fixed to an Adjustable Table

Figure 3.2: Optical Sensors for Speed Measurement

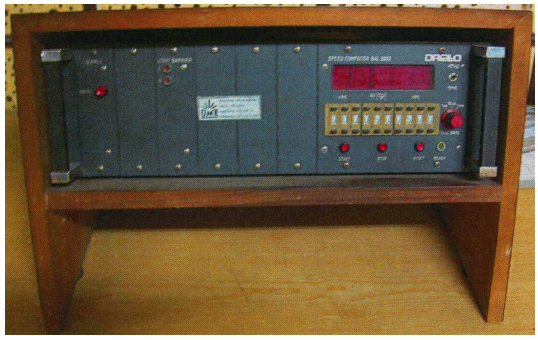

Figure 3.3: Speed Measurement Device

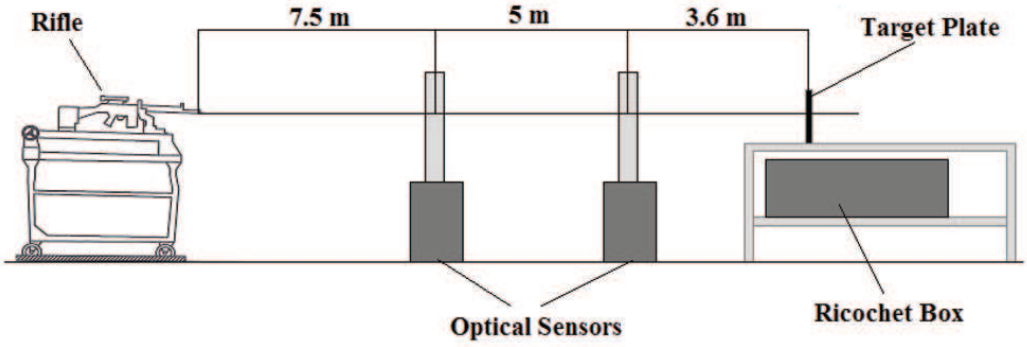

Figure 3.4: Test Setup in MKEK

3.1.2 Clamping Mechanism

Time is a big constraint while conducting experiments. To overcome this difficulty, an easy clamping and releasing mechanism is required. Since the scope of this thesis is to investigate the oblique impact, the clamping mechanism should also allow the target plates to be inclined to specified angles. In order to solve these problems simultaneously, a clamping mechanism is designed and manufactured.

As it can be seen in Figure 3.5, mechanism has a fixed and a moving plate to fix the target plate in between. When the lever arm is pulled, moving plate goes back compressing the springs. Target plate is then placed in between the moving and fixed plates and the arm is released, letting the springs press the moving plate against the target plate and fix it to its place. After fixing the target place, inclination of the target plate is set using the angle

adjusting arms. When the fixing assembly is inclined counterclockwise (Figure 3.5), angle adjustment arms slide freely inside the angle fixing blocks. These blocks have eight holes drilled on them, each representing the angle of attack of the bullet from 0 to 70° with 10° increments. When the holes on the angle adjustment arms become concentric with the desired holes on the angle fixing blocks, two pins are used to fix the angle adjustment arms and the whole assembly connected to them. The clamping assembly has a rectangular hole where the personnel triggering the rifle aims and shoots the target plate (Figure 3.6). Since the clamping mechanism leans forward (to the bullet approach direction), bullets ricocheting from the target materials moves down and falls into the ricochet box sticking into one of the wood blocks.

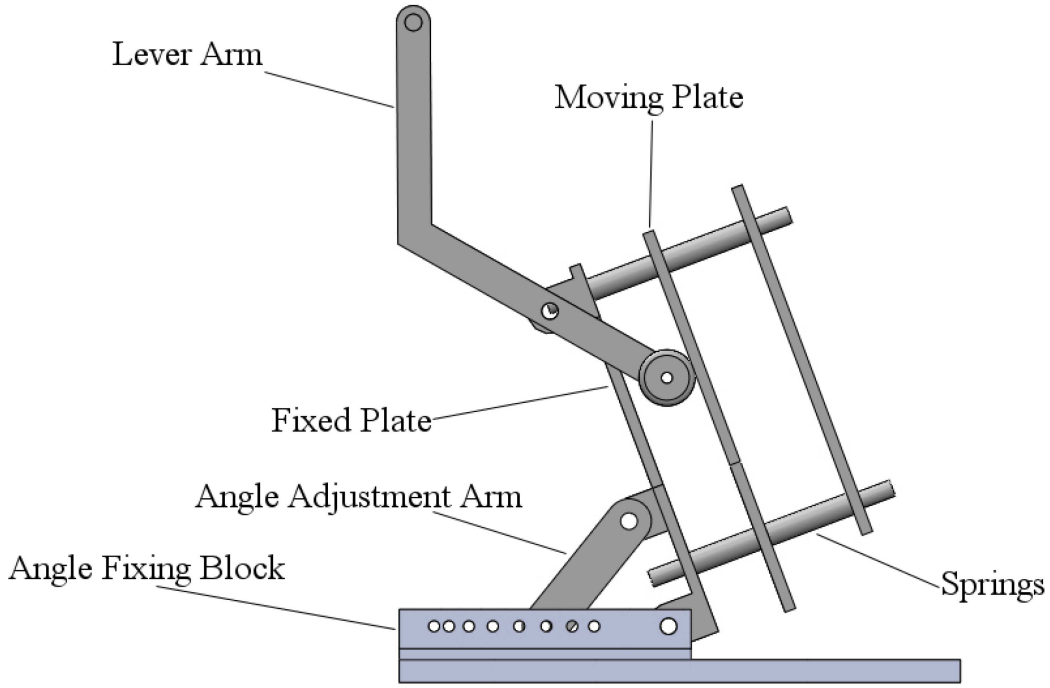

Figure 3.5: Designed Clamping Mechanism (Right View)

Manufacturing of the clamping mechanism and the ricochet box (sheet cutting, welding, milling and turning) is done in the main workshop of the Department of Mechanical Engineering, METU. Steel sheets of 10 mm thickness are used in general construction of the assembly and steel sheets of 2 mm thickness are used in the construction of the ricochet box. Manufactured clamping mechanism and ricochet box can be seen in Figures 3.7 and 3.8.

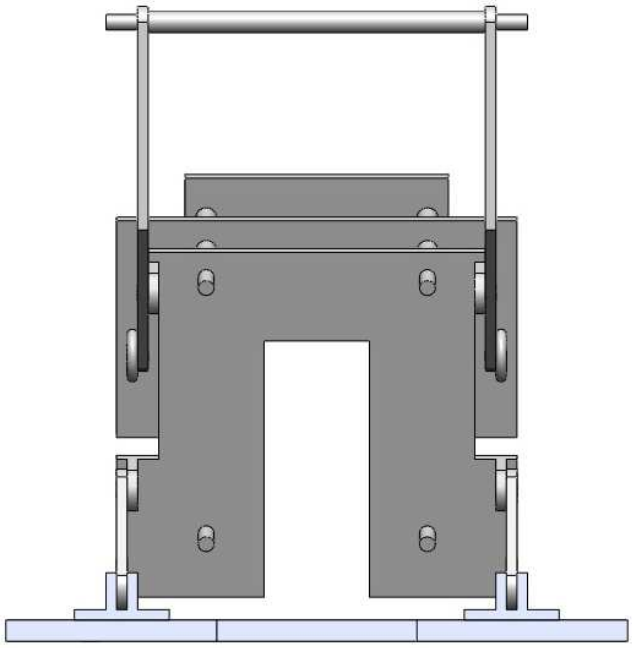

Figure 3.6: Designed Clamping Mechanism (Front View)

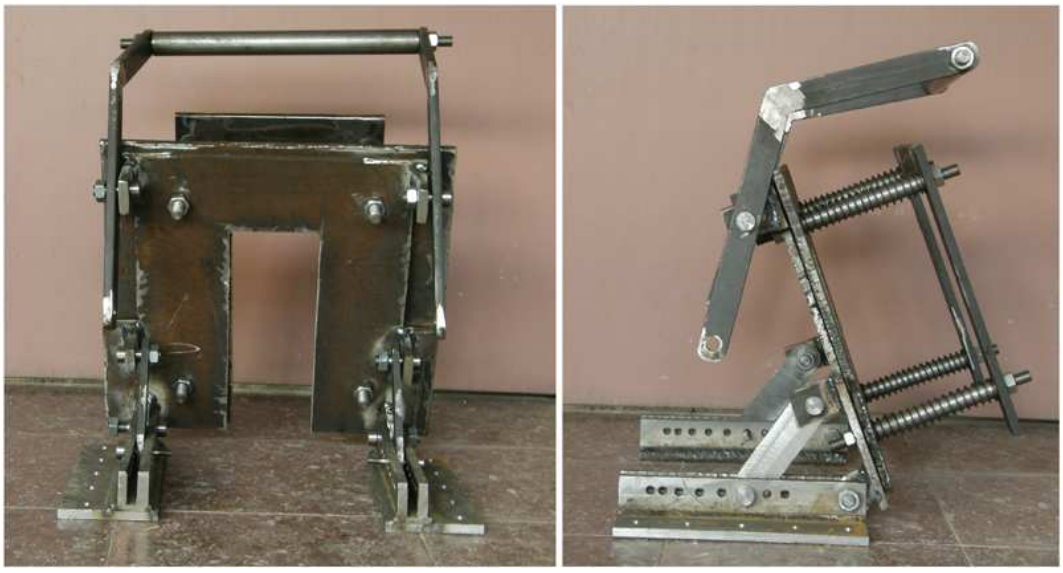

Figure 3.7: Manufactured Clamping Mechanism (Front and Right Views)

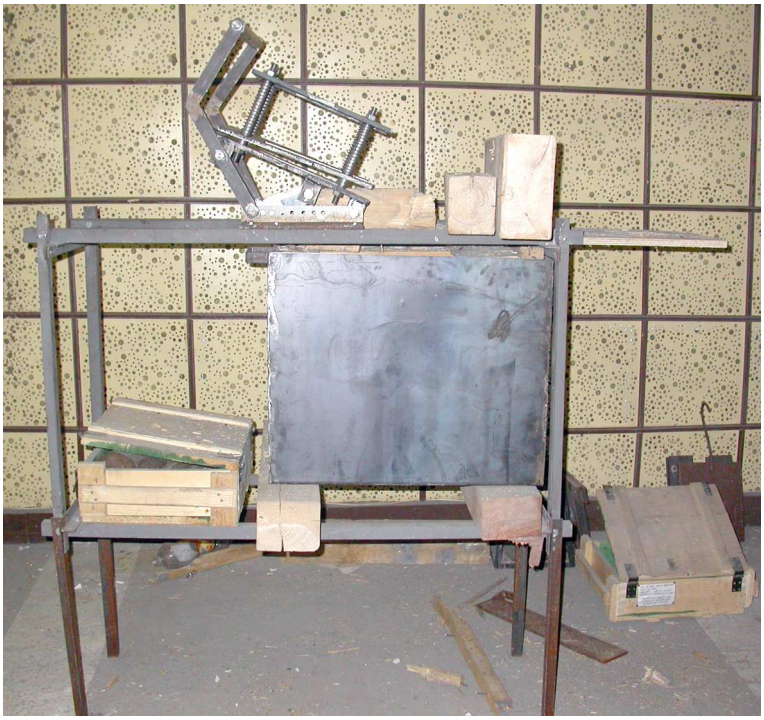

Figure 3.8: A View of the Ricochet Box

3.2 Target Materials

After a literature survey about the dynamic properties of the commercially available materials that can be purchased easily in sheet metal form, ST-37 steel is chosen for this thesis. Starting from 2 mm to 30 mm thicknesses (approximately 10 pieces of each thickness), 150 mm x 250 mm rectangular sheets of ST-37 are purchased from OSTİM. To check the mechanical properties of the plates, 2 tensile tests are conducted for each thickness in the Department of Metallurgical and Materials Engineering, METU. Results of these tests can be seen in Table 3.1.

3.3 Properties of 7.62 mm AP Bullet

The bullet used in the experimental analysis part of this thesis is a standard 7.62 x 51 mm AP (Armor Piercing) bullet (Figure 3.9). This bullet, having a hardened 100Cr6 (AISI E52100) steel core (see Table 3.2 for the nominal chemical composition), has been used in Turkish

Army with G1, G3 and MG3 rifles against armored targets. The core material of the bullet is hardened to 61 - 62 HRc with a yield strength of 2033 MPa for more effective perforation and penetration capabilities. Some specifications of the bullet are given in Table 3.3.

Table 3.1: Results of the Tensile Tests for the Target Plates

Nominal Plate Thickness [mm]	**Yield Strength** [MPa]	**Ultimate Tensile Strength** [MPa]
2	237	363
2	274	377
3	302	402
3	299	403
4	249	366
4	242	362
5	261	374
5	289	375
6	276	379
6	278	377
8	269	409
8	268	411
10	266	380
10	261	375
12	208	299
12	213	301
15	318	484
15	321	489
20	311	496
20	320	500
25	278	444
25	271	448
30	247	364
30	243	361

Table 3.2: Nominal Composition of 100Cr6 [26]

Element	**C**	**Mn**	**Cr**
Amount	1.00 %	0.35 %	1.50 %

Figure 3.9: 7.62 mm AP Bullet [26]

Table 3.3: Some Specifications of 7.62 mm AP Bullet [27]

Name	Value
Cartridge Length	71.12±0.76 mm
Cartridge Weight	25.47±1.75 g
Jacket Material	Brass (CuZn30)
Core Material	DIN 100Cr6 (61-62 HRc)
Bullet Length	32.95 mm
Bullet Weight	9.75±0.7 g
Nose Type	Conical (17 ° half conical angle)

3.4 Testing Procedure

Due to the limitations in the number of cartridges and target materials, it is decided to perform 3 shots for each impact case, i.e. a specified angle of attack and target thickness combination. A total of 94 ballistic tests are conducted each consisting of the following steps:

1. Labeling the target plate (shot number and aiming point)
2. Clamping the target plate to the clamping mechanism
3. Setting the angle of attack (if necessary)
4. Resetting the speed measurement device and leaving the ballistic tunnel (shooting)
5. Releasing the impacted target plate
6. Recording the impact speed and final condition of the plate

Tests are done for angle of attacks starting from 0° to 70° with 10° increments. First of all, the thickest target plate in hand (30 mm) is shot at 0° and at the same angle, the procedure continued trying a thinner plate until obtaining the thickest plate that is perforated at 0° angle of attack. Then the angle of attack is increased 10° and test procedure started again with the thickest plate perforated at the previous test, instead of the thickest plate in hand. After the thickest plate that is perforated and the thinnest plate that is not perforated are determined from 0° to 70°, for some selected angles (0°, 50° and 70°), layered plate combinations are tried. In these combinations, plates are in contact with each other by the help of the spring forces of the clamping mechanism. Definition of the angle of attack in this thesis can be seen in Figure 3.10. Results of the ballistic tests are presented in Section 3.5.

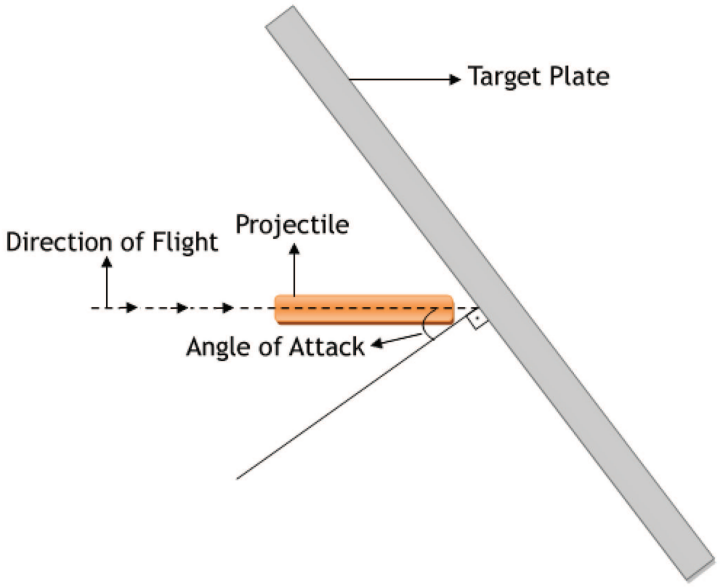

Figure 3.10: Angle of Attack Definition Used in This Thesis

3.5 Experimental Results

As explained in Section 3.4, 94 experimental shots are done by 7.62 mm AP bullets. After each shot, the post-impact conditions of the target plates are recorded as *Perforated* (P), *Stuck* (S) or *Ricocheted* (R). Results of the monolithic tests can be seen in Table 3.4 and the results of the layered tests can be seen in Table 3.5. Note that due to some problems during experiments, 4 of the 94 shots were unsuccessful. These shots are not mentioned in these tables.

While presenting the results of the monolithic plates, a designation system is used as shown in Figure 3.11. Also, in the *Result* column of the tables; *P* means the target plate is perforated, *S* means the bullet core is stuck into the target plate and *R* means the bullet core is ricocheted from the target plate or hit the target plate and fragmented.

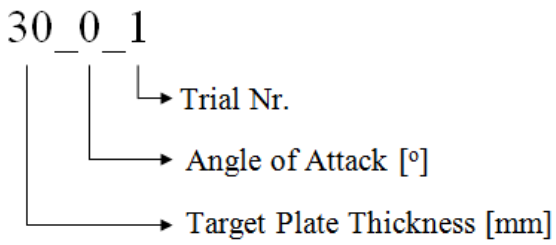

Figure 3.11: Explanation of the *Code* Column in Table 3.4

Table 3.4: Ballistic Test Results for Monolithic Case

Test Nr.	**Code**	**Thickness** [mm]	**Angle** [$^\circ$]	**Trial Nr.**	**Impact Speed** [m/s]	**Result**
1	30_0_1	30	0	1	815.0	R
2	30_0_2	30	0	2	-	R
3	30_0_3	30	0	3	-	R
4	25_0_1	25	0	1	794.0	S
5	25_0_2	25	0	2	809.5	S
6	25_0_3	25	0	3	810.6	S
7	20_0_1	20	0	1	794.4	P
8	20_0_2	20	0	2	-	S
9	20_0_3	20	0	3	796.0	P
10	15_0_1	15	0	1	805.0	P
11	15_0_2	15	0	2	793.5	P
12	15_0_3	15	0	3	806.8	P
13	15_10_1	15	10	1	793.1	P
14	15_10_2	15	10	2	797.9	P
15	15_10_3	15	10	3	-	P

Table 3.4 – continued

Test Nr.	Code	Thickness [mm]	Angle [$^\circ$]	Trial Nr.	Impact Speed [m/s]	Result
16	20_10_1	20	10	1	-	P
17	20_10_2	20	10	2	791.3	R
18	20_10_3	20	10	3	-	P
19	20_10_4	20	10	4	-	R
20	15_20_1	15	20	1	-	P
21	15_20_2	15	20	2	803.9	P
22	15_20_3	15	20	3	803.2	P
23	20_20_1	20	20	1	-	S
24	20_20_2	20	20	2	806.7	S
25	20_20_3	20	20	3	812.0	R
26	20_30_1	20	30	1	802.0	R
27	20_30_2	20	30	2	812.0	S
28	20_30_3	20	30	3	801.0	R
29	15_30_1	15	30	1	811.0	S
30	15_30_2	15	30	2	805.0	S
31	15_30_3	15	30	3	794.0	S
32	12_30_1	12	30	1	810.0	P
33	12_30_2	12	30	2	-	P
34	12_30_3	12	30	3	799.0	P
35	12_40_1	12	40	1	817.0	P
36	12_40_2	12	40	2	811.0	R
37	12_40_3	12	40	3	820.0	R
38	10_40_1	10	40	1	818.0	R
39	10_40_2	10	40	2	807.0	R
40	10_40_3	10	40	3	815.0	P
41	8_40_1	8	40	1	815.0	P
42	8_40_2	8	40	2	811.0	R
43	8_40_3	8	40	3	808.0	R
44	6_40_1	6	40	1	825.0	P

Table 3.4 – continued

Test Nr.	Code	Thickness [mm]	Angle [$^\circ$]	Trial Nr.	Impact Speed [m/s]	Result
45	6_40_2	6	40	2	818.0	P
46	6_40_3	6	40	3	817.0	P
47	8_50_1	8	50	1	819.0	R
48	8_50_2	8	50	2	813.0	P
49	8_50_3	8	50	3	817.0	P
50	10_50_1	10	50	1	817.4	R
51	10_50_2	10	50	2	835.4	R
52	10_50_3	10	50	3	815.0	R
53	6_50_1	6	50	1	816.3	P
54	6_50_2	6	50	2	811.4	P
55	6_50_3	6	50	3	822.1	P
56	6_60_1	6	60	1	813.1	P
57	6_60_2	6	60	2	811.0	P
58	6_60_3	6	60	3	816.3	P
59	8_60_1	8	60	1	811.4	R
60	8_60_2	8	60	2	815.7	R
61	8_60_3	8	60	3	826.0	R
62	6_70_1	6	70	1	816.7	R
63	6_70_2	6	70	2	816.7	R
64	6_70_3	6	70	3	818.8	R
65	4_70_1	4	70	1	819.8	P
66	4_70_2	4	70	2	825.7	P
67	5_70_1	5	70	1	818.0	R
68	5_70_2	5	70	2	828.7	R
69	5_70_3	5	70	3	822.7	R

Table 3.5: Ballistic Test Results for Layered Case

Test Nr.	**Thickness** [mm]	**Angle** [$^\circ$]	**Trial Nr.**	**Impact Speed** [m/s]	**Result**
70	6+12	0	1	811.0	P
71	8+12	0	1	-	P
72	8+12	0	2	821.0	P
73	8+12	0	3	821.0	P
74	10+12	0	1	-	P
75	10+12	0	2	815.0	P
76	10+12	0	3	815.0	P
77	12+12	0	1	-	P
78	12+12	0	2	814.0	P
79	12+12	0	3	814.0	P
81	3+3	70	1	811.0	R
82	3+3	70	2	812.0	R
83	3+3	70	3	819.0	R
84	2+3	70	1	813.0	P
85	2+3	70	2	818.0	P
86	2+3	70	3	798.0	Front: P
87	5+5	50	1	811.0	Front: P
88	5+5	50	2	813.0	P
90	5+5	50	4	817.0	Front: P, Back: S
93	4+5	50	1	811.3	P
94	4+5	50	2	824.3	P

Since 3 shots are conducted for each angle of attack - plate thickness combination, it can be said that the plate *fails* if the it is perforated in at least 2 of the 3 shots at an angle of attack. Otherwise, the plate can be named as *successful*.

Front and back views of some selected plates after impact can be seen in Figures 3.12-3.27 for the monolithic case and in Figures 3.28-3.37 for the layered case. Note that the plates are numbered according to the *Test Nr.* in Tables 3.4 and 3.5. In layered plate combinations, plates designated as *A* are the front plates and the plates designated as *B* are the rear plates.

In Figure 3.12, it can be seen that the bullet has penetrated and stuck into the 25 mm plate at normal impact condition. Tip of the bullet is clearly visible in the back view. In Figure 3.13, however, bullet has perforated the 20 mm plate. Failure type seems to be the *Ductile Hole Growth* in this case (see Figure 2.10).

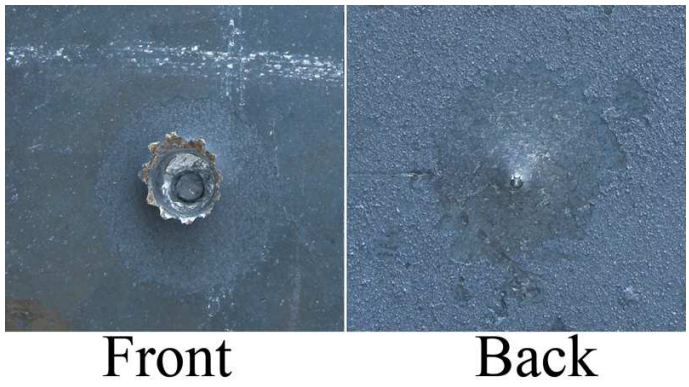

Figure 3.12: Front and Back Views of Test Nr. 6

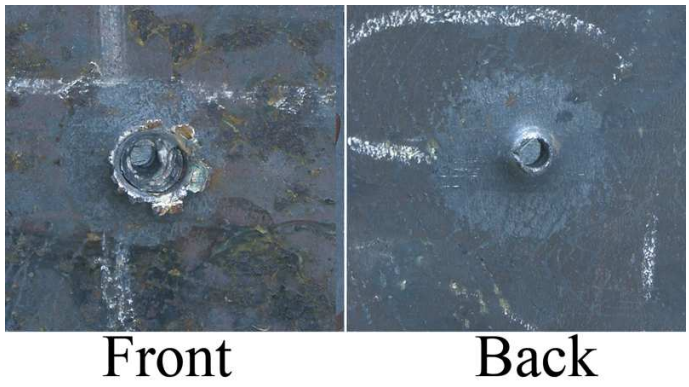

Figure 3.13: Front and Back Views of Test Nr. 7

When Figure 3.14 is investigated, we can say that the bullet was unsuccessful in perforating the 20 mm plate at 10 ° angle of attack while it perforates the 15 mm as in Figure 3.15. Again the failure is in the *Ductile Hole Growth* form.

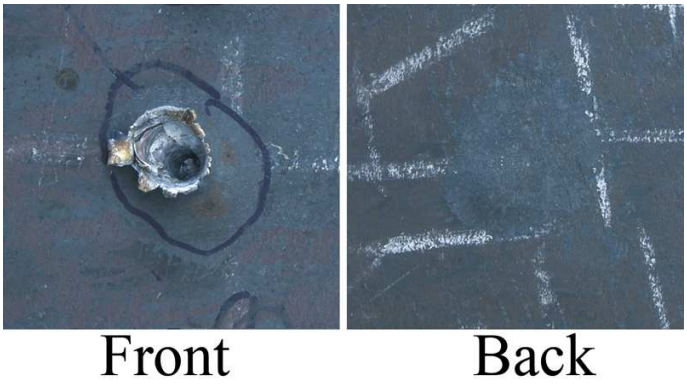

Figure 3.14: Front and Back Views of Test Nr. 17

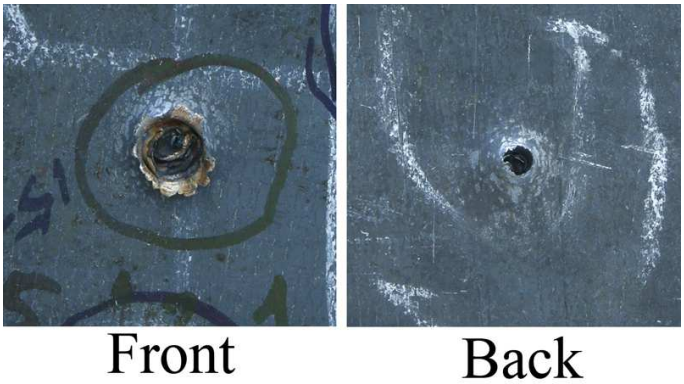

Figure 3.15: Front and Back Views of Test Nr. 13

When it comes to 20° angle of attack, thicknesses of the not-perforated (Figure 3.16) and perforated (Figure 3.17) plates are the same as 10°.

In 30° angle of attack - 15 mm plate thickness combinations, tips of the two bullets can be clearly seen on the back surface (Figure 3.18, shot numbers 30 and 31). This shows that the kinetic energy of the bullets have been consumed when they are almost completing the perforation. Such a behavior is very close to the *Ballistic Limit Thickness* [18] of the plate at 30° angle of attack. High deviation from the initial angle of attack is also visible when the tip directions of both bullets are examined.

Figure 3.16: Front and Back Views of Test Nr. 23

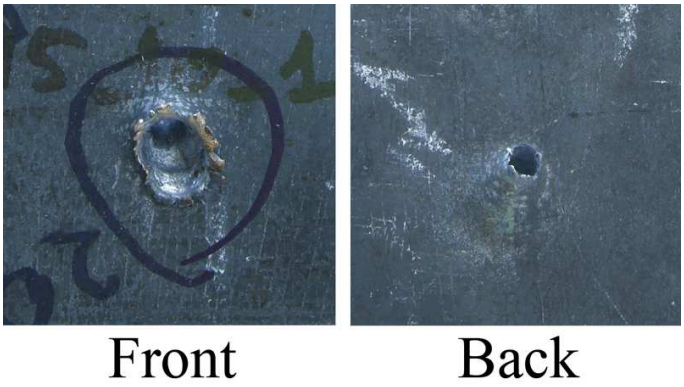

Figure 3.17: Front and Back Views of Test Nr. 20

As it can be seen in Figure 3.20, bullet ricocheted after causing a small tear in the back side of the 8 mm thick impacted target plate at 40° angle of attack. In the 6 mm plate (Figure 3.21), however, a clear *Petaling* type failure can be witnessed.

When the angle of attack is increased to 50°, an increase in the minimum perforated plate thickness occurred and 8 mm plates are perforated by the bullets (Figure 3.23), contrary to the 40° angle of attack case. At the same angle of attack (i.e. 50°), 10 mm plates cause the ricochet of all three bullets in test numbers 50 (Figure 3.22),51 and 52.

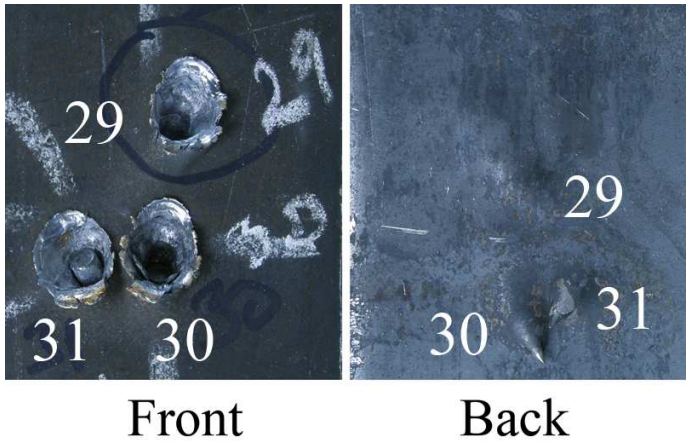

Figure 3.18: Front and Back Views of Test Nr. 29, 30 & 31

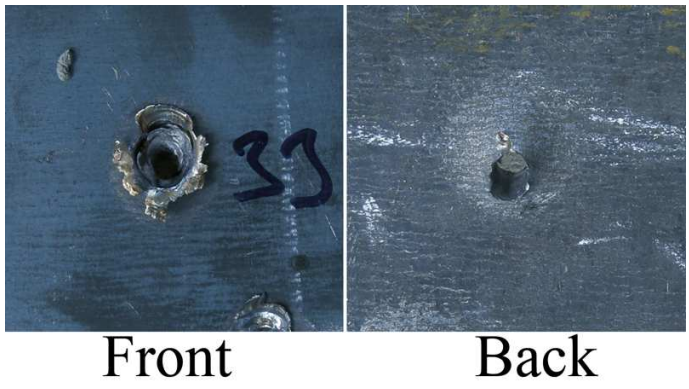

Figure 3.19: Front and Back Views of Test Nr. 33

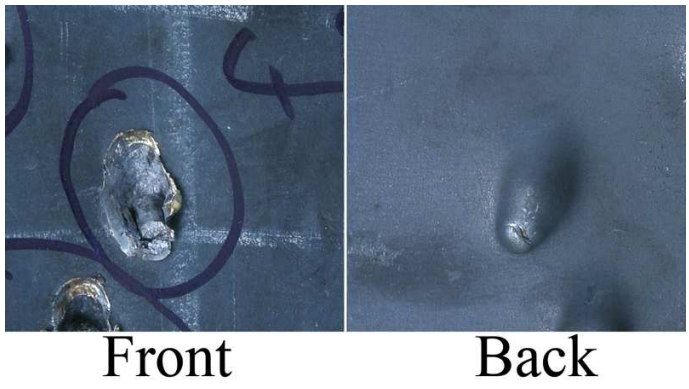

Figure 3.20: Front and Back Views of Test Nr. 42

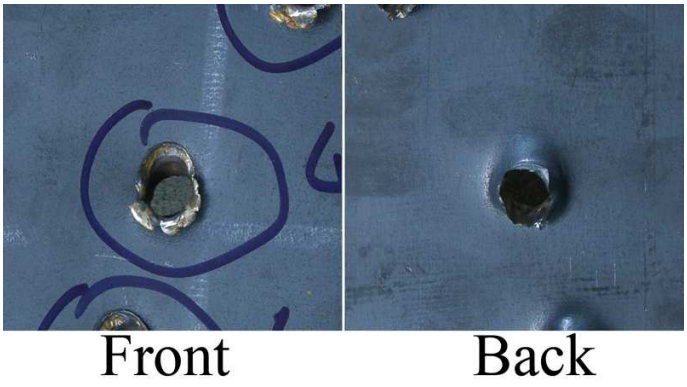

Figure 3.21: Front and Back Views of Test Nr. 45

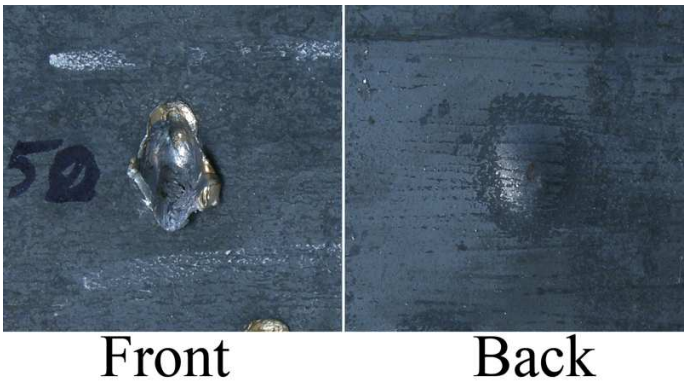

Figure 3.22: Front and Back Views of Test Nr. 50

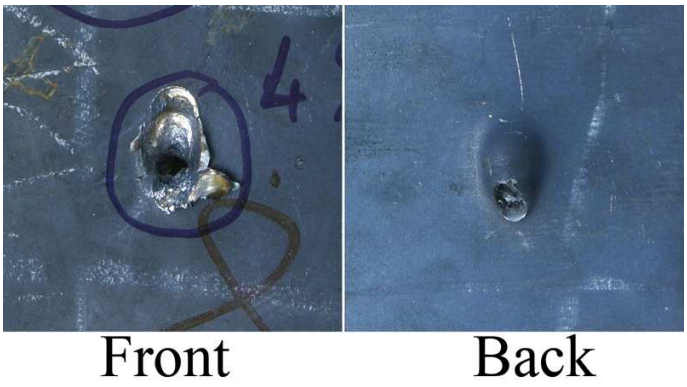

Figure 3.23: Front and Back Views of Test Nr. 49

Same as 40° angle of attack tests, 6 mm plates are perforated (Figure 3.25) and 8 mm plates are not perforated (Figure 3.24) in 60°. At this angle of attack, *Petaling* occurred in all the

perforated plates and ricochet occurred in the not-perforated ones.

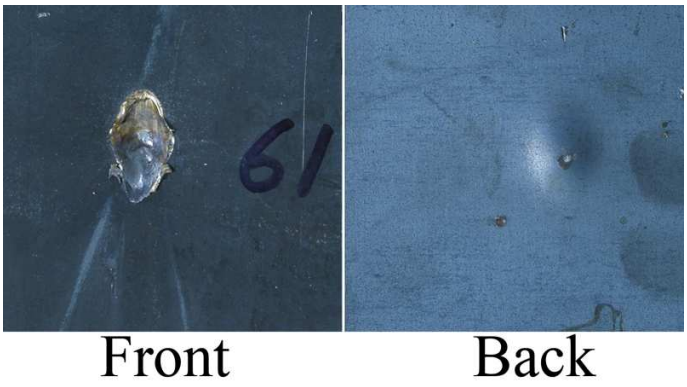

Figure 3.24: Front and Back Views of Test Nr. 61

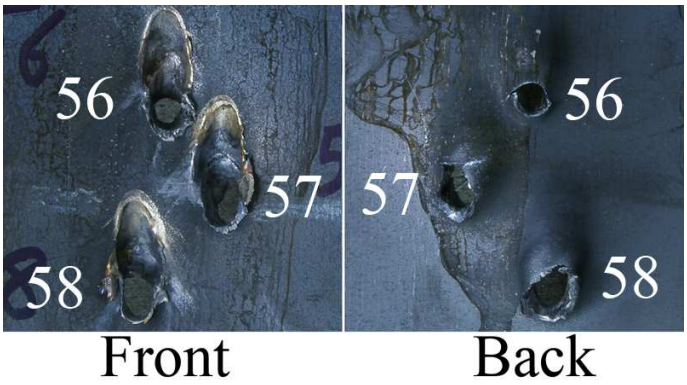

Figure 3.25: Front and Back Views of Test Nr. 56, 57 & 58

For the last case of the monolithic plate studies, plates are tested at 70 ° angle of attack. As it can be seen in Figures 3.26 and 3.27, 5 mm plates successfully ricochets the bullets while the 4 mm ones are perforated in all tests. Type of failure is again *Petaling* at this angle of attack.

After all the tests for the monolithic plates, layered plate combinations for three angles of attack are also tested. First of all, at 0 °, both the front (Figure 3.28) and back (Figure 3.29) plates are perforated for 12 mm + 12 mm layered plate thickness combination.

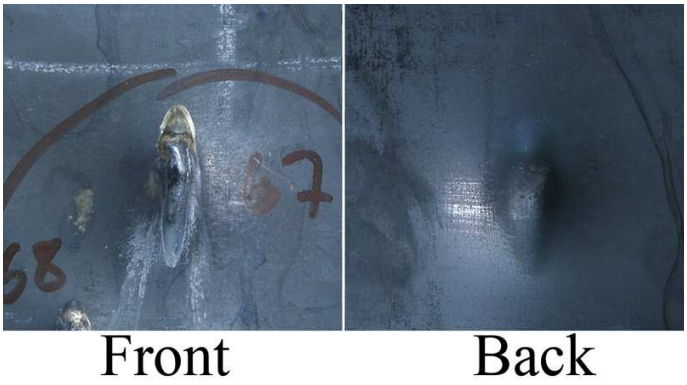

Figure 3.26: Front and Back Views of Test Nr. 67

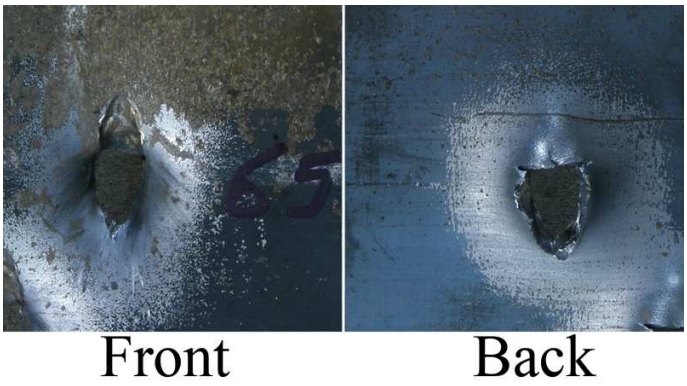

Figure 3.27: Front and Back Views of Test Nr. 65

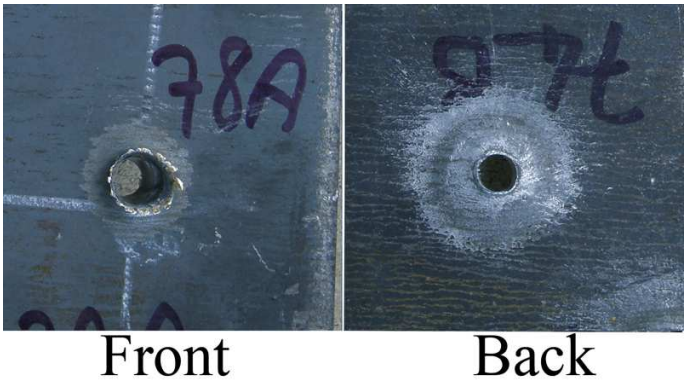

Figure 3.28: Front and Back Views of Test Nr. 78A

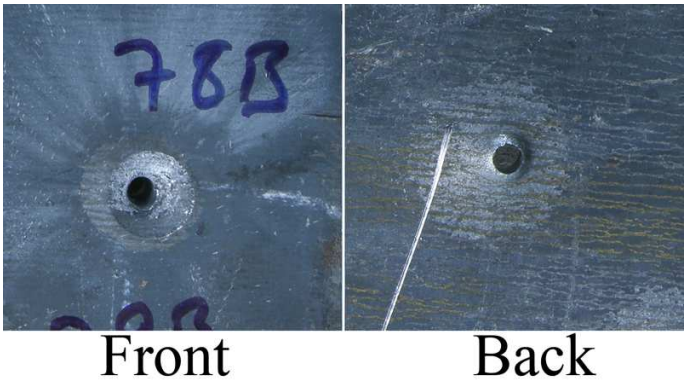

Figure 3.29: Front and Back Views of Test Nr. 78B

In 70 ° angle of attack - 3mm + 3mm plate thickness combinations, the front plates are teared but the rear plates are not perforated (see Figures 3.30 and 3.31). Complete perforation occurs when the thickness of the front plates are decreased and a 2 mm + 3 mm combination is shot, although 5 mm monolithic plates are not perforated at the same angle of attack. Petaling failure in both the front and the rear plates are observed in these tests (Figures 3.32 and 3.33).

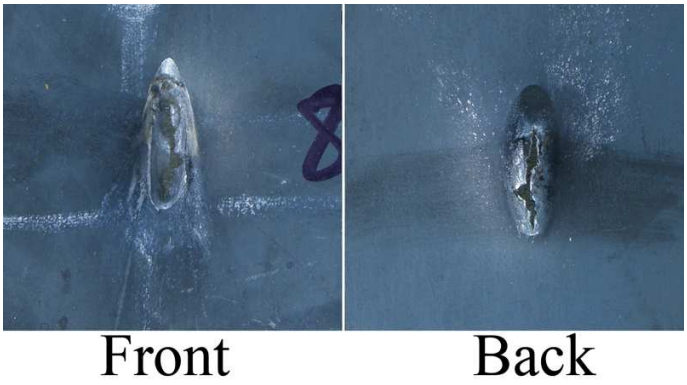

Figure 3.30: Front and Back Views of Test Nr. 82A

Last group of tests are conducted at 50 ° angle of attack. At this angle of attack, 8 mm plates are perforated and 10 mm plates are not perforated in monolithic plate tests. In layered plate tests, back plates of 5 mm + 5 mm combinations (Figures 3.34 and 3.35) successfully stopped the bullets while 4 mm + 5 mm combinations (Figures 3.36 and 3.37) are perforated.

Figure 3.31: Front and Back Views of Test Nr. 82B

Figure 3.32: Front and Back Views of Test Nr. 84A

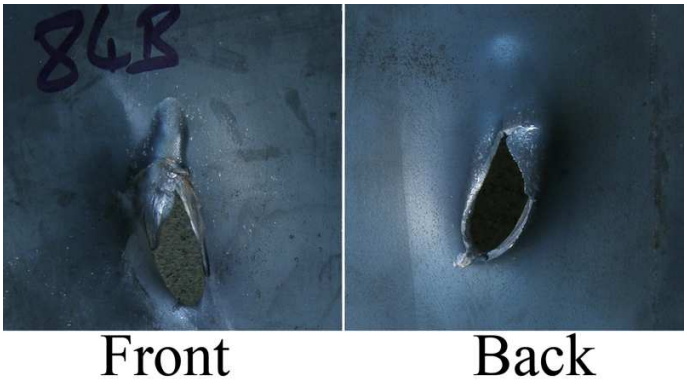

Figure 3.33: Front and Back Views of Test Nr. 84B

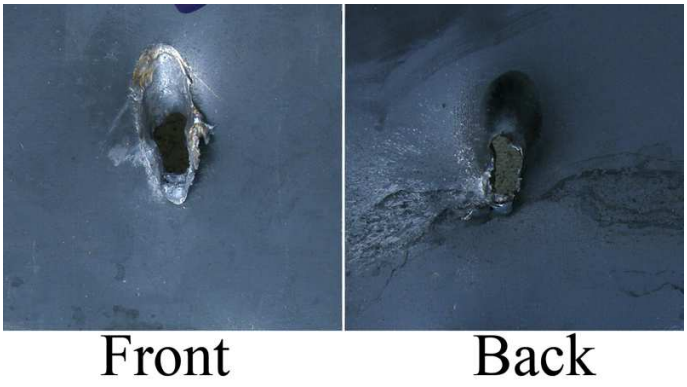

Figure 3.34: Front and Back Views of Test Nr. 90A

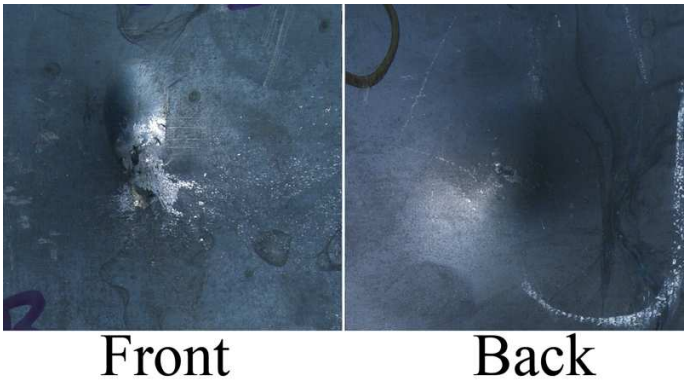

Figure 3.35: Front and Back Views of Test Nr. 90B

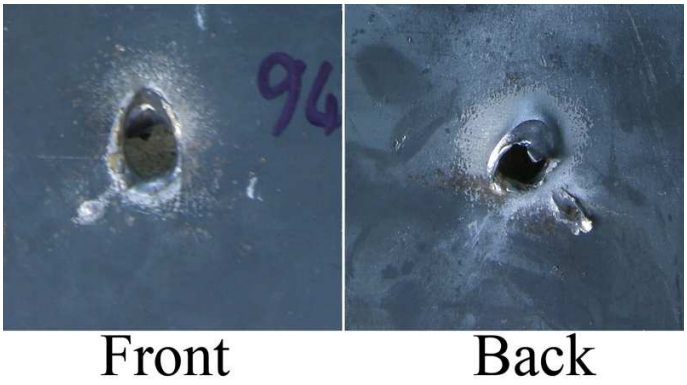

Figure 3.36: Front and Back Views of Test Nr. 94A

Figure 3.37: Front and Back Views of Test Nr. 94B

A summary of the thickest perforated and the thinnest not-perforated plate thicknesses for each angle of attack can be seen in Figure 3.38 for the monolithic plate studies.

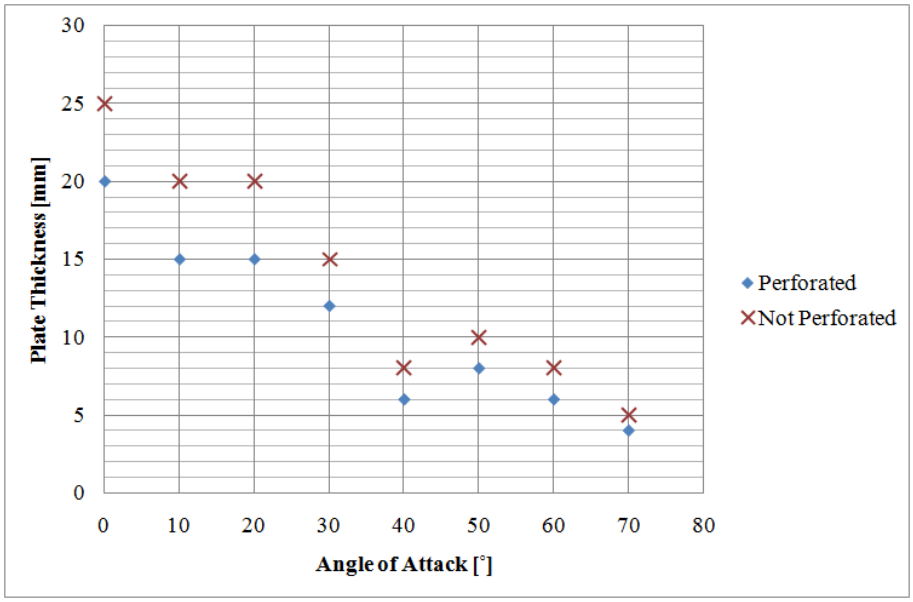

Figure 3.38: Summary of the Experimental Work for Monolithic Plates

Note that at 40 ° angle of attack, due to some reason (most probably an experimental error), results do not agree with the general trend. Especially the increase in the perforated plate thicknesses at 50 ° proves that. A possible reason of this fact is the missetting of the clamping mechanism to 60 ° instead of 40 °. Therefore this data is omitted.

To make a meaningful comparison about the effect of obliquity on the effectiveness of an armor system, areal density of the system should be checked as explained in Section 2.7. The graph showing this comparison can be seen in Figure 3.39. In this figure, t_2 refers to the required thickness of the plate at an angle of attack so that its areal density is the same as a 25 mm plate with 0 ° angle of attack, i.e. the thinnest plate that provides protection under normal impact conditions.

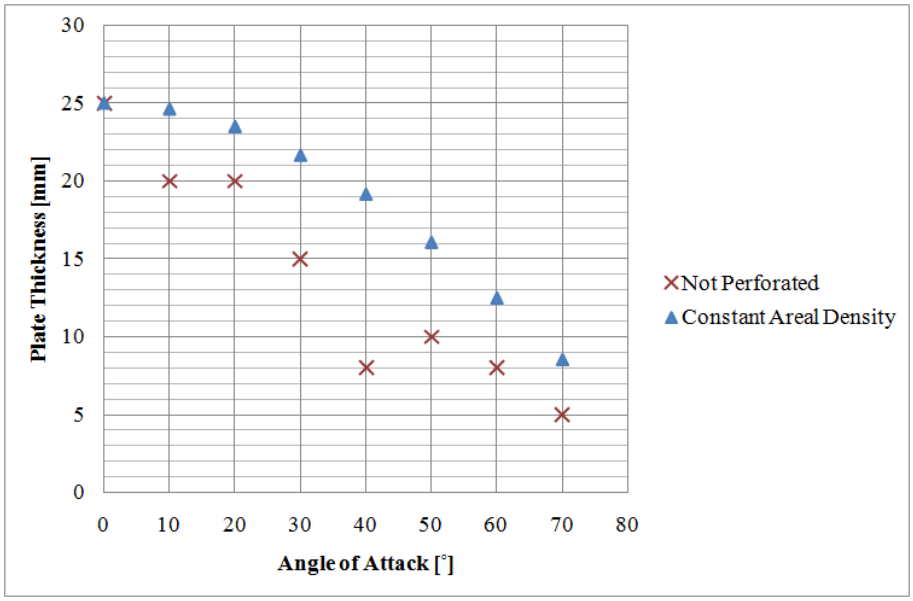

Figure 3.39: Comparison Graph of the Experimental Results According to Constant Areal Density

As a final effort, a straight line can be fitted to the experimental results. Excluding the data for 40 ° angle of attack and knowing that at 90 ° angle of attack the plate thickness approaches to 0, a straight line is fitted to the experimental results and it is shown in Figure 3.40.

As shown in the figure, the straight line fitted to the data has an R^2 (coefficient of determination) value of 0.988. This value means that 98.8% of the experimental shots can be explained by the line fitted. The equation of the line is also shown in the same figure.

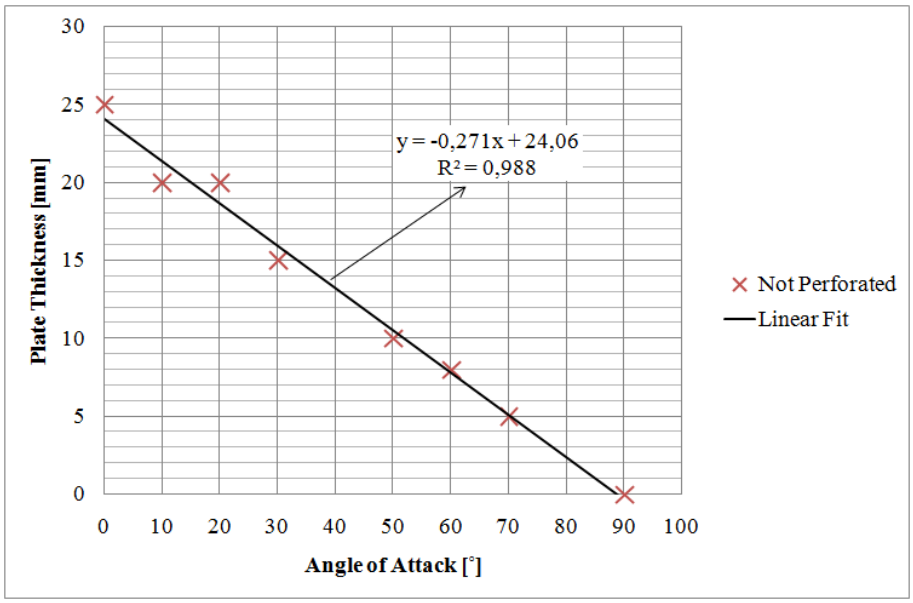

Figure 3.40: Linear Line Fitted to the Results of the Experiments

CHAPTER 4

NUMERICAL SIMULATION STUDIES

In this chapter, numerical modeling and simulation process of the experimental results (Section 3.5) are presented.

4.1 Hydrocodes

In late 1950's at Los Alamos National Laboratory, a method called *particle-in-cell* (PIC) is developed. When Robert Bjork at Rand Corporation applied this method to the problem of steel impacting steel and aluminum impacting aluminum at velocities of 5.5, 20 and 72 km/s, the first numerical investigation of high strain rate impact problem cited in literature is conducted. Since at such high velocities of approach, impacting materials create very high pressures on each other, i.e. exceeding their strength by several orders of magnitude, the method did not include the material strength in calculations, assuming a hydrodynamic behavior. Although contemporary hydrocodes employ quite successful material models, the term *hydrocode* originates from the hydrodynamic behavior assumption of the first numerical investigation studies [28].

For the numerical simulation studies of this thesis, ANSYS AUTODYN, embedded in ANSYS Workbench v.12 environment is used. AUTODYN is an explicit non-linear commercial hydrocode software package which was first introduced by Century Dynamics in 1986. It uses the techniques of finite element, finite volume and finite difference to solve non-linear solid, fluid and gas dynamics problems. The most appropriate numerical technique for the domain of the problem, e.g. structures, fluids, gases etc. is employed to obtain an optimum numerical solution. The ability of coupling these techniques makes AUTODYN strong and

effective especially in solving interaction problems between different domains [29].

In AUTODYN, both time and space are discretized, i.e. divided into increments. Time is discretized into time-steps (Δt), each presenting a *cycle* while solving the problem. While selecting the time step for a cycle, AUTODYN calculates the local time step for all elements in the numerical grid and selects the minimum of them. Finally the time step is calculated by multiplying the minimum value with a safety factor (default safety factor is 2/3). As a minimum criteria, time step is selected by checking the CFL (Courant-Friedrichs-Lewy [30]) condition (Equation 4.1) [29]. Using CFL condition as the minimum condition of determining time step ensures that no wave (i.e. disturbance) will be able to travel through an element in a single cycle and the effect due to that wave will not be missed.

$$\Delta t \leq \frac{d}{c} \tag{4.1}$$

where;

Δt : Time step
d : Typical length of a mesh element
c : Local wave speed

Note that the parameter d in Equation 4.1 is calculated by dividing the volume of a mesh element by the square of the length of the longest diagonal in that element and scaling this value by $\sqrt{\frac{2}{3}}$ [29].

Space, on the other hand, is discretized by dividing the solution into grids and assigning an I, J and K index to each mesh element in the grid. Then the variables like initial condition, boundary condition or material parameters are imposed to the I, J, K index. Space can also be divided into subgrids. This division feature of AUTODYN allows the user to define a different solver, initial condition, material etc. for each subgrid resulting in a successful coupling of solvers and materials (e.g. liquid-solid and gas-solid interactions, blast effect on structures etc.) [29, 31, 32].

4.1.1 Lagrange Solver

In Lagrange solver, computation grid moves with the material, contrary to Euler grid which is commonly used in fluid mechanics problems. This solver is used generally for modeling of solid continua as in this thesis. A typical cycle of the Lagrange solver is as follows [33];

1. The nodal velocities are integrated in time leading to the new nodal positions
2. Using new nodal positions, new density of the cell and strain rate is obtained
3. Knowing the strains, stresses in the cell are calculated
4. Using the new stresses, nodal forces are calculated
5. Adding the external forces by interaction or boundary conditions, total nodal forces are calculated
6. Simply using the $F = m.a$ equation, nodal accelerations are obtained
7. By integrating the nodal accelerations, nodal velocities are calculated (Figure 4.1).

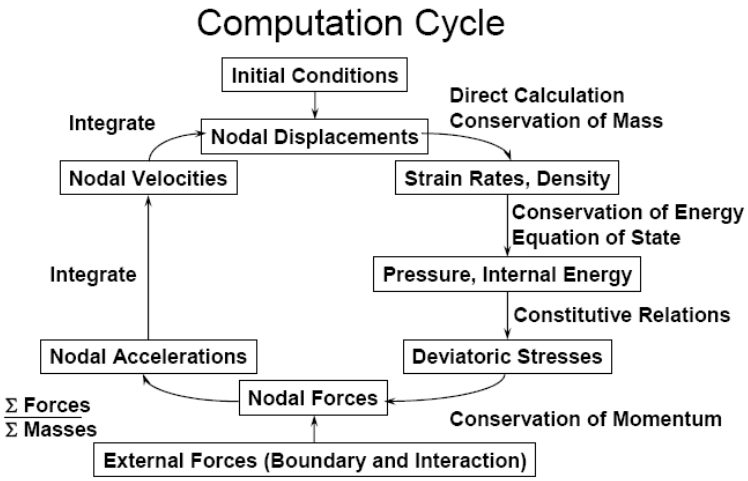

Figure 4.1: Lagrange Computation Cycle [33]

Since the mesh moves with the material, loading histories of materials are kept in each cell fixed to the material. This characteristic of the Lagrange solver provides the usage of special material models easier than the Euler solver.

4.1.2 Erosion Algorithm

Although Lagrange solver is ideal for the cases where there is low mesh distortion and large displacement, it can also be used for high strain rate solid-solid interaction problems where there are high deformations. For such an analysis, since the mesh moves with the material, excessive deformation on cells can cause inaccurate and inefficient results. Since the time step is calculated before every cycle in Lagrange solver, an extremely distorted element will lead to a very small time step. In such a case, simulation becomes extremely slow and may even stop. To prevent these, an algorithm called *erosion* is implemented.

In erosion algorithm, excessively distorted mesh elements (at a predefined strain value, determined by the user) are removed from the solution grid. Depending on the preference of the user, inertia of the eroded element can be kept as a free point mass interacting with the mesh. But whatever is done, internal energy and the compressive strength of the eroded element is lost. Although it is a non-physical process, erosion is generally used in the Lagrange solver where there are large deformations [29].

4.1.3 Johnson - Cook Constitutive Model

In high velocity impact problems, strain hardening, temperature softening and strain rate effects are quite important. To implement these effects into analysis, a complex constitutive model should be used. Since it is capable of modeling these effects, Johnson-Cook constitutive equation is selected while modeling the bullet core and the target plate materials for the numerical analysis part of this theses.

Johnson-Cook constitutive model is a purely empirical equation (Equation (4.2)) using the material data obtained by some high strain rate (e.g. Split Hopkinson Pressure Bar) tests. To include the temperature softening behavior of the material, tests are also conducted at a constant strain rate and different temperatures [35].

$$\sigma = [A + B\varepsilon^{n}][1 + C \ln \dot{\varepsilon}^{*}][1 - T^{*m}] \tag{4.2}$$

In Equation (4.2);

σ : Stress

A : Yield stress

B : Strain hardening constant

ε : Strain

n : Strain hardening exponent

C : Strain rate constant

$\dot{\varepsilon}^* = \frac{\dot{\varepsilon}}{\dot{\varepsilon}_0}$: Dimensionless plastic strain rate

$\dot{\varepsilon}$: Strain rate

$\dot{\varepsilon}_0$: Reference strain rate

$T^* = \frac{T-T_0}{T_m-T_0}$: Homologous temperature

T : Temperature

T_0 : Reference temperature

T_m : Melting temperature

In Johnson-Cook model (Equation (4.2)), first expression in brackets deals with the strain (work) hardening. This equation is the well-known Ludwik's Equation. The expression in second brackets takes the strain rate effect into account. Parameter C is obtained by using the results of high strain rate tests. Finally the expression in the last brackets in Equation (4.2) implements the temperature softening effect into material's strength characteristic.

4.1.4 Johnson - Cook Failure Model

Johnson-Cook failure model is also an empirical model based on the tests with several metallic materials. It implements the effects of temperature softening and strain rate hardening. The basic form of the model, using the damage accumulation, can be seen in Equation (4.3).

$$D = \sum \frac{\Delta\varepsilon}{\varepsilon_f} \tag{4.3}$$

where;

D: Damage

$\Delta\varepsilon$: Increment of equivalent plastic strain during 1 integration cycle

ε_f : Failure strain

Failure strain is defined as follows;

$$\varepsilon_f = [D_1 + D_2 \exp(D_3 \frac{\sigma_m}{\sigma})][1 + D_4 \ln \dot{\varepsilon}^*][1 + D_5 T^*] \tag{4.4}$$

where;

$D_1, \ldots, D_5$: Material constants

σ_m : Mean stress

σ : Stress

$\dot{\varepsilon}^* = \frac{\dot{\varepsilon}}{\dot{\varepsilon}_0}$: Dimensionless plastic strain rate

$T^* = \frac{T - T_0}{T_m - T_0}$: Homologous temperature

When D in Equation (4.3) becomes unity, failure occurs and the element is removed (eroded) from the computational grid [36].

4.2 Modeling of Target and Bullet Materials

As described in Section 3.3, 7.62 mm AP bullet is used for both experimental and numerical analysis parts of this thesis. This bullet consists of 3 layers of materials (Figure 4.2). The outmost layer is the jacket, made of brass. Inside the jacket, there is a thin layer of liner material, made of antimonial lead. The final part of the bullet, i.e. the core, is made of hardened steel (DIN 100Cr6).

Material properties of cartridge brass and antimonial lead are taken from previous works [26, 37] and presented in Tables 4.1 and 4.2, respectively. Von-Misses constitutive model is used for these materials. For the core material, material properties (Table 4.3), using Johnson-Cook constitutive model are taken from another work [31]. In this PhD Thesis, author used a wise estimation process to obtain the Johnson-Cook constitutive model parameters for hardened DIN 100Cr6 core material using the tensile test data given in [38]. Geometric modeling of the bullet (Figure 4.2) is also taken from the same work, i.e. [31].

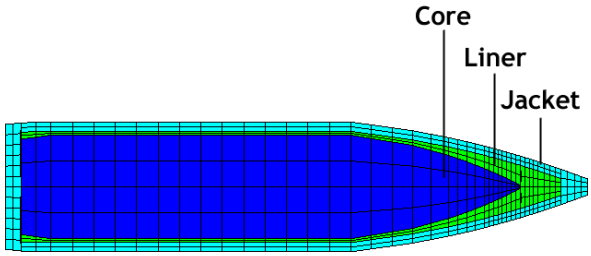

Figure 4.2: Section of 7.62 mm AP Bullet Used in Simulations

Table 4.1: Material Properties of Brass [26, 37]

Parameter	Value [Unit]
Reference Density	8530 $[kg/m^3]$
Bulk Modulus	117 $[GPa]$
Shear Modulus	38 $[GPa]$
Yield Stress	112 $[MPa]$

Table 4.2: Material Properties of Antimonial Lead [26, 37]

Parameter	Value [Unit]
Reference Density	10740 $[kg/m^3]$
Bulk Modulus	46 $[GPa]$
Shear Modulus	56 $[GPa]$
Yield Stress	20 $[MPa]$

Table 4.3: Material Properties of Hardened 100Cr6 [31]

Parameter	Value [Unit]
Reference Density	7853 $[kg/m^3]$
Bulk Modulus	169 $[GPa]$
Shear Modulus	80 $[GPa]$
Yield Stress (**A**)	2033 $[MPa]$
Strain Hardening Constant (**B**)	895 $[MPa]$
Strain Hardening Exponent (**n**)	0.3
Strain Rate Constant (**C**)	0.0095
Thermal Softening Exponent (**m**)	1.03
Melting Temperature	1793 $[K]$

As explained in Section 3.2, target plates (ST-37) have a range of yield strengths. To be more accurate, Johnson-Cook material model parameters are determined specifically for each plate thickness. Parameter A is the yield strength value of the material and it is directly taken from the tensile test results (Table 3.1). Strain hardening parts of the Johnson-Cook constitutive model (i.e. parameters B and n) are obtained by fitting curves to the resulting graphs of tensile tests for each plate thickness.

Strain rate coefficient and temperature softening exponent parameters (C and m, respectively) are still required for the analysis. Since determination of these parameters require special equipment and tests at high strain rates and different temperatures, these parameters should be taken from the literature. As the mechanical properties of the target materials are examined, it can be seen that these values are quite similar to AISI 1006 steel which has a yield strength of 285 MPa [34]. Therefore, C and m values of AISI 1006 steel [35] are used for the numerical simulations. As a result, Johnson-Cook constitutive model parameters are completely defined for each thickness and presented in Table 4.4.

Table 4.4: Johnson-Cook Constitutive Model Parameters for ST-37

Plate Thickness [mm]	**A** [MPa]	**B** [MPa]	**n**	**C**	**m**
25	278.45	188.00	0.0881	0.0220	1.0000
20	310.92	213.04	0.0888	0.0220	1.0000
15	319.24	206.56	0.1214	0.0220	1.0000
12	210.45	109.86	0.1272	0.0220	1.0000
10	263.51	130.05	0.0915	0.0220	1.0000
8	268.74	161.77	0.0888	0.0220	1.0000
6	277.03	125.47	0.1673	0.0220	1.0000
5	275.09	117.27	0.1127	0.0220	1.0000
4	245.92	142.70	0.1277	0.0220	1.0000
3	300.58	127.86	0.1577	0.0220	1.0000
2	255.98	162.58	0.2571	0.0220	1.0000

Johnson-Cook failure model is used while modeling the failure behaviors of target materials. Again, using the similarity between AISI 1006 and the target plates, failure model parameters of AISI 1006 steel [39] are used as presented in Table 4.5.

As mentioned earlier, model for the bullet is obtained from a previous work, [31]. Initial velocity of the bullet is set to the average of the three experimentally measured impact speeds

for that specific condition and applied to the bullets in -z direction.

Table 4.5: Johnson-Cook Failure Model Parameters for ST-37 [39]

Parameter	Value
Damage Parameter 1 ($\mathbf{D_1}$)	0.05
Damage Parameter 2 ($\mathbf{D_2}$)	3.44
Damage Parameter 3 ($\mathbf{D_3}$)	-2.12
Damage Parameter 4 ($\mathbf{D_4}$)	0.002
Damage Parameter 5 ($\mathbf{D_5}$)	0.61

While modeling the target plates, Lagrange solver is used. To be consistent with the bullet model, they are modeled as half-symmetric with respect to x-z plane (Figures 4.3 and 4.4).

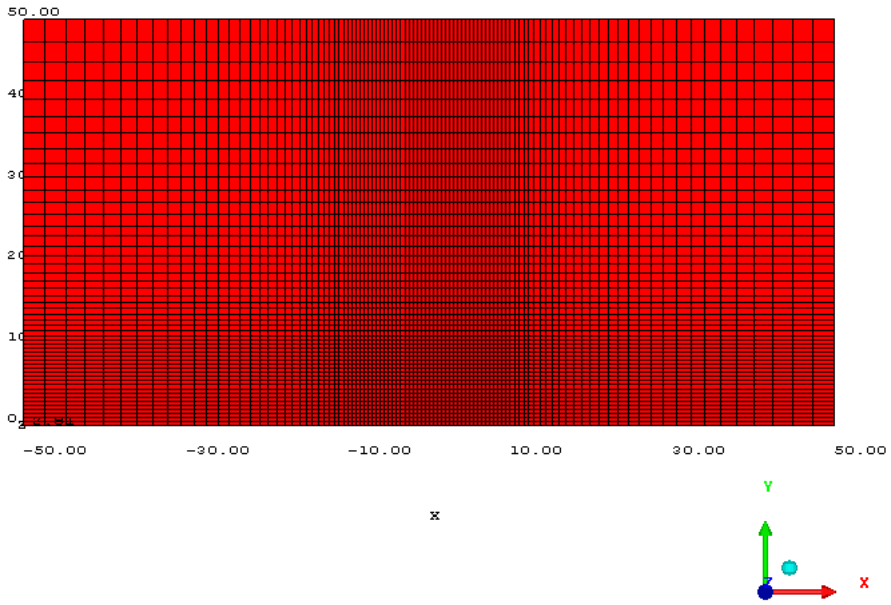

Figure 4.3: Front View of Target Plate

While meshing the target plates, nodes are set to be finer around the center of the plate, where the bullet hits. After meshing, boundary conditions are applied to the plates (Figure 4.5) in order to represent the clamping behavior of the experimental set-up.

After modeling the target material in front of the bullet (Figure 4.6), giving the necessary initial condition to the bullet and the necessary boundary condition to the plate, angle of attack is set by rotating the plate around y-axis and the analysis is started. One numerical analysis

is conducted for each *plate thickness - angle of attack* combination tested experimentally. Including layered plate combinations, list of all the numerical modeling work is presented in Table 4.6. After completing all the numerical simulations, results are presented in Section 4.3.

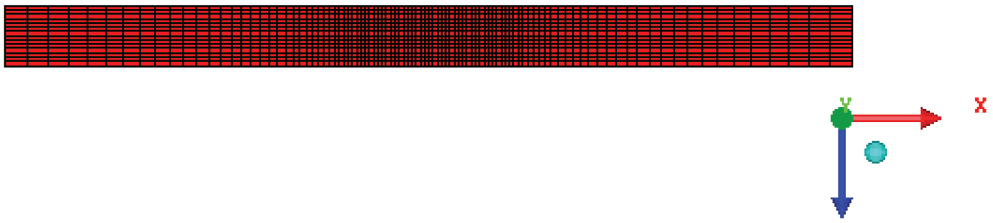

Figure 4.4: Section View of Target Plate

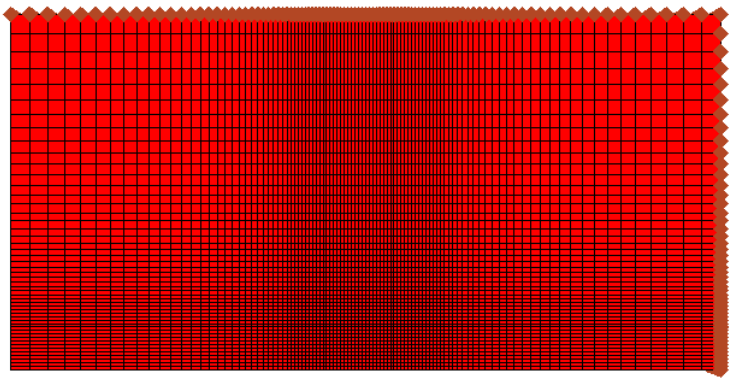

Figure 4.5: Boundary Conditions Around the Target Plate

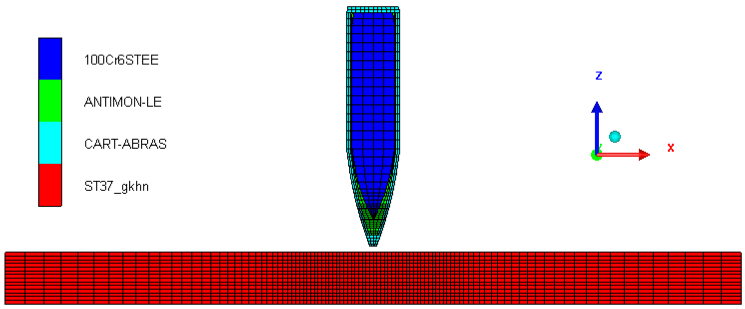

Figure 4.6: Model of Bullet and Target Plate

Table 4.6: List of Numerical Simulations for Experimental Tests

Angle of Attack [$^\circ$]	**Plate Thickness** [mm]	**Impact Speed** [m/s]
0	25	795
0	20	795
10	20	791
10	15	796
20	20	809
20	15	803
30	15	803
30	12	805
40	8	811
40	6	820
50	10	823
50	8	816
60	8	817
60	6	813
70	5	823
70	4	823
0	12+12	814
50	5+5	814
50	4+5	818
70	3+3	814
70	2+3	810

4.3 Results of the Numerical Simulation Studies for Selected Samples

After obtaining the Johnson-Cook constitutive and failure models for the target plate materials by using a combination of literature survey and tensile test results, computer simulations are conducted using ANSYS AUTODYN embedded in ANSYS Workbench v.12 environment. Summary of the numerical results can be seen in Table 4.7. Note that in the *Simulation Result* column of this table, as in Section 3.5, *P* means the target plate is perforated, *S* means the bullet core is stuck into the target plate, *R* means the bullet core is ricocheted from the target plate or hit the target plate and fragmented.

Results of each numerical simulation are presented in Figures 4.8 - 4.48. In these figures, each color symbolizes a different material as shown in Figure 4.7.

Table 4.7: Summary of Numerical Simulation Results

Angle of Attack [$^\circ$]	**Plate Thickness** [mm]	**Simulation Result**
0	25	S
0	20	P
10	20	S
10	15	P
20	20	S
20	15	P
30	20	S
30	15	P
30	12	P
40	15	S
40	12	P
40	10	P
40	8	P
40	6	P
50	15	S
50	12	P
50	10	P
50	8	P
60	8	R
60	6	P
70	5	R
70	4	R
0	12+12	P
50	5+5	P
50	4+5	P
70	3+3	R
70	2+3	Front: P

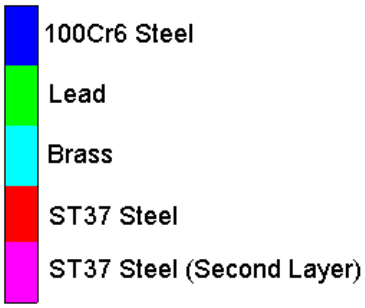

Figure 4.7: Materials Corresponding to Each Color

4.3.1 Monolithic Plates Impacted by 7.62 mm AP Bullets

First of all, numerical simulations of the experimental shots conducted for monolithic plates are done. Results of these simulations are presented in this subsection starting from 0 ° to 70 ° angles of attack.

In Figures 4.8 and 4.9, it can be seen that under normal impact conditions, the bullet perforates 20 mm target plate and stuck into 25 mm where the tip of the bullet is almost out of the target plate when all its kinetic energy is consumed during penetration (Figure 4.10). The bullet perforating 20 mm plate, however, still has 110m/s residual velocity in -z direction (Figure 4.11).

Figure 4.8: Simulation Result of the 20 mm Plate Impacted by the Bullet at 0 °

Figure 4.9: Simulation Result of the 25 mm Plate Impacted by the Bullet at 0 °

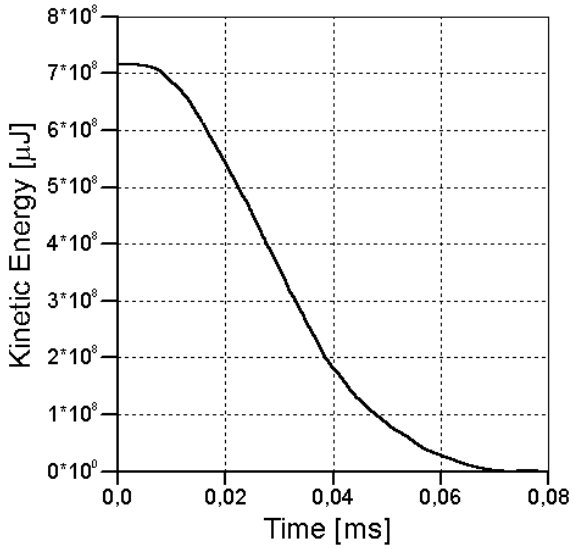

Figure 4.10: Kinetic Energy Plot of the Bullet Core During Impact to 25 mm Plate at 0 °

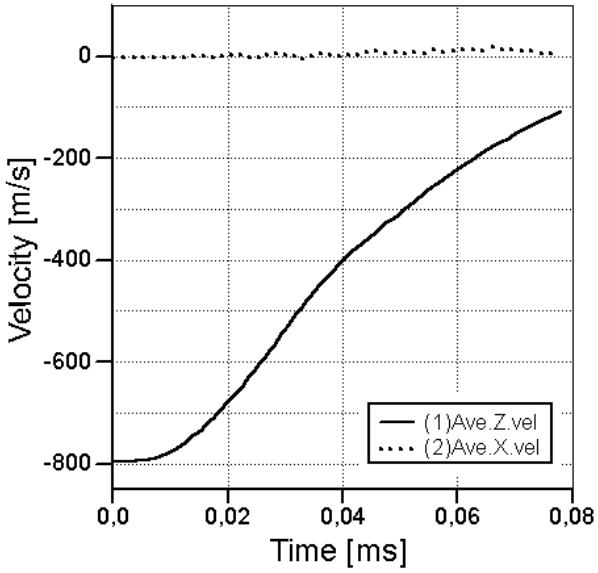

Figure 4.11: Average Velocity of the Bullet Core During Impact to 20 mm Plate at 0 °

At 10 ° angle of attack, 7.62 mm AP bullet perforates 15 mm monolithic plate (Figure 4.12) while it is stuck into the 20 mm one. As in 0 ° angle of attack - 25 mm plate thickness combination, tip of the bullet core is emerging from the back of the target plate at the end of the penetration process (Figure 4.13). The bullet perforating 15 mm plate has a residual velocity of $395 m/s$ in -z direction (Figure 4.14). In -x direction, on the other hand, there is

not a big change in the velocity of the bullet core meaning that the bullet did not deflected significantly from its direction of motion before impact and perforation.

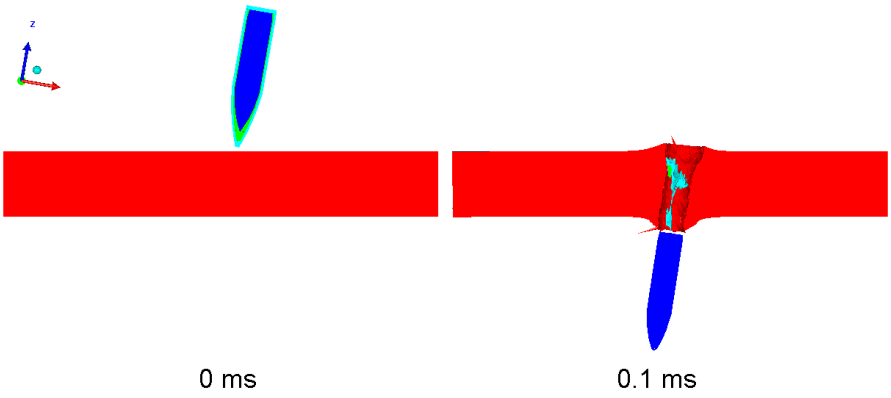

Figure 4.12: Simulation Result of the 15 mm Plate Impacted by the Bullet at 10°

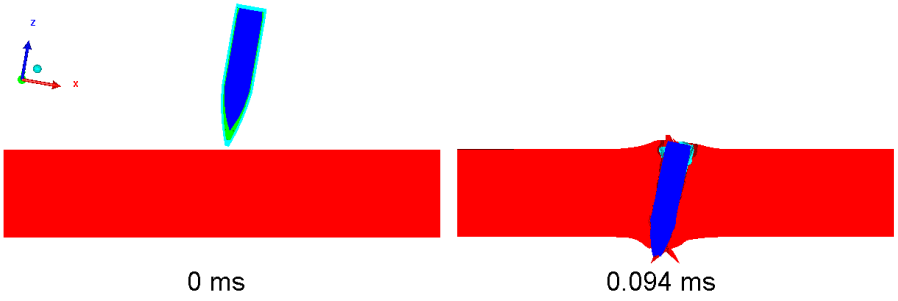

Figure 4.13: Simulation Result of the 20 mm Plate Impacted by the Bullet at 10°

When the same plate thicknesses are simulated at 20° angle of attack (Figures 4.15 and 4.16), almost the same results are obtained as in 10° angle of attack case except from the residual velocity of the bullet core (in -z direction) after perforation 15 mm plate which is around $345 m/s$ in this case (Figure 4.17). Again, there is no significant deflection in the original direction of flight of the bullet after perforation 15 mm target plate.

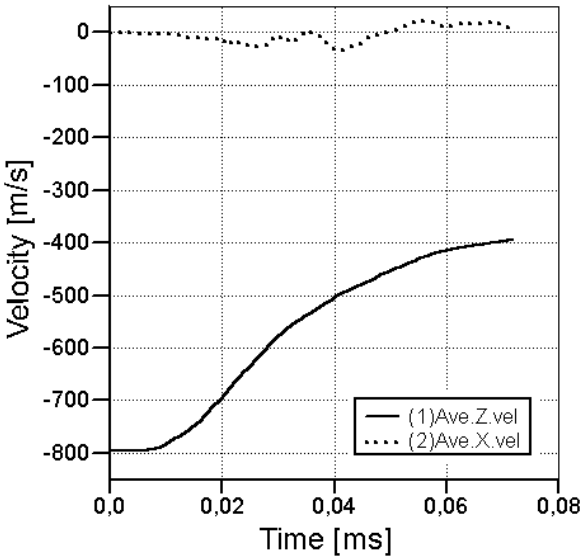

Figure 4.14: Average Velocity of the Bullet Core During Impact to 15 mm Plate at 10°

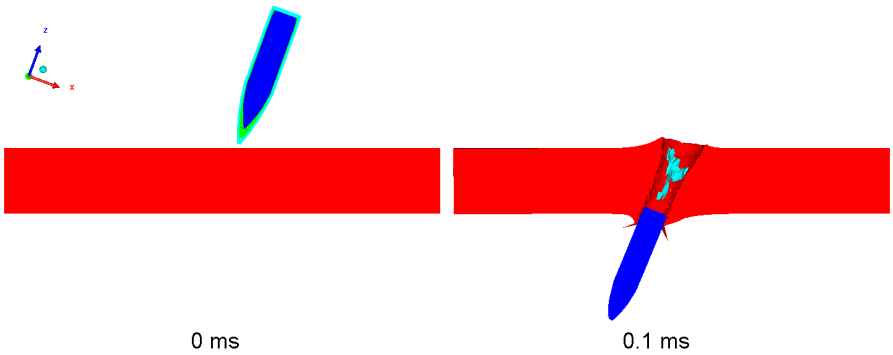

Figure 4.15: Simulation Result of the 15 mm Plate Impacted by the Bullet at 20°

Figure 4.16: Simulation Result of the 20 mm Plate Impacted by the Bullet at 20°

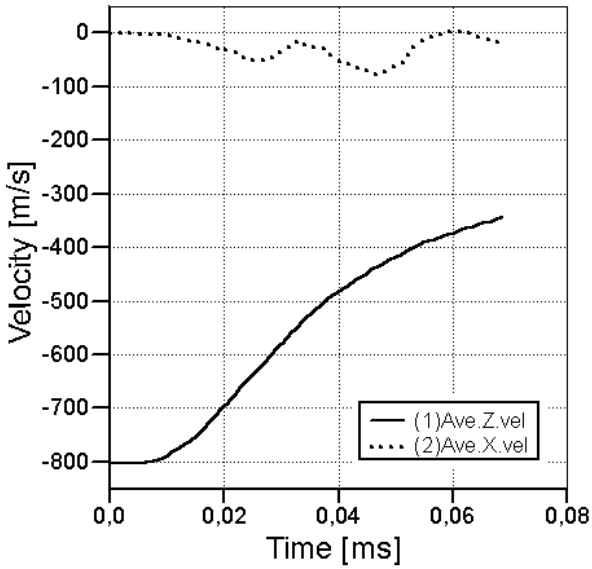

Figure 4.17: Average Velocity of the Bullet Core During Impact to 15 mm Plate at 20°

As a result of the simulations of a 7.62 mm AP bullet impacting 15 mm (Figure 4.18) and 12 mm (Figure 4.19) ST-37 plates, it is seen that both of the target plates are perforated at 30° angle of attack. During perforation of 15 mm target plate, 95.8% of the initial kinetic energy of the bullet core is consumed (Figure 4.20) while the kinetic energy loss is 35.6% for 12 mm plate perforated at the same angle of attack (Figure 4.21).

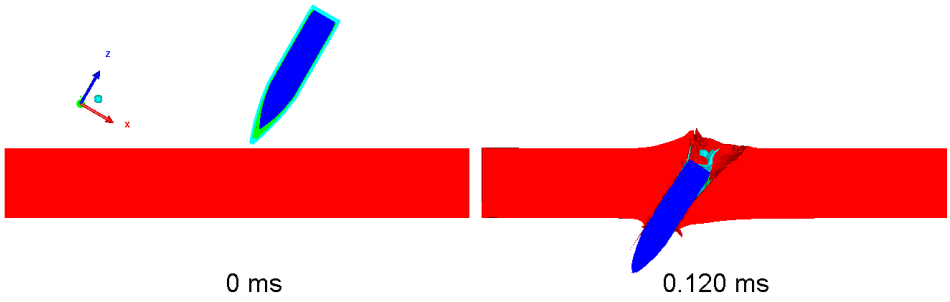

Figure 4.18: Simulation Result of the 15 mm Plate Impacted by the Bullet at 30 °

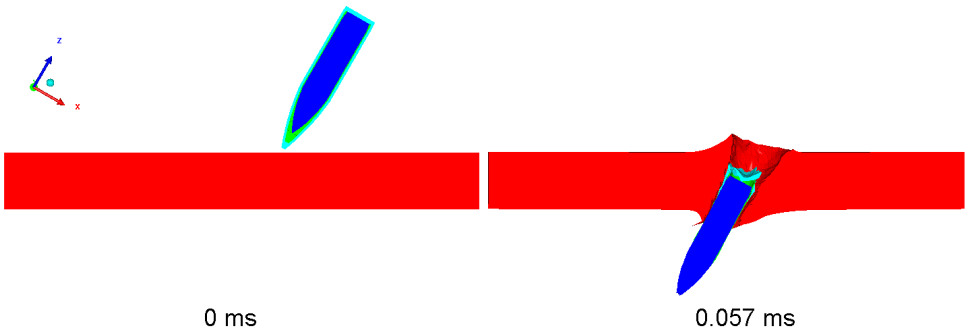

Figure 4.19: Simulation Result of the 12 mm Plate Impacted by the Bullet at 30 °

At 40 ° angle of attack, 8 mm (Figure 4.22) and 6 mm (Figure 4.23) target plates are simulated. Both plates are perforated quite easily by the bullets and the residual velocities of them are 645m/s for the 8 mm case and 753m/s for the 6 mm case (Figures 4.24 and 4.25).

As in 30 ° and 40 ° angles of attack, both plates that are simulated are perforated at 50 ° angle of attack (Figures 4.26 and 4.27). When we investigate the velocity changes of the bullet cores for both cases (Figures 4.28 and 4.29) it can be clearly seen that both bullets gained around 100m/s velocity in +x direction resulting in the change of the original directions of flight. Their residual velocities in -z direction, on the other hand, are 440m/s and 500m/s for 10 mm and 8 mm plates, respectively.

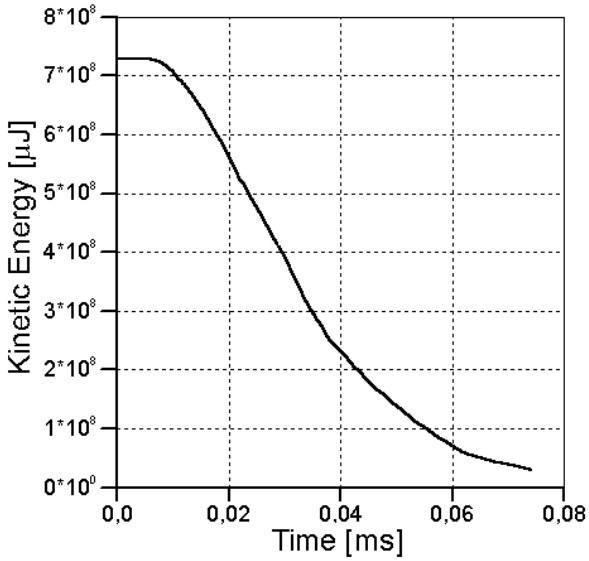

Figure 4.20: Kinetic Energy Plot of the Bullet Core During Impact to 15 mm Plate at 30°

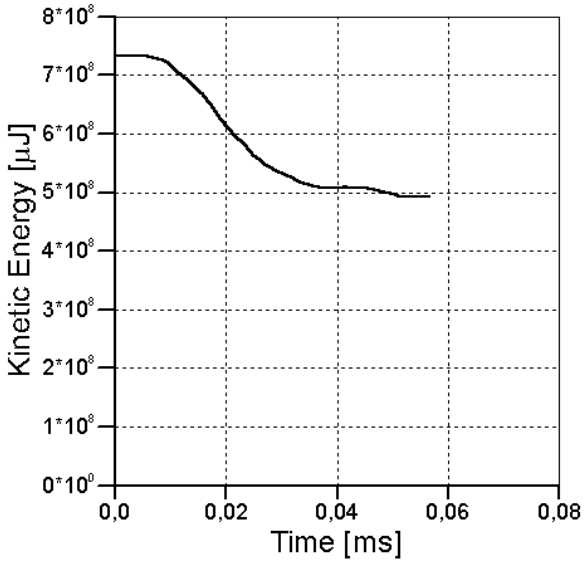

Figure 4.21: Kinetic Energy Plot of the Bullet Core During Impact to 12 mm Plate at 30°

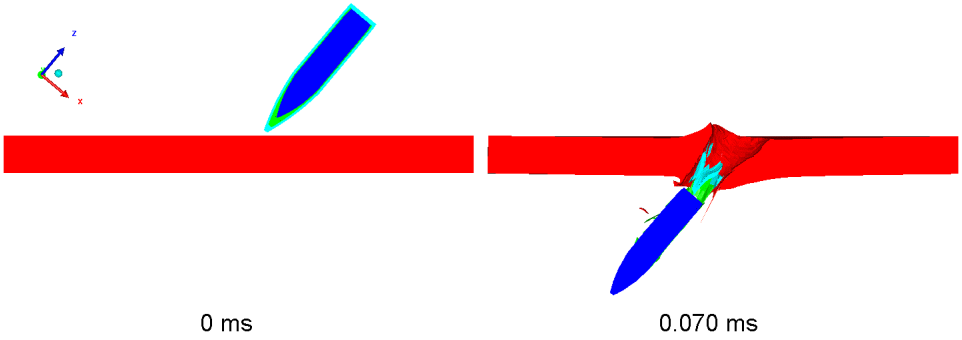

Figure 4.22: Simulation Result of the 8 mm Plate Impacted by the Bullet at 40°

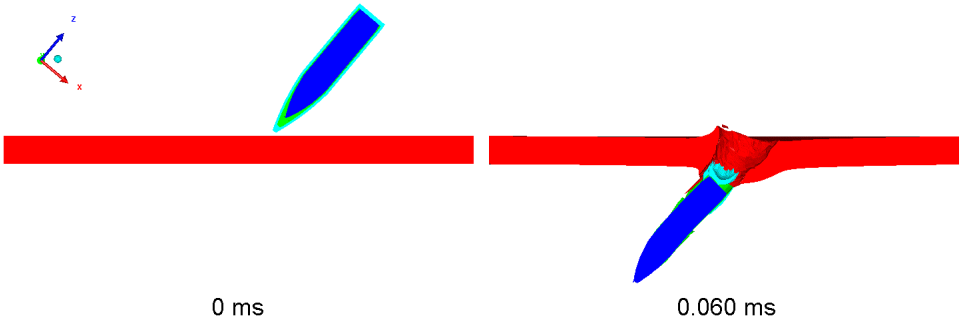

Figure 4.23: Simulation Result of the 6 mm Plate Impacted by the Bullet at 40°

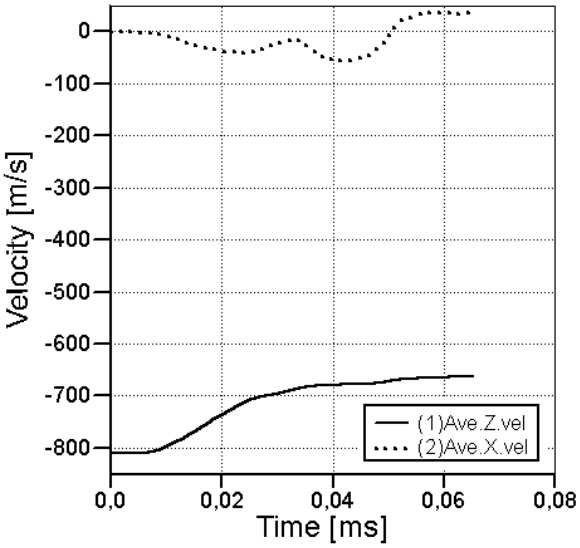

Figure 4.24: Average Velocity of the Bullet Core During Impact to 8 mm Plate at 40°

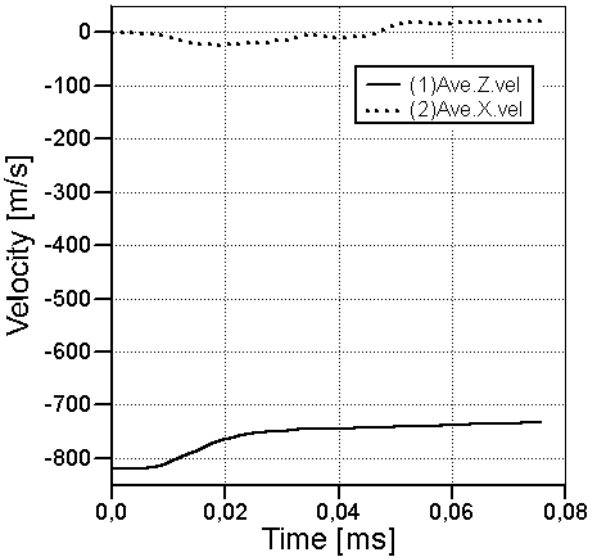

Figure 4.25: Average Velocity of the Bullet Core During Impact to 6 mm Plate at 40°

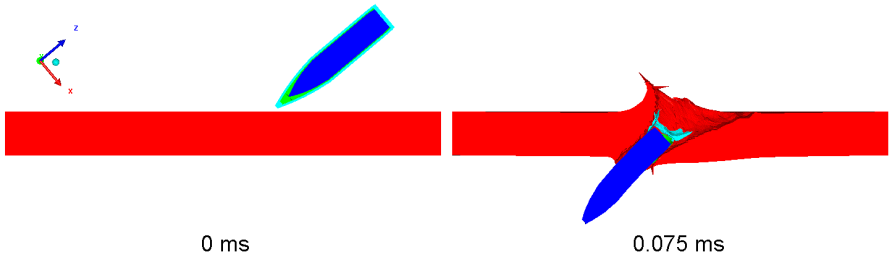

Figure 4.26: Simulation Result of the 10 mm Plate Impacted by the Bullet at 50°

At 60° angle of attack, 7.62 mm AP bullet is ricocheted (Figure 4.30) after impacting 8 mm plate. However, 6 mm target plate is completely perforated (Figure 4.31). When the velocity change plot of the 60° angle of attack - 8 mm plate thickness combination (Figure 4.32) is examined, it can be seen that residual velocities of the bullet in -x and -z directions are almost the same. This clearly indicates that there is a 45° angle between the direction of flight of the bullet after ricochet and the horizontal plane (i.e. y-z plane). The bullet perforating 6 mm plate has a 534m/s velocity in -z direction and 43m/s in +x direction indicating no significant deflection from the pre-impact direction of flight (Figure 4.33).

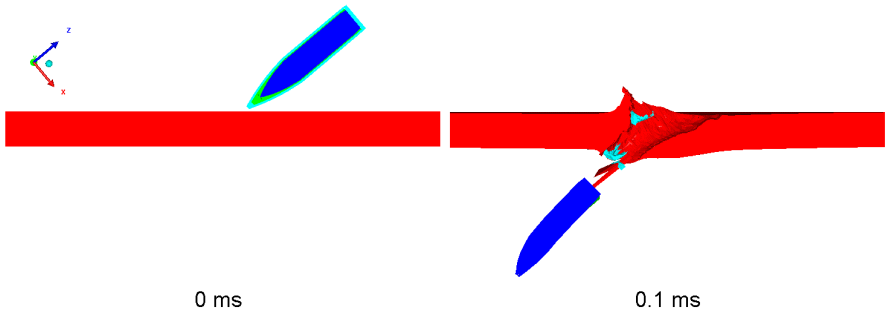

Figure 4.27: Simulation Result of the 8 mm Plate Impacted by the Bullet at 50°

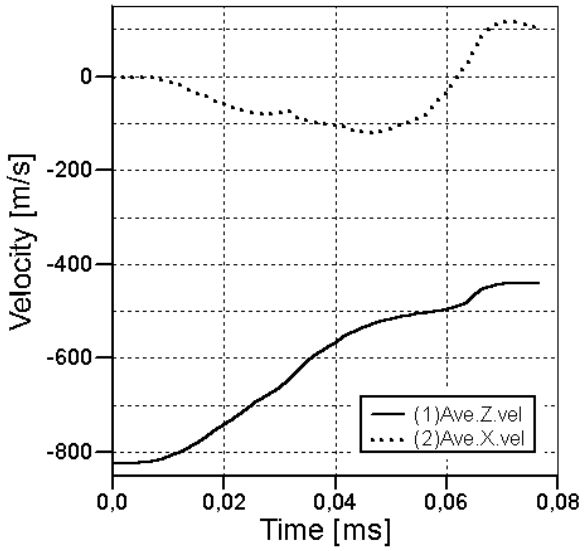

Figure 4.28: Average Velocity of the Bullet Core During Impact to 10 mm Plate at 50°

At the last simulation group of the monolithic plate cases, 5 mm and 4 mm plate thicknesses are impacted by bullets at 70° angle of attack. Although both bullets are ricocheted after the impact, 4 mm target plate is severely damaged and torn (Figure 4.34). 5 mm plate, on the other hand, has a dent on the impacted face and a bump on the rear face (Figure 4.35). Due to ricochet, both bullets are deflected from their original direction of flight. Their residual velocities are $409 m/s$ and $384 m/s$ in -x direction and $467 m/s$ and $590 m/s$ in -z direction for 4 mm and 5 mm plate thicknesses, respectively (Figures 4.36 and 4.37).

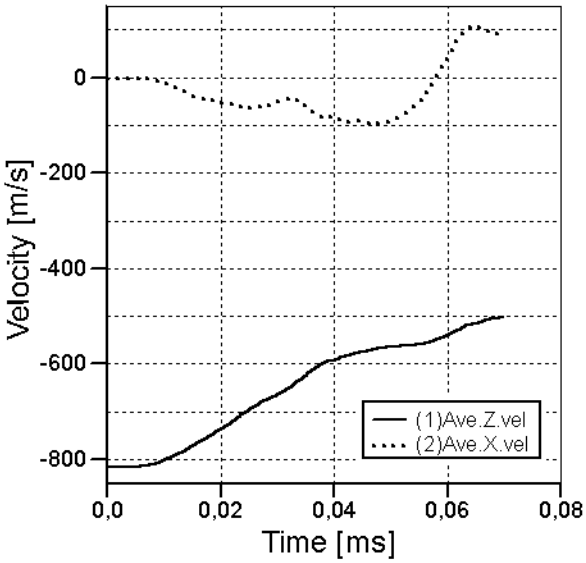

Figure 4.29: Average Velocity of the Bullet Core During Impact to 8 mm Plate at 50°

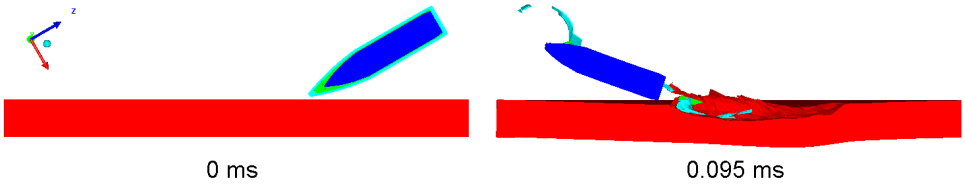

Figure 4.30: Simulation Result of the 8 mm Plate Impacted by the Bullet at 60°

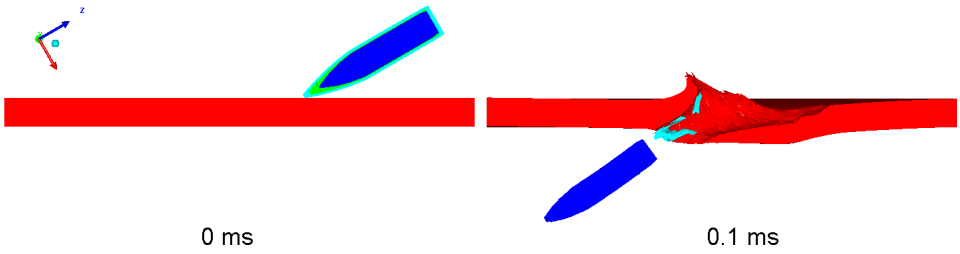

Figure 4.31: Simulation Result of the 6 mm Plate Impacted by the Bullet at 60°

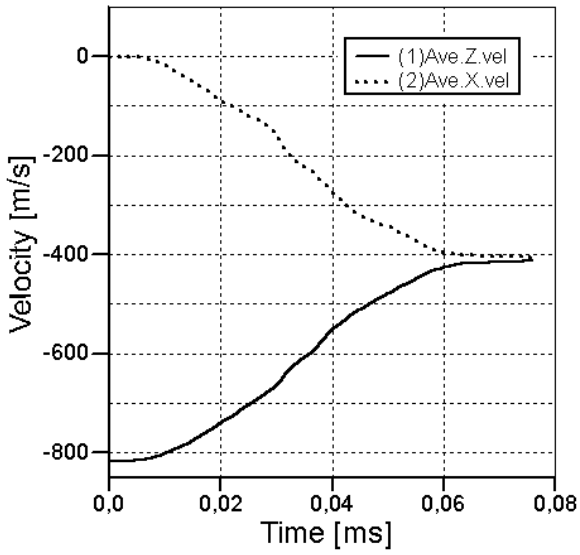

Figure 4.32: Average Velocity of the Bullet Core During Impact to 8 mm Plate at 60°

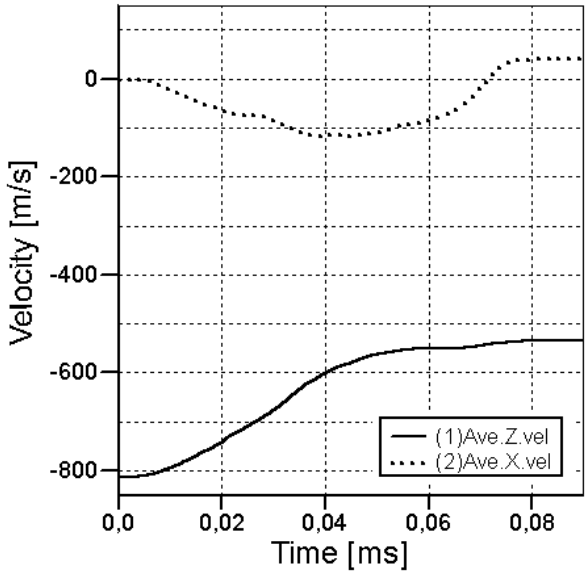

Figure 4.33: Average Velocity of the Bullet Core During Impact to 6 mm Plate at 60°

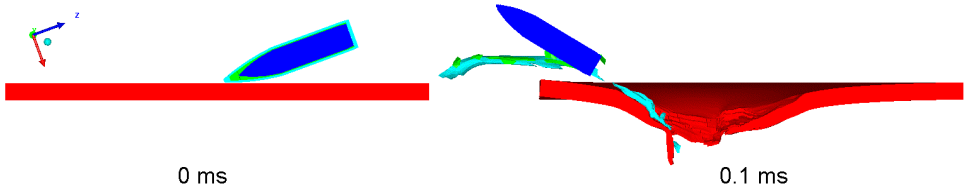

Figure 4.34: Simulation Result of the 4 mm Plate Impacted by the Bullet at 70°

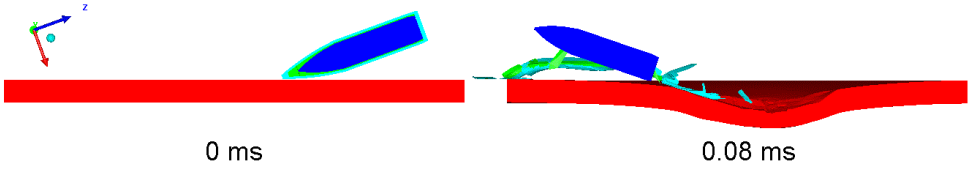

Figure 4.35: Simulation Result of the 5 mm Plate Impacted by the Bullet at 70°

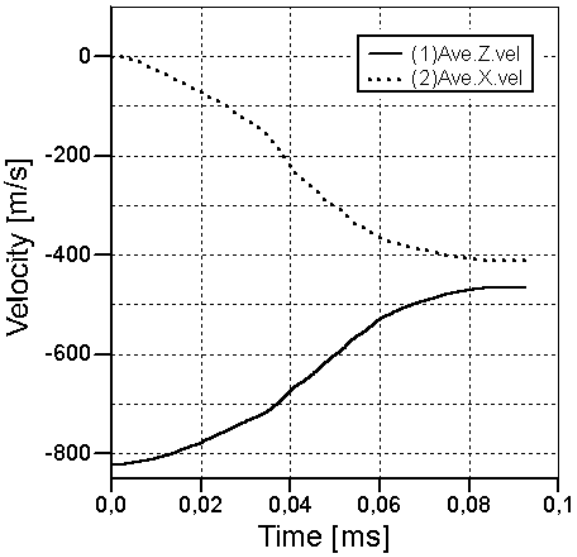

Figure 4.36: Average Velocity of the Bullet Core During Impact to 4 mm Plate at 70°

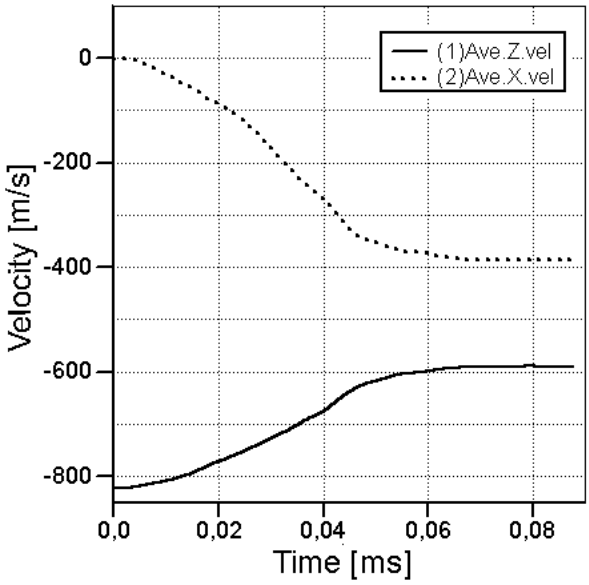

Figure 4.37: Average Velocity of the Bullet Core During Impact to 5 mm Plate at 70°

When the numerical simulation of monolithic plates used in the experimental part of the thesis are completed, it is seen that for some angles of attack, the minimum plate thicknesses that are not perforated could not be determined. In order to eliminate this absence, some more simulations are conducted to find the minimum plate thicknesses that are not perforated at 30°, 40° and 50° angles of attack. As a result, it is found that the minimum plate thickness that is not perforated at 30° angle of attack is 20 mm while it is 15 mm for both 40° and 50° angles of attack. Figure 4.38 shows the summary of the numerical simulations for the monolithic plates and Figure 4.39 can be checked in order to see a comparison according to constant areal density as explained in Section 2.7.

As it is done for the results of the experiments, a straight line is also fitted to the numerical simulation results of the monolithic plates impacted by 7.62 mm AP bullets. This line, its equation and the coefficient of determination (R^2) values can be seen in Figure 4.40. It should be noted that theoretically the line should pass through the 0 thickness at 90° angle of attack. But due to curve fitting, there is a slight offset from that point.

The straight line fitted to the numerical simulation results has a coefficient of determination of 0.946. This means that 94.6% of the numerical simulation results fall into the line that is

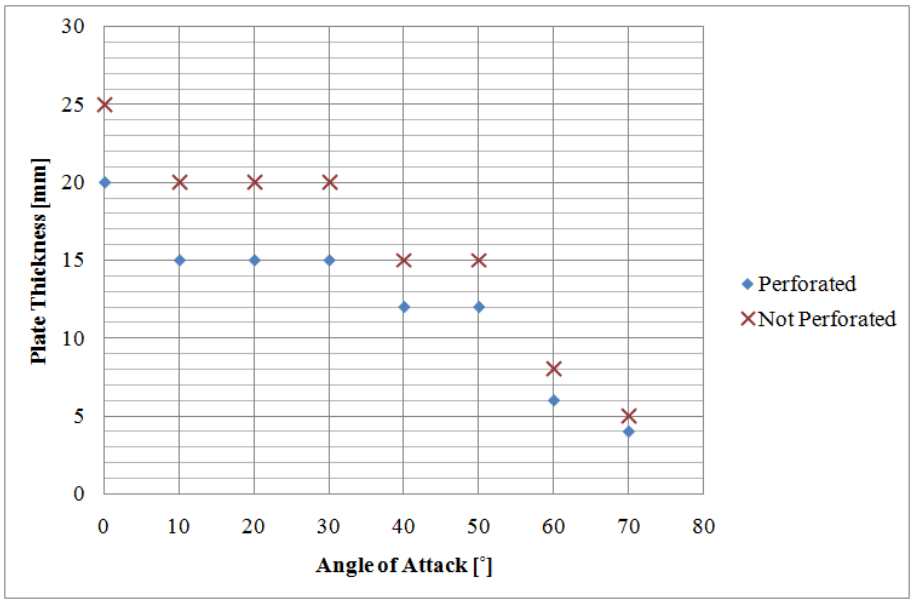

Figure 4.38: Summary of the Numerical Simulations for Monolithic Plates

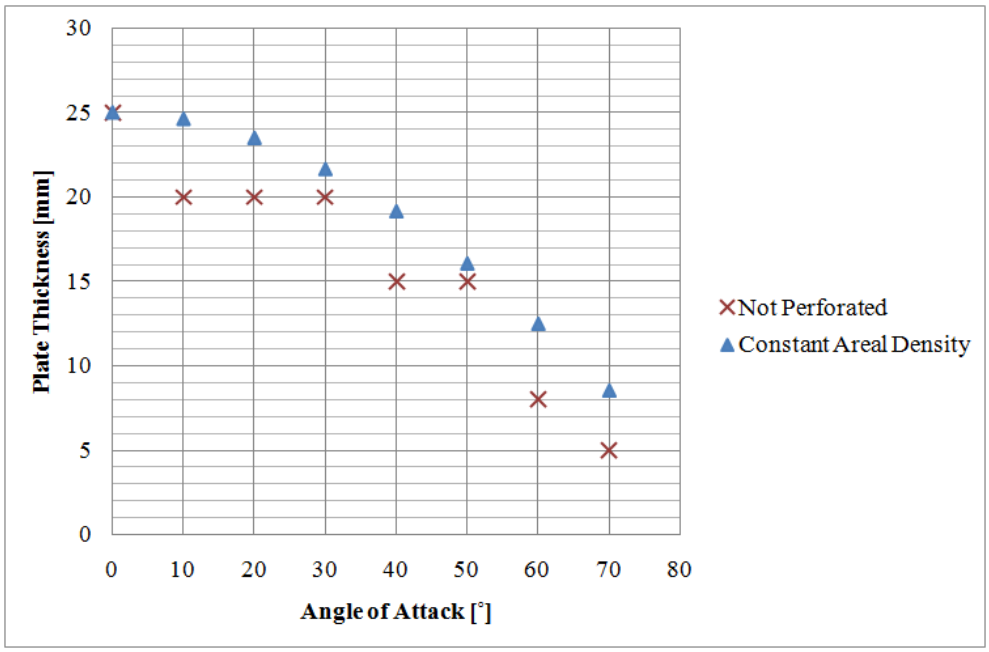

Figure 4.39: Comparison Graph of the Numerical Simulation Results According to Constant Areal Density

fitted.

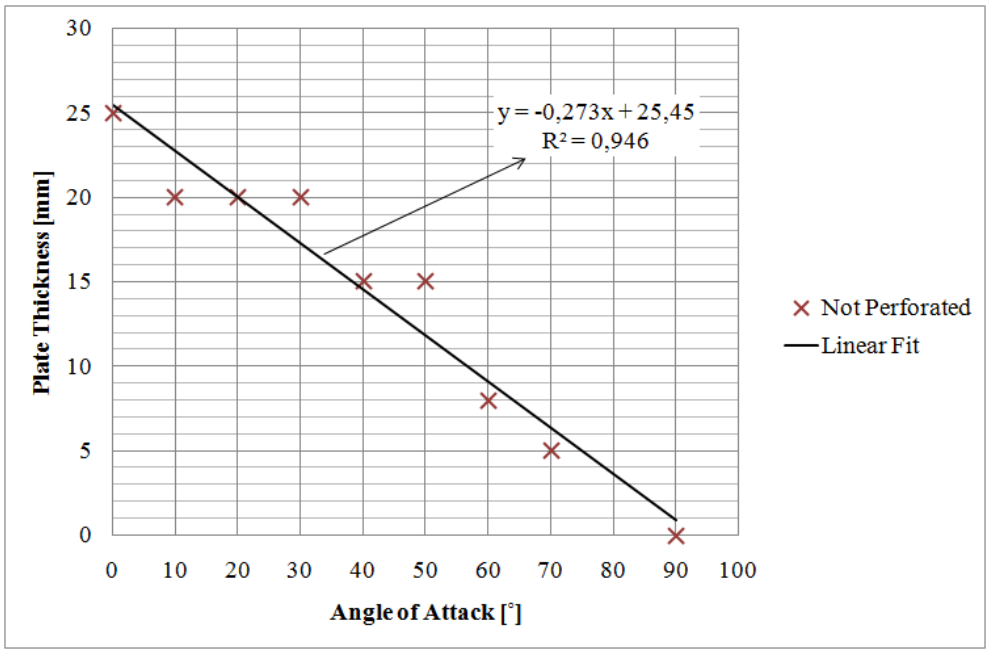

Figure 4.40: Linear Line Fitted to the Results of the Numerical Simulations

4.3.2 Layered Plates Impacted by 7.62 mm AP Bullets

After presenting the simulation results for monolithic plates in Subsection 4.3.1, in this last subsection of the Numerical Simulation Studies chapter, results of the numerical simulations conducted to simulate the experimental behaviors of layered ST-37 plate combinations impacted at 0°, 50° and 70° angles of attack are presented.

First simulation in layered plate combinations is conducted for the perforation of 12 mm + 12 mm plate combination under normal impact. As a result of this simulation, it is seen that the plate combination is perforated (Figure 4.41) and the bullet has a residual velocity of about $500 m/s$ in -z direction and no significant raise in its velocity in x direction (Figure 4.42).

In second set of numerical simulations, 4 mm + 5 mm (4 mm on the front face) and 5 mm + 5 mm layered plate combinations are impacted at 50° angle of attack. As a result, both layered plate combinations are perforated by 7.62 mm AP bullets (Figures 4.43 and 4.44). Velocities of the bullets after perforation are $86 m/s$ and $94 m/s$ in +x direction and $609 m/s$ and $524 m/s$ in -z direction for 4 mm + 5 mm and 5 mm + 5 mm, respectively (Figures 4.45 and 4.46).

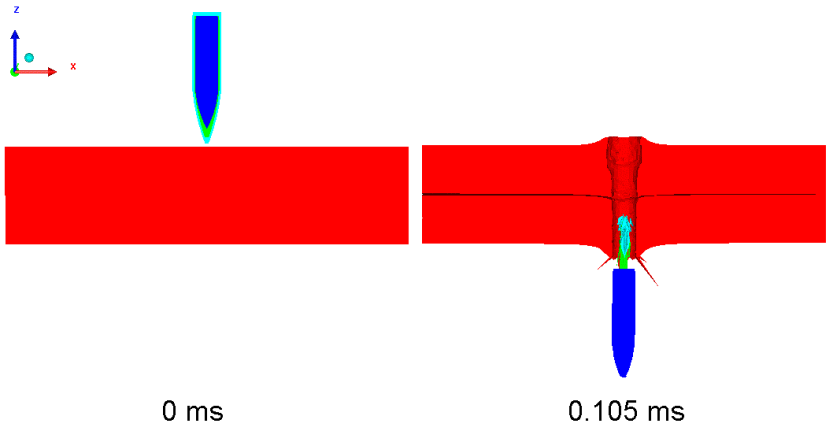

Figure 4.41: Simulation Result of the 12 mm + 12 mm Layered Plate Combination Impacted at 0 °

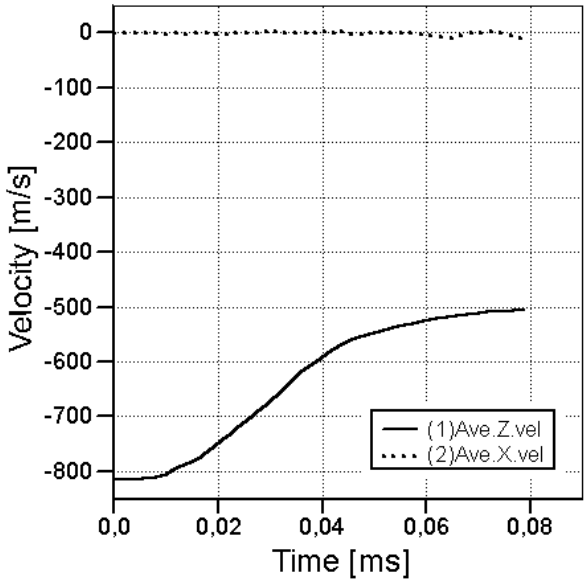

Figure 4.42: Average Velocity of the Bullet Core During Impact to 12 mm + 12 mm Layered Plate Combination at 0 °

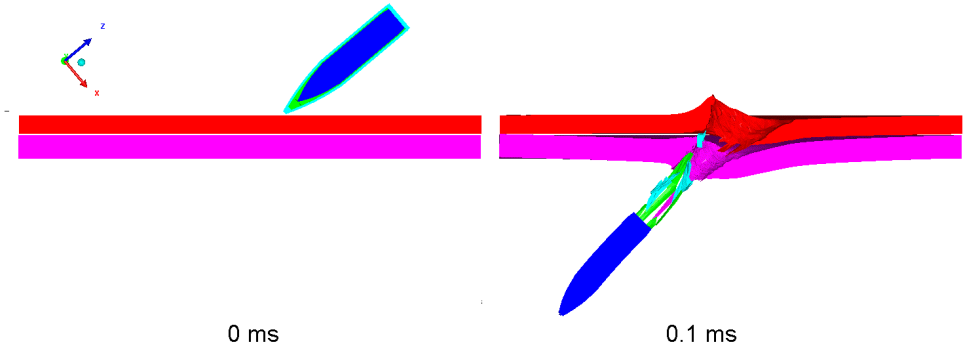

Figure 4.43: Simulation Result of the 4 mm + 5 mm Layered Plate Combination Impacted at 50 °

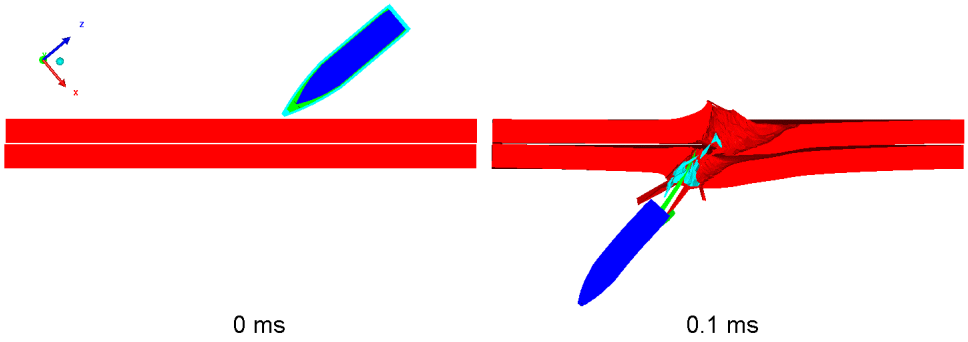

Figure 4.44: Simulation Result of the 5 mm + 5 mm Layered Plate Combination Impacted at 50 °

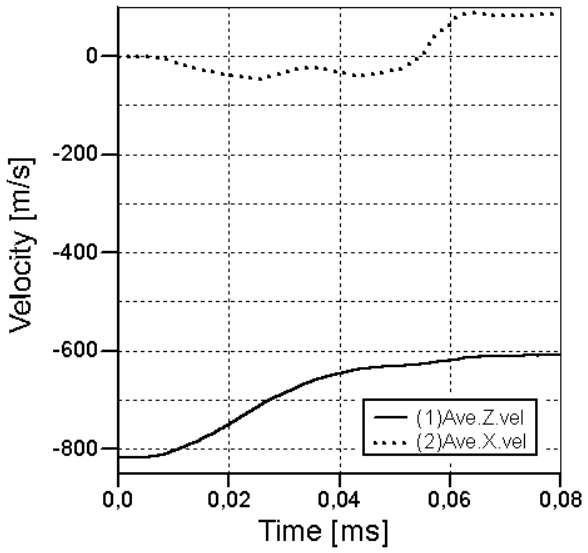

Figure 4.45: Average Velocity of the Bullet Core During Impact to 4 mm + 5 mm Layered Plate Combination at 50 °

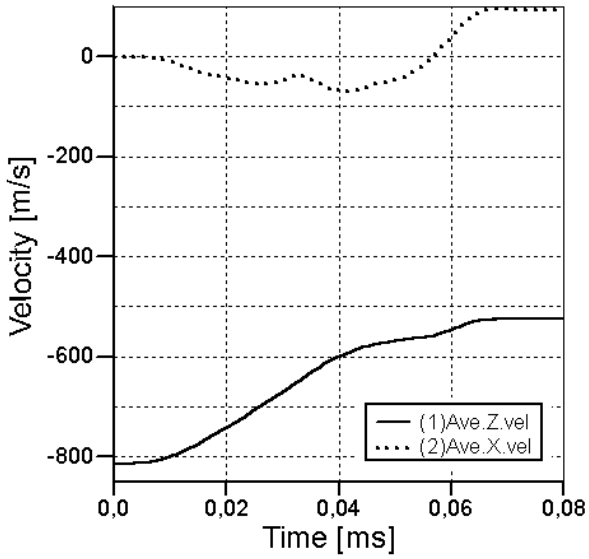

Figure 4.46: Average Velocity of the Bullet Core During Impact to 5 mm + 5 mm Layered Plate Combination at 50 °

Last set of numerical simulations is conducted for bullets impacting 2 mm + 3 mm (2 mm on front face) and 3 mm + 3 mm layered plate combinations at 70° angle of attack. In 2 mm + 3 mm plate combination, front plate is completely perforated but the bullet ricocheted without perforating the back plate (Figure 4.47). In 3 mm + 3 mm combination, however, there is some erosion on the front plate but neither of the plates is completely perforated and the bullet is ricocheted (Figure 4.48). Residual velocities of the bullet after ricocheting from 2 mm + 3 mm plate combination are around $380 m/s$ in both -z and -x directions (Figure 4.49) resulting in a ricochet having almost 45° angle with the horizontal (y-z plane). Residual velocities of the bullet for the 3 mm + 3 mm plate combination case are $545 m/s$ in -z direction and $390 m/s$ in -x direction (Figure 4.50).

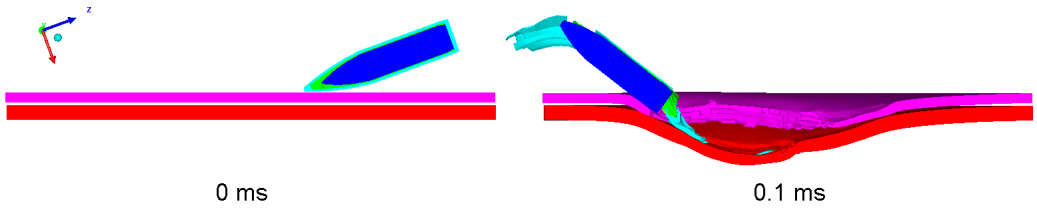

Figure 4.47: Simulation Result of the 2 mm + 3 mm Layered Plate Combination Impacted at 70°

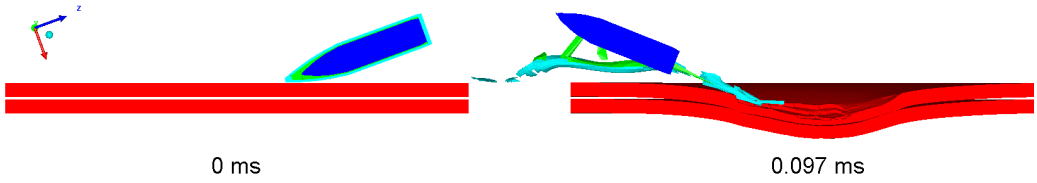

Figure 4.48: Simulation Result of the 3 mm + 3 mm Layered Plate Combination Impacted at 70°

As a final note, the angles of exit of the bullets that perforate the plates can be seen in Table 4.8 together with the perforated plate thicknesses.

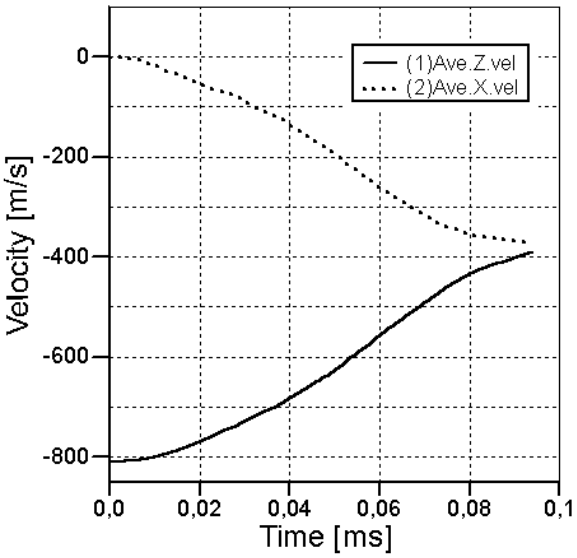

Figure 4.49: Average Velocity of the Bullet Core During Impact to 2 mm + 3 mm Layered Plate Combination at 70 °

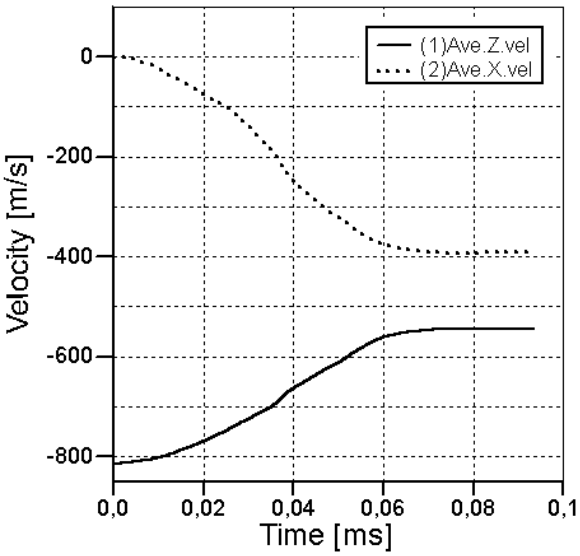

Figure 4.50: Average Velocity of the Bullet Core During Impact to 3 mm + 3 mm Layered Plate Combination at 70 °

Table 4.8: Exit Angles of the Bullets After Perforation

Angle of Attack	Plate Thickness	Angle of Exit
[°]	[*mm*]	[°]
10	15	10
10	20	11
20	15	22
20	20	23
30	12	28
30	15	33
40	6	43
40	8	40
50	8	44
50	4+5	43
50	10	43
50	5+5	43
60	6	55

When the results of the experimental shots are compared to the results of the numerical simulations it is obvious that they are in quite good agreement. This means the curve fitting on tensile tests results of the ST-37 plates and combining the results with the Johnson-Cook constitutive and damage model parameters of AISI 1006 steel explains the behavior of ST-37 steel plates under oblique impact successfully.

CHAPTER 5

COMPARISON OF THE EXPERIMENTAL AND NUMERICAL RESULTS

As explained before, 21 different numerical simulations are conducted to investigate the perforation of ST-37 steel plates under oblique impact. In this chapter, results of these numerical simulations (presented in Section 4.3) are compared to the results of the experimental work (presented in Section 3.5).

5.1 Monolithic Plates Impacted by 7.62 mm AP Bullets

While conducting experimental part of this thesis, a total of 71 monolithic plates are shot by 7.62 mm AP bullets. Using these 71 shots, the minimum plate thickness that is not perforated and the maximum plate thickness that is perforated are determined for each angle of attack from 0° to 70° by 10° increments. As a result, 16 plate thickness - angle of attack combinations are determined and numerical simulations are conducted for each combination.

First of all, under normal impact conditions, the bullet penetrated and stuck into 25 mm target plates in the experimental work. When we investigate the result of the numerical simulation for this combination, we can see the same result. As in the experimental shot, tip of the bullet is almost out of the target plate in the numerical simulation (Figure 5.1). 20 mm plate, at the same angle of attack, is completely perforated, as in the experimental shots (Figure 5.2).

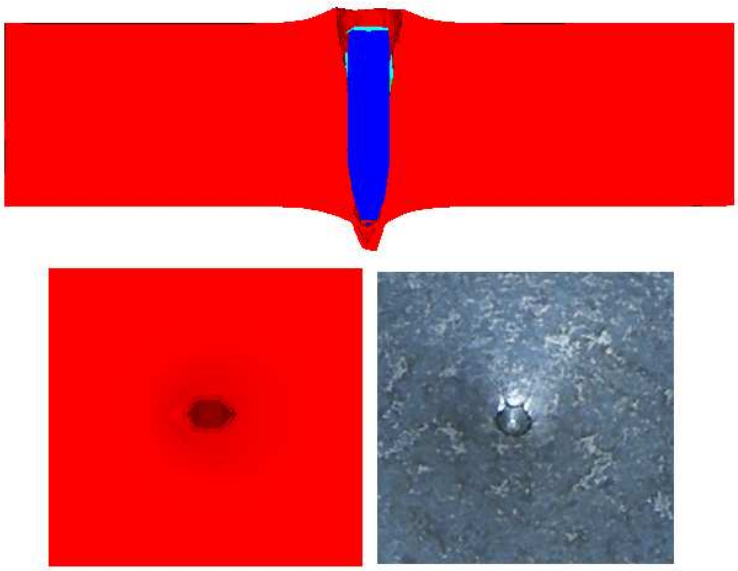

Figure 5.1: Comparison of the Experimental and Simulation Results of the 25 mm Plate Impacted by the Bullet at 0 °

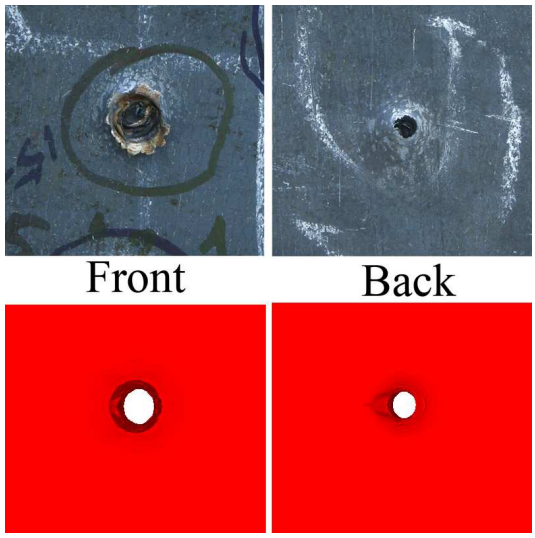

Figure 5.2: Comparison of the Experimental and Simulation Results of the 20 mm Plate Impacted by the Bullet at 0 °

Experimental shots and numerical simulations conducted at 10 ° and 20 ° angles of attack are yielded to similar results. Both experimental shots and numerical simulations show that at these angles of attack, 15 mm plates are perforated (Figure 5.3) while 20 mm plates are not (Figure 5.4).

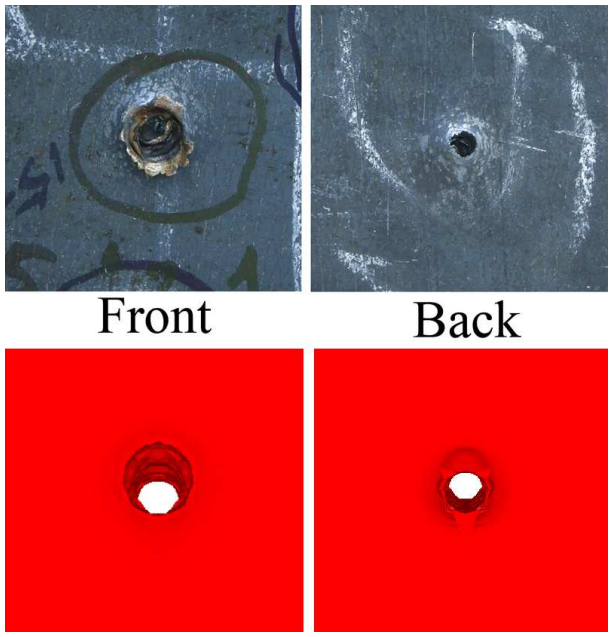

Figure 5.3: Comparison of the Experimental and Simulation Results of the 15 mm Plate Impacted by the Bullet at 10 °

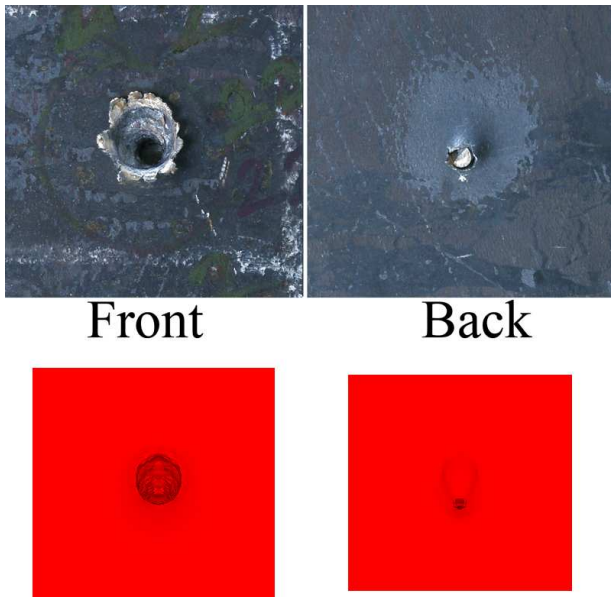

Figure 5.4: Comparison of the Experimental and Simulation Results of the 20 mm Plate Impacted by the Bullet at 20 °

In experiments, it is seen that at 30° angle of attack, 12 mm plates are perforated and 15 mm plates are not. In the numerical simulations, on the other hand, both plate thicknesses are perforated. But when the kinetic energy plot of 15 mm plate is investigated (Figure 4.20), it can be said that since the kinetic energy loss is quite large (95.8%) we can say that simulations done for 30° angle of attack are quite successful in explaining the results of the experimental shots. Comparison of the results of experimental and numerical studies for 15 mm and 12 mm plates can be seen in Figures 5.5 and 5.6, respectively.

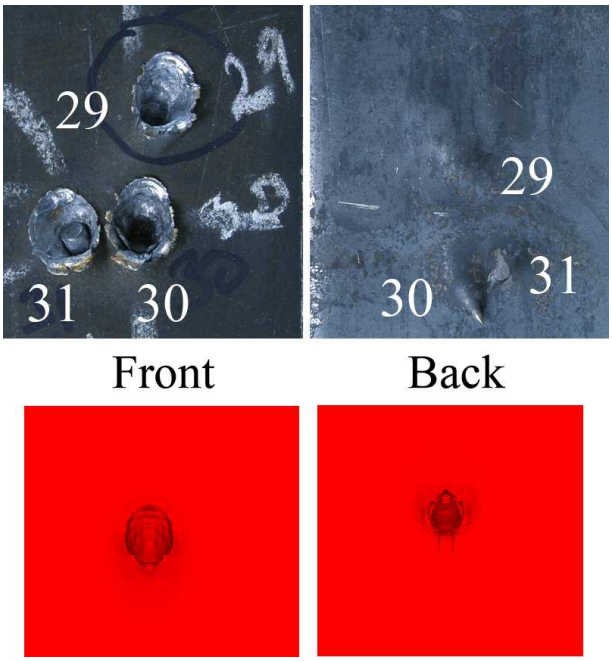

Figure 5.5: Comparison of the Experimental and Simulation Results of the 15 mm Plate Impacted by the Bullet at 30°

Results of the numerical simulations conducted at 40° angle of attack show that both 6 mm and 8 mm plates are perforated. In experimental shots, however, two of the three bullets, impacting to 8 mm target plates are ricocheted while the third one perforates. Figures 5.7 and 5.8 show the similarities and differences between numerical simulations and experimental shots for 6 mm and 8 mm plates impacted at 40°, respectively. By looking at Figure 5.8, one can clearly say that the simulation result resembles the shot that perforated the 8 mm plate, instead of two shots that are ricocheted.

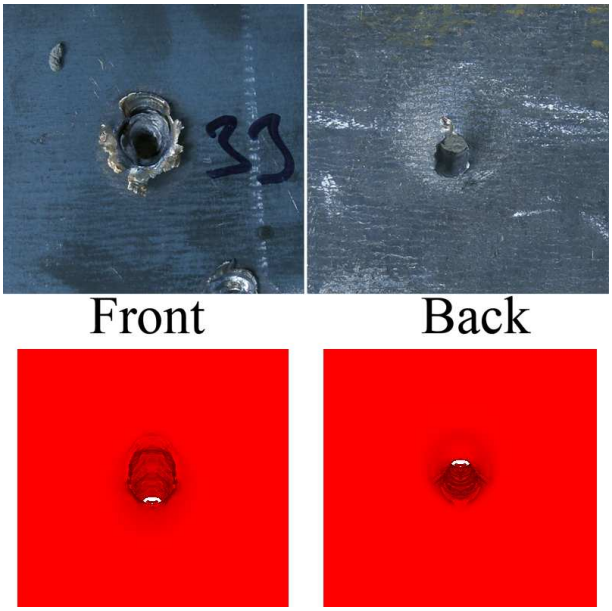

Figure 5.6: Comparison of the Experimental and Simulation Results of the 12 mm Plate Impacted by the Bullet at 30 °

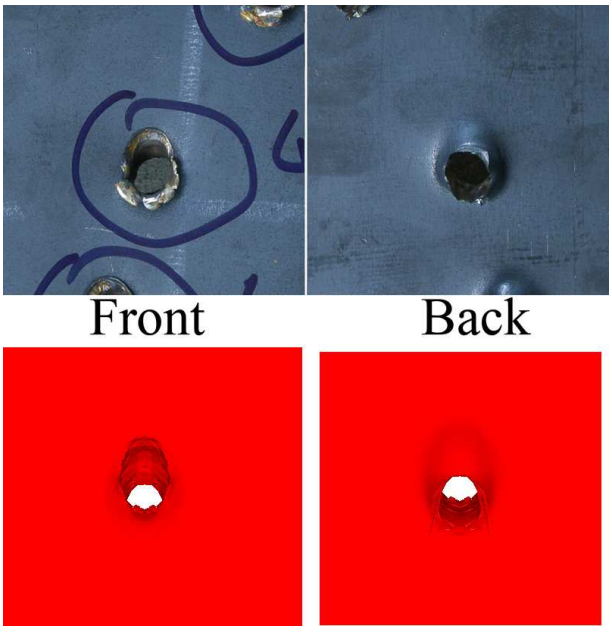

Figure 5.7: Comparison of the Experimental and Simulation Results of the 6 mm Plate Impacted by the Bullet at 40 °

In experimental studies, it is seen that at 50° angle of attack, 8 mm target plate is perforated while the bullet ricocheted after impacting 10 mm target plate. In the numerical simulations, on the other hand, both plates are perforated. Comparison of 10 mm plates after impact can be seen in Figure 5.9.

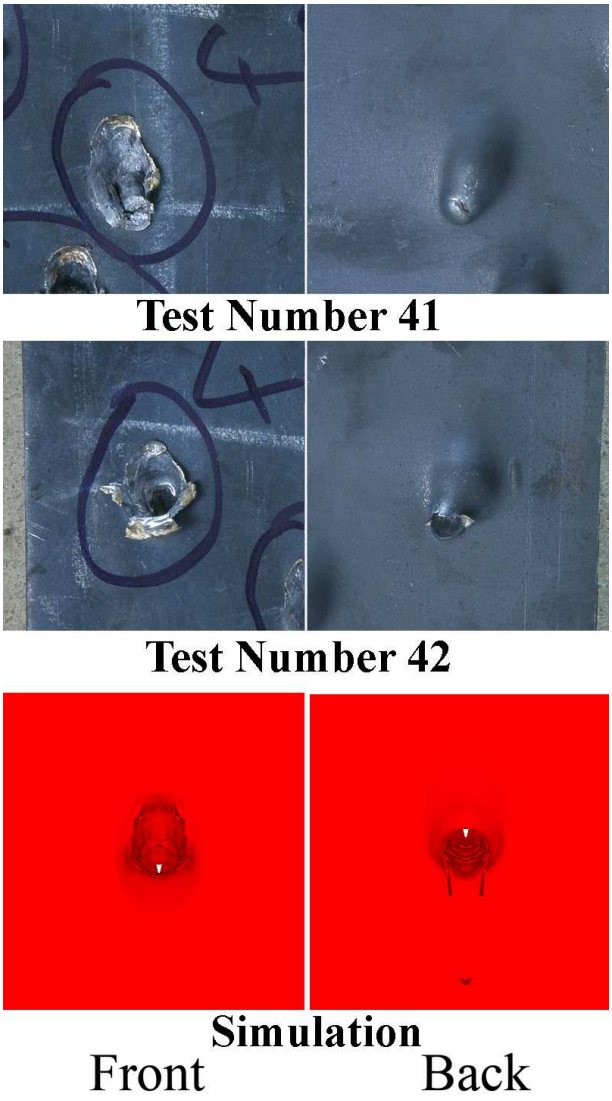

Figure 5.8: Comparison of the Experimental and Simulation Results of the 8 mm Plate Impacted by the Bullet at 40°

At 60° angle of attack, both the experimental and numerical work provide the result that bullets ricochet from 8 mm plates but perforate the 6 mm ones. Figures 5.10 and 5.11 can be investigated to compare these results.

Last case of monolithic plate sets is conducted at 70 °. At this angle of attack, bullet ricocheted from plates having 5 mm thicknesses. Comparison of the experimental and numerical work results for this angle of attack - plate thickness combination can be seen in Figure 5.12. While conducting experimental shots, 4 mm plates are recorded as *perforated* at this angle of attack. When the numerical simulation is done, it is seen that although the post-impact appearance of the plate is quite similar to the experimentally shot plate (Figure 5.13), the bullet actually ricocheted. This may mean that the bullet is also ricocheted in the experimental shot but the plate is incorrectly recorded as *perforated* just by looking at the gap on the plate.

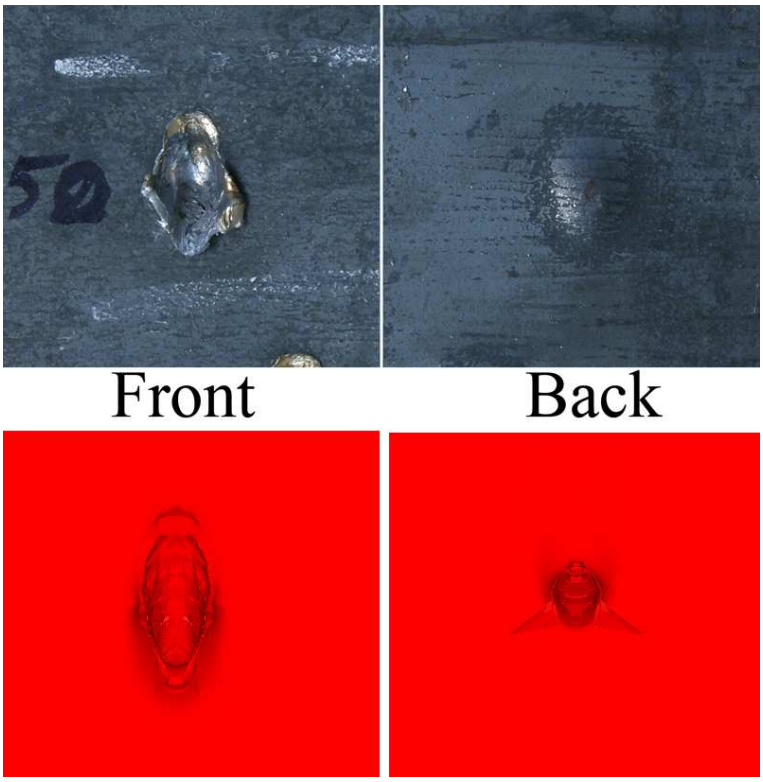

Figure 5.9: Comparison of the Experimental and Simulation Results of the 10 mm Plate Impacted by the Bullet at 50 °

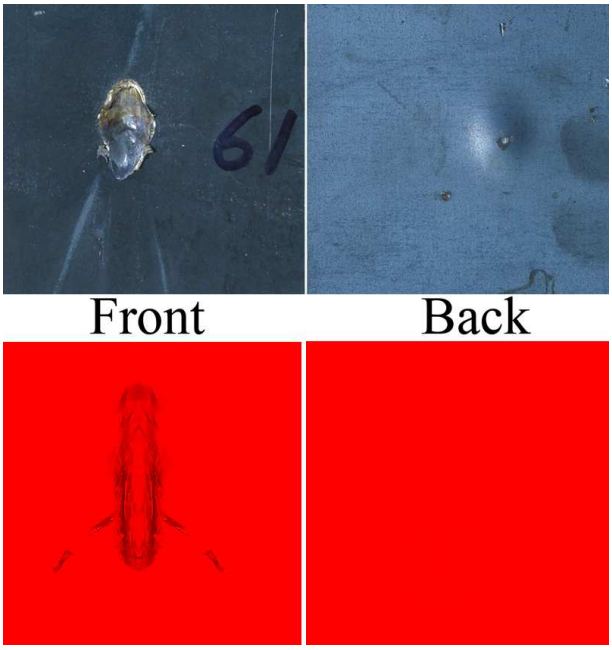

Figure 5.10: Comparison of the Experimental and Simulation Results of the 8 mm Plate Impacted by the Bullet at 60 °

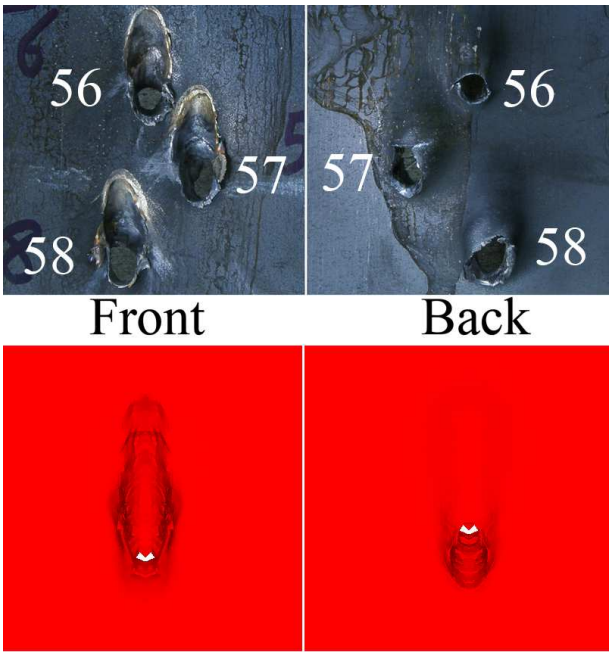

Figure 5.11: Comparison of the Experimental and Simulation Results of the 6 mm Plate Impacted by the Bullet at 60 °

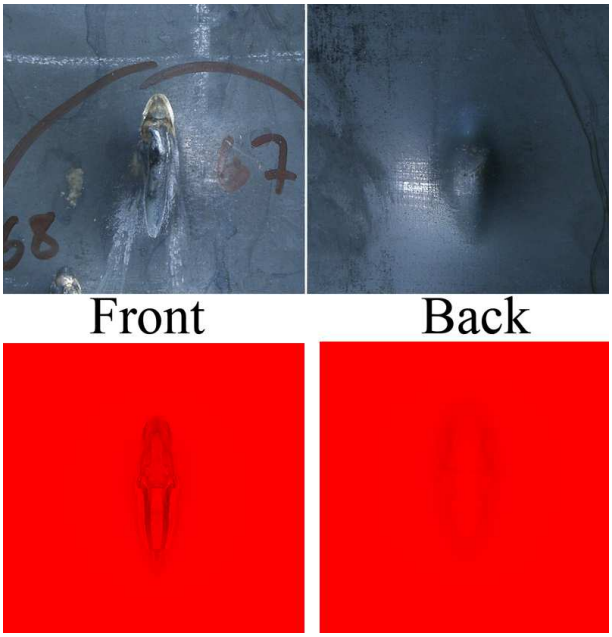

Figure 5.12: Comparison of the Experimental and Simulation Results of the 5 mm Plate Impacted by the Bullet at 70 °

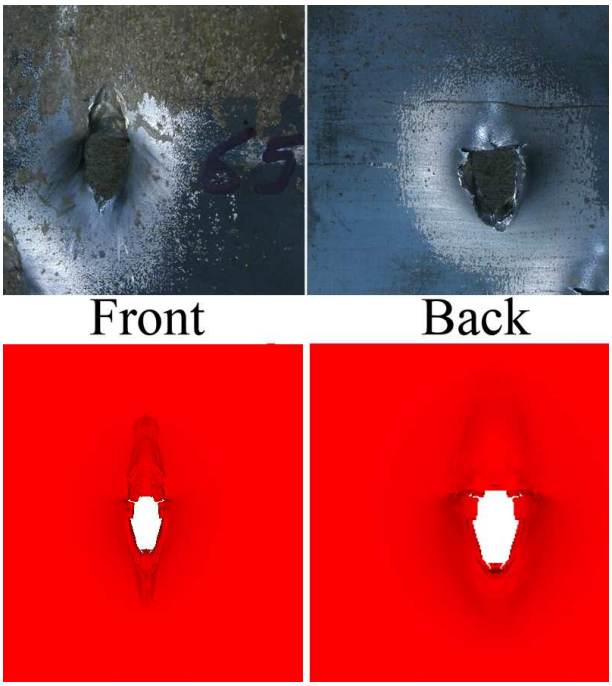

Figure 5.13: Comparison of the Experimental and Simulation Results of the 4 mm Plate Impacted by the Bullet at 70 °

Summary of the results including both experimental and numerical work for the above explained 16 shots can be seen in Table 5.1. Not perforated plate thicknesses for both experimental and numerical simulation results can be compared in Figure 5.14.

Table 5.1: Summary of the Results of Experiments and Numerical Simulations for Monolithic Plates

Angle of Attack [°]	**Plate Thickness** [*mm*]	**Experimental Result**	**Simulation Result**
0	25	S	S
0	20	P	P
10	20	R	S
10	15	P	P
20	20	S	S
20	15	P	P
30	15	S	P
30	12	P	P
40	8	R	P
40	6	P	P
50	10	R	P
50	8	P	P
60	8	R	R
60	6	P	P
70	6	R	R
70	4	P	R

5.2 Layered Plates Impacted by 7.62 mm AP Bullets

Three different angles of attack are tested both numerically and experimentally for the layered plate combinations, i.e. 0°, 50° and 70°. Among 22 experimental shots conducted for these three angle of attack, five different angle of attack - plate thickness combinations are simulated numerically.

At 0°, numerical modeling and simulation is done for 12 mm + 12 mm plate thickness combination, i.e. the thickest layered plate combination that is perforated at this angle of attack. As a result, it is seen that 12 mm + 12 mm layered plate combination is perforated as a result of both experimental and numerical studies. Comparison of the results that are presented in Sections 3.5 and 3.5 for this specific combination can be seen in Figures 5.15 and 5.16.

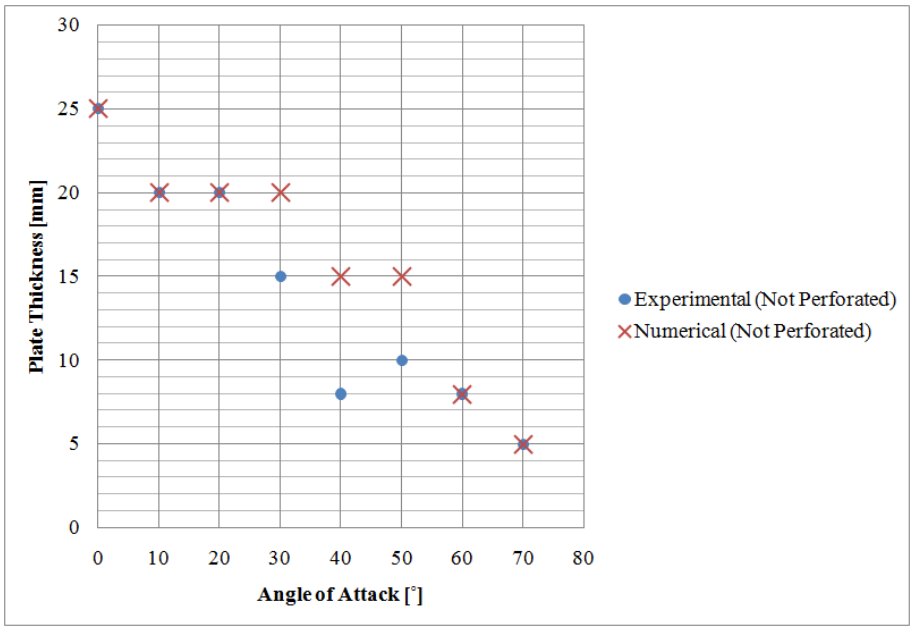

Figure 5.14: Comparison of Not Perforated Plate Thicknesses for Monolithic Plates

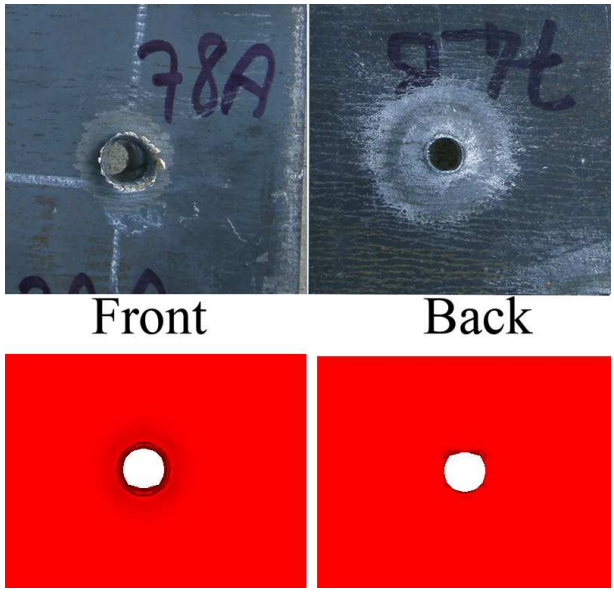

Figure 5.15: Comparison of the Experimental and Simulation Results of the 12 mm + 12 mm Layered Plate Combination Impacted at 0 ° (Front Plate)

Second angle of attack, chosen for layered plate combinations is 50 °. At this angle of attack, in experimental shots, 5 mm + 5 mm plate combinations are not perforated (bullet ricocheted from second plate) while 4 mm + 5 mm plate combinations are perforated. In the numerical

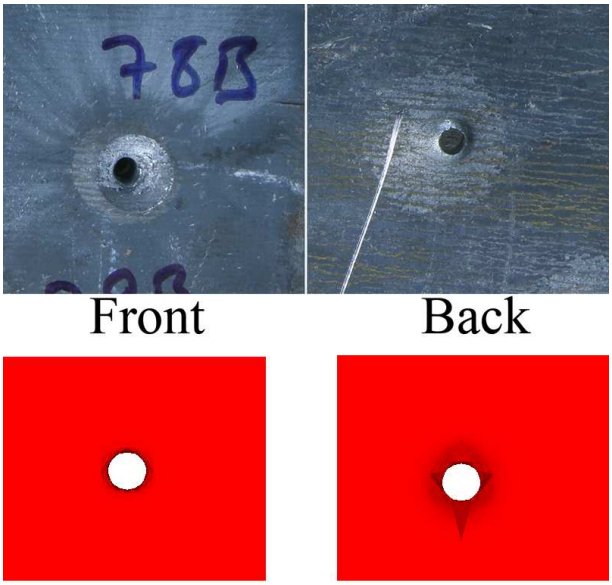

Figure 5.16: Comparison of the Experimental and Simulation Results of the 12 mm + 12 mm Layered Plate Combination Impacted at 0 ° (Back Plate)

simulations, however, both 5 mm + 5 mm and 4 mm + 5 mm plate combinations are perorated by 7.62 mm AP bullets. In Figures 5.17 and 5.18, similarities and differences between experimental and numerical studies for 5 mm + 5 mm layered plate combinations can be seen, while comparison for 4 mm + 5 mm plate combinations are presented in Figures 5.19 and 5.20.

The last case investigated both numerically and experimentally is layered plate combinations impacted at 70 ° angle of attack. In experimental shots conducted at this angle of attack, 7.62 mm AP bullets are ricocheted from 3 mm + 3 mm layered ST-37 plates tearing the front (impacted) plate and fully perforated 2 mm + 3 mm layered plate combinations. In numerical simulations, on the other hand, bullets impacting both combinations are ricocheted. When the post-impact status of plates after numerical simulations are investigated, it is seen that the plate having 2 mm plate thickness (front plate of 2 mm + 3 mm layered plate combination) is teared. Comparison of the experimental and numerical studies can be seen in Figures 5.21 and 5.22 for 3 mm + 3 mm and in Figures 5.23 and 5.24 for 2 mm + 3 mm layered plate combinations.

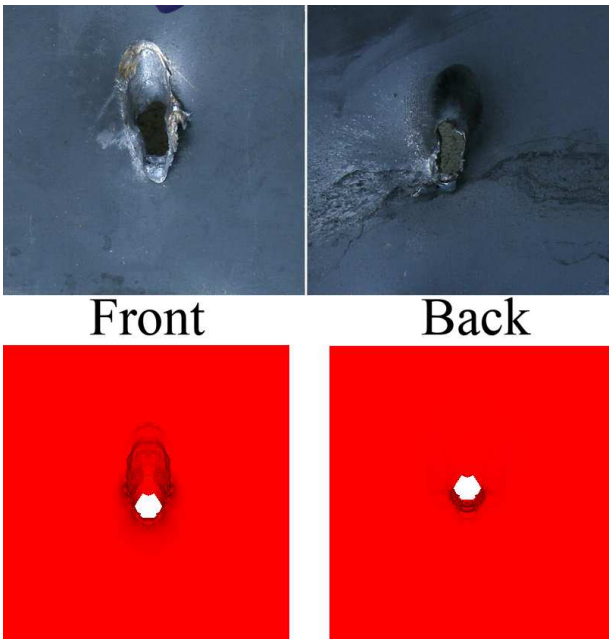

Figure 5.17: Comparison of the Experimental and Simulation Results of the 5 mm + 5 mm Layered Plate Combination Impacted at 50 ° (Front Plate)

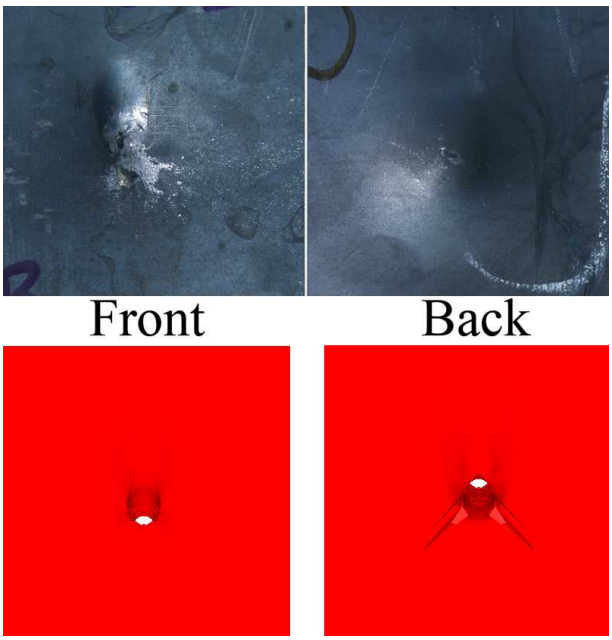

Figure 5.18: Comparison of the Experimental and Simulation Results of the 5 mm + 5 mm Layered Plate Combination Impacted at 50 ° (Back Plate)

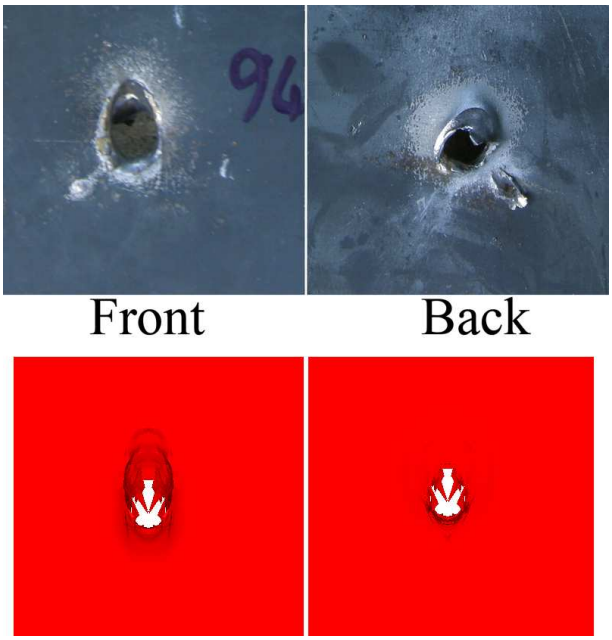

Figure 5.19: Comparison of the Experimental and Simulation Results of the 4 mm + 5 mm Layered Plate Combination Impacted at 50° (Front Plate)

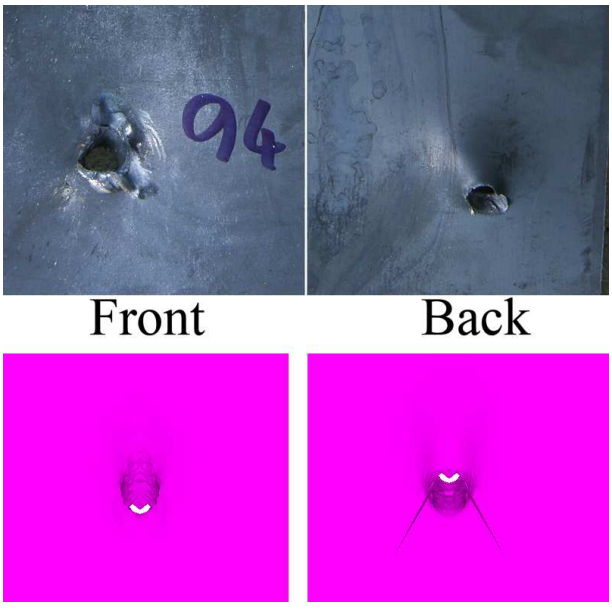

Figure 5.20: Comparison of the Experimental and Simulation Results of the 4 mm + 5 mm Layered Plate Combination Impacted at 50° (Back Plate)

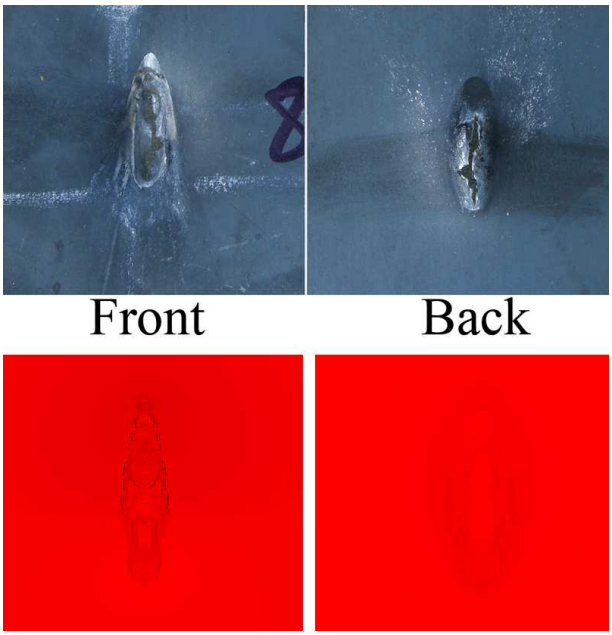

Figure 5.21: Comparison of the Experimental and Simulation Results of the 3 mm + 3 mm Layered Plate Combination Impacted at 70° (Front Plate)

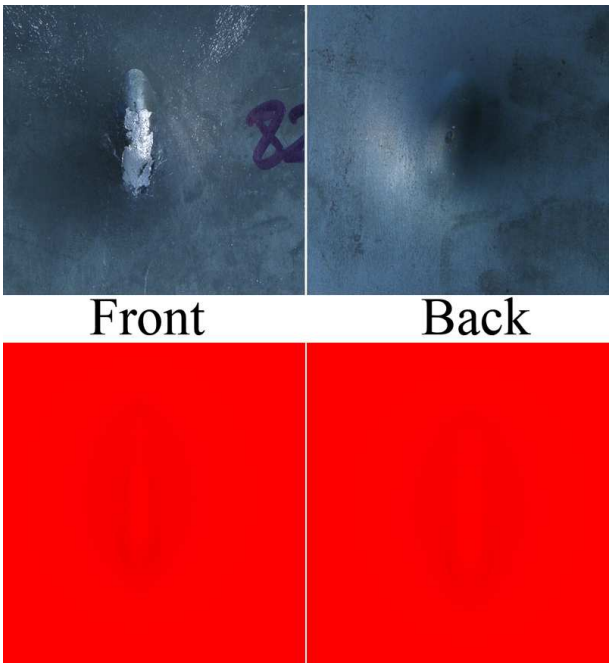

Figure 5.22: Comparison of the Experimental and Simulation Results of the 3 mm + 3 mm Layered Plate Combination Impacted at 70° (Back Plate)

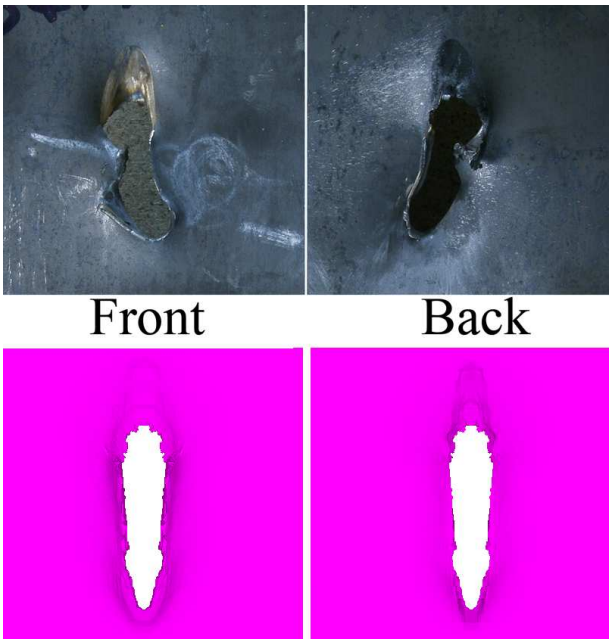

Figure 5.23: Comparison of the Experimental and Simulation Results of the 2 mm + 3 mm Layered Plate Combination Impacted at 70° (Front Plate)

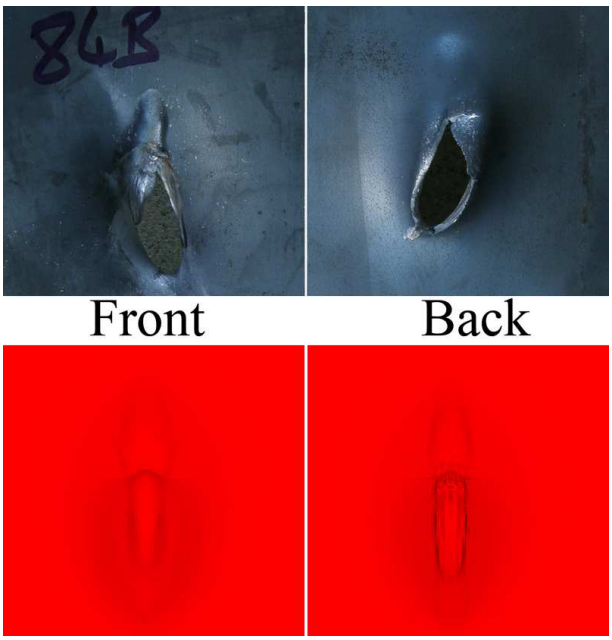

Figure 5.24: Comparison of the Experimental and Simulation Results of the 2 mm + 3 mm Layered Plate Combination Impacted at 70° (Back Plate)

CHAPTER 6

CONCLUSIONS AND RECOMMENDATIONS

In this last chapter of the thesis, the main conclusions of the experimental and numerical studies are presented (Section 6.1). In Section 6.2, some recommendations for the future work on this topic are given.

6.1 Conclusions

In this thesis study, effects of change of plate thickness and angle of attack on the perforation behavior of ST-37 steel plates under oblique impact conditions are investigated. To perforate the plates, 7.62 mm AP bullets are used. First of all, experiments are conducted at MKEK Small Arms Weapon Factory (Kırıkkale/TURKEY). Afterwards, numerical simulations of the experimental conditions are performed using a commercial nonlinear hydrocode solver, ANSYS AUTODYN. Results of the both methods are compared in Chapter 5. The main conclusions of this thesis are:

- In general, after checking the tensile test results, it is seen that plates having different thicknesses have slightly different material properties. Also the number of shots for each angle of attack-plate thickness combination is limited to 3 due to insufficient number of cartridges in hand. These should be considered while investigating the results of the experiments.

- As a result of the experimental studies for the monolithic plates, it can be said that as the angle of attack increases, the maximum plate thickness that is perforated at that angle of attack decreases or vice versa.

- As presented in Figure 3.39, since the constant areal density values start to become larger than not perforated plate thicknesses for all experimental shots, the areal density (as a result, the weight) of the plates that provide protection against 7.62 mm AP bullet can actually be decreased by changing the obliquity of the plates. The largest difference between the minimum plate thickness that is not perforated and the plate thickness providing a constant areal density is observed at 70 ° angle of attack resulting in a 41.5% lighter armor compared to 25 mm plate impacted under normal impact conditions. The least efficient angle of attack is 20 ° with only 14.9% decrease in the total armor weight. An application area of this property can be an active armor system that detects a treat and aligns itself to 70 ° angle of attack.

- Due to insufficient number of layered plate shots, no meaningful conclusion could be obtained for the layered plates in comparison to monolithic ones.

- Since it was impossible to trace the bullet after impact 4 mm plates impacted at 70 ° angle of attack are recorded as *Perforated* in the experimental results. However, it is seen in the numerical studies that they actually did not let the bullet pass through. They just look like they are perforated.

- When a straight line is fitted to the results of the experiments for the monolithic plates, it is seen that the line shows the behavior of ST-37 plates impacted by 7.62 mm AP bullets under oblique impact conditions by 98.8% certainty. This value is 94.6% for the numerical simulations. By checking these results, it can be concluded the relation between the minimum not perforated plate thickness and the angle of attack can be explained by a linear relation.

- As in the results of experimental studies for the monolithic plates, the numerical simulation results also indicate that as the angle of attack increases, the maximum plate thickness that is perforated at that angle of attack decreases or vice versa.

- When Figure 4.39 is investigated, it can be concluded that by changing the obliquity of the ST-37 steel plates, the weight of the total armor can be decreased in numerical simulations as well. The minimum armor weight is obtained when the angle of attack is 70 ° which provides a 41.5% lighter armor compared to the 25 mm plate impacted by the bullet at 0 °. At 50 ° angle of attack, however, total armor weight is decreased by 6.7% only.

6.2 Recommendations for Future Work

Recommendations for the researchers who will deal with a similar topic in future can be listed as follows:

- Since this thesis aims to understand the basic behavior of steel under oblique impact conditions, an ordinary steel (ST-37) is used in both experimental and numerical analyses. However, in real applications, armor materials commonly used in practice could be investigated.

- In experimental studies, systems like high speed cameras, could be implemented, wherever possible. Such systems enable the researcher to determine the exact velocities and directions of the bullets after impact. Such data would be very helpful in understanding the oblique impact phenomenon and comparing the results with the numerical simulations in an easier and more detailed way.

- Layered plate combinations could be investigated for every angle of attack where the monolithic plates are examined. By this way, a better and broader understanding of the effect of layered plates would be obtained.

- Also in layered plate combinations, thicknesses of the front and back plates and number of plates could be changed without altering the total thickness. By this way, effects of the number of layers and layer thicknesses would be investigated.

- After obtaining a better understanding of the layered plates, spacing between the plates could be changed. This would enable the researcher to understand the effect of spacing between plates under oblique impact conditions.

- To get more reliable results in numerical simulations, more realistic material model parameters should be obtained. Although the curve fitting approach used in this thesis works quite well, more precise simulations require material tests conducted at high stain rates and temperatures such as Split-Hopkinson Pressure Bar (SHPB) test. Results of these tests can provide more reliable parameters for the material model used.

- Since the geometric model and Johnson-Cook model parameters for the bullet are taken from a previous study ([31]) and they are obtained by an estimation process by the

author, high stain rate and temperature material tests could also be conducted for the bullet core material (hardened DIN 100Cr6) to obtain more realistic simulation results. A suitable failure model and its parameters could also be determined by material tests to explain the fracture behavior of the core as occurred in the experiments.

- Although Johnson-Cook constitutive and damage models provide good results in this thesis, effect of different material models on the results of numerical simulations could be an interesting topic to investigate.

- The increment of the angle of attack is determined to be $10\,^{\circ}$ in this thesis due to limited number of cartridges. This increment value could be decreased to a smaller value (as small as possible) to obtain more precise results.

REFERENCES

[1] Britannica Online Encyclopedia, http://www.britannica.com, last visited on 17.10.2009

[2] Heard B. J., *Handbook of Firearms and Ballistics*, Second Edition ,Wiley - Blackwell, 2008

[3] Carlucci D. E., Jacobson S. S., *Ballistics: Theory and Design of Guns and Ammunitions*, CRC Press, 2008

[4] Bhatnagar A., *Lightweight Ballistic Composites*, Woodhead Publishing, Cambridge, 2006

[5] Garibaldi J., Storti M., Battaglia L., D'Elia J., *Numerical Simulations of the Flow Around a Spinning Projectile in Subsonic Regime*, Latin American Applied Research, Volume 38, p.p. 241-247, 2008

[6] Meyers M. A., *Dynamic Behavior of Materials*, John Wiley & Sons, 1994

[7] Zukas J. A., Nicholas T., Swift H. F., Greszczuk L. B., Curran D. R., *Impact Dynamics*, John Wiley & Sons, 1982

[8] Carleone J., *Tactical Missile Warheads*, American Institute of Aeronautics and Astronautics, 1993

[9] Bashford D., *Helmets and Body Armor in Modern Warfare*, Yale University Press, 1920

[10] Payne C. M., *Principles of Naval Weapon Systems*, Naval Institute Press, 2006

[11] NIJ Standard-0101.04: *Ballistic Resistance of Personal Body Armor*, U.S. Department of Justice, National Institute of Justice, 2000

[12] NIJ Standard-0106.01: *Ballistic Helmets*, U.S. Department of Justice, National Institute of Justice, 1981

[13] Gálvez V. S., Paradela L. S., *Analysis of Failure of Add-on Armour for Vehicle Protection against Ballistic Impact*, Journal of Engineering Failure Analysis, Vol 16, Issue 6, p.p. 1837-1845, 2009

[14] Pinder J., *Reactive Armor Tiles for Army and Marine Corps Armored Vehicles*, An Independent Report to the Department of Defense and the United States Congress, 1999

[15] Shin H., Lee W., *A Numerical Study on the Detonation Behaviour of Double Reactive Cassettes by Impacts of Projectiles with Different Nose Shapes*, International Journal of Impact Engineering, Volume 28, p.p. 349-362

[16] Jonas G. H., Zukas J. A., *Mechanics of Penetration: Analysis and Experiment*, Technical Report Submitted to US Army Research and Development Command, Ballistic Research Laboratory, Maryland, 1979

[17] Awerbuch J., Bodner S. R., *An Investigation of Oblique Perforation of Metallic Plates by Projectiles*, Technion-Israel Institute of Technology, 1975

[18] Gupta V., Madhu N. K., *An Experimental Study of Normal and Oblique Impact of Hard-core Projectile on Single and Layered Plates*, International Journal of Impact Engineering, Volume 19, Issues 5-6, p.p. 395-414, 1997

[19] Woong L., Heon-Joo L., Hyunho S., *Ricochet of a tungsten heavy alloy long-rod projectile from deformable steel plates*, Journal of Physics D: Applied Physics, Volume 35, p.p. 2676-2686, 2002

[20] Daneshjou K., Sahravi M., *Analysis of Critical Ricochet Angle Using Two Space Discretization Methods*, Engineering with Computers, Volume 25, p.p. 191-206, 2008

[21] Zhou D. W., Stronge W. J., *Ballistic Limit for Oblique Impact of Thin Sandwich Panels and Spaced Plates*, International Journal of Impact Engineering, Volume 35, p.p. 1339-1354, 2008

[22] Lee W. S., Liu C. Y., *The Effects of Temperature and Strain Rate on the Dynamic Flow Behaviour of Different Steels*, Materials Science and Engineering: A, Volume 426, Issues 1-2, p.p. 101-113, 2006

[23] Hertzberg R. W., *Deformation and Fracture Mechnics of Engineering Materials*, Fourth Edition, John Wiley & Sons, 1996

[24] Lee W. S., Chen T. H., Hwang H. H., *Impact Response and Microstructural Evolution of Biomedical Titanium Alloy under Various Temperatures*, Journal of Metallurgical and Materials Transactions A, Volume 39, Issue 6, p.p. 1435-1448, 2008

[25] Demir T., *Metal ve Katmanlı Zırh Malzemelerinin 7,62 mm'lik Zırh Delici Mermiler Karşısında Balistik Başarımlarının İncelenmesi*, An MSc Thesis Submitted to the Graduate School of Natural and Applied Sciences of TOBB University of Economics and Technology, 2008

[26] Übeyli M., *A Comparison of Ballistic Behavior of Steel and Laminated Composite Armors*, PhD Thesis Submitted to the Graduate School of Natural and Applied Sciences of Middle East Technical University, 2005

[27] MIL-C-60617A, *Military Specification, Cartrige, 7.62 mm: NATO, Armor Piercing, M61*, 1991

[28] Zukas J. A., *Introduction to Hydrocodes*, Elsevier Ltd., 2004

[29] CENTURY DYNAMICS, *AUTODYN Theory Manual*, West Sussex, 1998

[30] Courant R., Friedrichs K., Lewy H., *On the Partial Difference Equations of Mathematical Physics*, Mathematische Annalen, Volume 100, p.p. 32-7, 1928

[31] Bilici M. A., *An Investigation on the Ballistic Behaviour of Alumina/Aluminum Armor Structures*, PhD Thesis Submitted to the Graduate School of Natural and Applied Sciences of Middle East Technical University, 2007

[32] Zhang P., *Joining Enabled by High Velocity Deformation*, PhD Thesis Submitted to the Graduate School of the Ohio State University, 2003

[33] CENTURY DYNAMICS, *AUTODYN Version 6.0 Training Course*, 2006

[34] American Society of Metals, Edited by J. R. Davis, *Metals Handbook Desk Edition, 2nd edition*, ASM International, 1998

[35] Johnson G. R., Cook W. H., *A Constitutive Model and Data for Metals Subjected to Large Strains, High Strain Rates and High Temperatures*, Proceedings of the 7th International Symposium on Ballistics, The Hague, The Netherlands, 1983

[36] Dey S., Børvik T., Hopperstad O.S., Langseth M., *On the Influence of Constitutive Relation in Projectile Impact of Steel Plates*, International Journal of Impact Engineering, Volume 34, p.p. 464-486, 2007

[37] Gökgöz O., *Investigation of Monolithic and Multi-layered Metallic Plates against Projectile Impact*, An MSc Thesis Submitted to the Graduate School of Natural and Applied Sciences of Middle East Technical University, 2002

[38] *52100 Chrome Steel Balls*, National Precision Ball Product Catalogue, 2002

[39] Karim M. R., Fatt M. S. H., *Impact of the Boeing 767 Aircraft into the World Trade Center*, Journal of Engineering Mechanics, Volume 131, p.p. 1066-1072, 2005